

การเพิ่มสมรรถนะของเบตเตอร์ี่สังกะสี-อากาศแบบยืดหยุ่นได้ที่พิมพ์ขึ้นรูปโดยการปรับปรุงระบบ  
อิเล็กทรอนิกส์



นางสาวจุฑามาศ โชติพานิช

จุฬาลงกรณ์มหาวิทยาลัย

CHULALONGKORN UNIVERSITY

บทคัดย่อและแฟ้มข้อมูลฉบับเต็มของวิทยานิพนธ์ตั้งแต่ปีการศึกษา 2554 ที่ให้บริการในคลังปัญญาจุฬาฯ (CUIR)  
เป็นแฟ้มข้อมูลของนิสิตเจ้าของวิทยานิพนธ์ ที่ส่งผ่านทางบัณฑิตวิทยาลัย

The abstract and full text of theses from the academic year 2011 in Chulalongkorn University Intellectual Repository (CUIR)  
are the thesis authors' files submitted through the University Graduate School.

วิทยานิพนธ์นี้เป็นส่วนหนึ่งของการศึกษาตามหลักสูตรปริญญาวิทยาศาสตรดุษฎีบัณฑิต

สาขาวิชาวิศวกรรมเคมี ภาควิชาวิศวกรรมเคมี

คณะวิศวกรรมศาสตร์ จุฬาลงกรณ์มหาวิทยาลัย

ปีการศึกษา 2559

ลิขสิทธิ์ของจุฬาลงกรณ์มหาวิทยาลัย

PERFORMANCE ENHANCEMENT OF A FLEXIBLE PRINTED  
ZINC–AIR BATTERY BY IMPROVING ELECTROLYTE SYSTEM

Miss Jutamart Chotipanich



A Dissertation Submitted in Partial Fulfillment of the Requirements  
for the Degree of Doctor of Engineering Program in Chemical Engineering  
Department of Chemical Engineering  
Faculty of Engineering  
Chulalongkorn University  
Academic Year 2016  
Copyright of Chulalongkorn University

Thesis Title                         PERFORMANCE ENHANCEMENT OF A  
FLEXIBLE PRINTED ZINC–AIR BATTERY BY  
IMPROVING ELECTROLYTE SYSTEM

By   Miss Jutamart Chotipanich

Field of Study                        Chemical Engineering

Thesis Advisor                       Associate Professor Soorathep Kheawhom, Ph.D.

---

Accepted by the Faculty of Engineering, Chulalongkorn University in Partial  
Fulfillment of the Requirements for the Doctoral Degree

..... Dean of the Faculty of Engineering  
(Associate Professor Supot Teachavorasinskun, D.Eng.)

THESIS COMMITTEE

..... Chairman  
(Assistant Professor Pornchai Bumroongsri, D.Eng.)

..... Thesis Advisor  
(Associate Professor Soorathep Kheawhom, Ph.D.)

..... Examiner  
(Assistant Professor Amornchai Arpornwichanop, D.Eng.)

..... Examiner  
(Chalida Klaysom, Ph.D.)

..... Examiner  
(Palang Bumroongsakulsawat, Ph.D.)

..... External Examiner  
(Assistant Professor Prakorn Ramakul, D.Eng.)

จุฑามาศ โชติพานิช : การเพิ่มสมรรถนะของแบตเตอรี่สังกะสี-อากาศแบบยืดหยุ่นได้ที่พิมพ์ขึ้นรูป โดยการปรับปรุงระบบอิเล็กโทรไลต์ (PERFORMANCE ENHANCEMENT OF A FLEXIBLE PRINTED ZINC-AIR BATTERY BY IMPROVING ELECTROLYTE SYSTEM) อ.ที่ปรึกษาวิทยานิพนธ์หลัก: รศ. ดร. สุรเทพ เขียวหอม, 102 หน้า.

แบตเตอรี่สังกะสี-อากาศแบบยืดหยุ่นได้ที่พิมพ์ขึ้นรูป คือเทคโนโลยีการกักเก็บพลังงานชนิดหนึ่งซึ่งมีความหนาแน่นของพลังงานที่สูง อย่างไรก็ตาม ความแตกต่างระหว่างความหนาแน่นของพลังงานทางทฤษฎีและทางปฏิบัติมีค่าค่อนข้างสูง ดังนั้น ในการศึกษา การใช้ประโยชน์ของสังกะสีในแบตเตอรี่สังกะสี-อากาศแบบยืดหยุ่นได้ที่พิมพ์ขึ้นรูปจึงถูกทำให้เพิ่ม โดยการเติมสารลดแรงดึงผิวประเภทไอออนลบในโปแตสเซียมไฮดรอกไซด์เข้มข้น  $7 \text{ mol L}^{-1}$  ซึ่งคืออิเล็กโทรไลต์ดั้งเดิม สารลดแรงดึงผิวเหล่านี้ซึ่งถูกใช้ ประกอบด้วยโซเดียมโคเดซิลเบนซีนซัลโฟเนต (SDBS) และโซเดียมโคเดซิลซัลเฟต (SDS) นอกจากนี้ เอทานอลยังถูกใช้เพื่อปรับปรุงความสามารถของ SDBS และ SDS ด้วย จากนั้นเซลล์แบตเตอรี่ซึ่งใช้อิเล็กโทรไลต์ที่มีการปรับเปลี่ยนหลายแบบถูกศึกษาโดยใช้เครื่องวิเคราะห์แบตเตอรี่ ยิ่งไปกว่านั้น พื้นผิวของขั้วไฟฟ้าสังกะสีถูกศึกษาโดยกล้องจุลทรรศน์อิเล็กตรอนแบบส่องกราด ผลการทดลองที่ได้ แสดงให้เห็นว่า ค่าความจุและพลังงานของแบตเตอรี่ถูกทำให้เพิ่มขึ้นสองเท่าโดยใช้อิเล็กโทรไลต์ที่มีการปรับเปลี่ยนด้วย SDBS และ SDS การใช้อิเล็กโทรไลต์ที่มีการปรับเปลี่ยนด้วย SDS โดยปราศจากเอทานอล มีความจุและพลังงานสูงกว่าการใส่สารเติมแต่ง SDBS ความเข้มข้นที่เหมาะสมสำหรับ แบตเตอรี่สังกะสี-อากาศแบบยืดหยุ่นที่พิมพ์ขึ้นรูปของทั้ง SDBS และ SDS คือ  $0.4 \text{ mmol L}^{-1}$  ทั้ง SDBS และ SDS ปรับเปลี่ยนพื้นผิวของขั้วไฟฟ้าสังกะสีให้กลายเป็นมีความพรุนมากขึ้น นำไปสู่การปรับปรุงความสามารถในการเปียกของขั้วไฟฟ้าสังกะสี ดังนั้น อิเล็กโทรไลต์ที่มีการปรับเปลี่ยนสามารถแทรกซึมสู่ขั้วไฟฟ้าสังกะสีได้อย่างง่ายดาย ส่งผลต่อการปรับปรุงการแพร่ของสปีชีส์ที่ทำงานได้มากกว่านั้น การเติมเอทานอลในอิเล็กโทรไลต์ที่มีการปรับเปลี่ยนสามารถปรับปรุงความสามารถของ SDBS และ SDS เมื่อความเข้มข้นของสารลดแรงดึงผิวมีค่าสูงกว่าค่าความเข้มข้นวิกฤติของการเกิดไมเซลล์ของสารลดแรงดึงผิวนั้นๆ และโมเลกุลของสารลดแรงดึงผิวที่มีโครงสร้างโมเลกุลขนาดใหญ่ถูกใช้งาน นอกจากนี้ คุณสมบัติ (เช่น โครงสร้างโมเลกุลและค่า CMC) ของสารลดแรงดึงผิว ควรจะถูกพิจารณาเนื่องจากคุณลักษณะดังกล่าวมีผลต่อสมรรถนะของแบตเตอรี่

ภาควิชา วิศวกรรมเคมี

ลายมือชื่อนิติต .....

สาขาวิชา วิศวกรรมเคมี

ลายมือชื่อ อ.ที่ปรึกษาหลัก .....

ปีการศึกษา 2559

# # 5471403721 : MAJOR CHEMICAL ENGINEERING

KEYWORDS: FLEXIBLE PRINTED ZINC-AIR BATTERY / ZINC UTILIZATION / MODIFIED ELECTROLYTE / SODIUM DODECYLBENZENESULFONATE / SODIUM DODECYL SULFATE

JUTAMART CHOTIPANICH: PERFORMANCE ENHANCEMENT OF A FLEXIBLE PRINTED ZINC-AIR BATTERY BY IMPROVING ELECTROLYTE SYSTEM. ADVISOR: ASSOC. PROF. SOORATHEP KHEAWHOM, Ph.D., 102 pp.

Flexible printed zinc-air battery is an energy storage technology which has the high energy density. However, the difference between theoretical and practical energy densities is quite high. Therefore, in this study, zinc utilization in flexible printed zinc-air battery was enhanced by adding anionic surfactants in  $7 \text{ mol L}^{-1}$  KOH which is a traditional electrolyte. These surfactants which are employed consisted of sodium dodecyl benzene sulphonate (SDBS) and sodium dodecyl sulfate (SDS). In addition, an ethanol was also used to improve SDBS and SDS capabilities. Then the battery cells which used various modified electrolytes were examined by the battery analyzer. Additionally, the surface of discharged zinc electrodes was investigated by scanning electron microscope. The results reveal that the capacity and the energy of the batteries are doubled by using SDBS and SDS modified electrolyte. The use of SDS modified electrolyte without ethanol is higher capacity and energy than the use of SDBS additive. The proper concentration for a flexible printed zinc-air battery of both SDBS and SDS is  $0.4 \text{ mol L}^{-1}$ . Both SDBS and SDS modify the zinc electrode surface to become more porosity, leading to improve the wettability of zinc electrode. Therefore the modified electrolytes can easily penetrate to the zinc electrode, resulting in improvement of active species diffusion. Moreover, addition of ethanol in the modified electrolytes can improve SDBS and SDS capabilities when the surfactant concentration is higher than their critical micelle concentration and the surfactant molecule with the large molecular structure is employed. Furthermore, characteristics of surfactants (such as molecular structure and the CMC) should be taken into account because they also affect the battery performance.

Department: Chemical Engineering

Student's Signature .....

Field of Study: Chemical Engineering

Advisor's Signature .....

Academic Year: 2016

## ACKNOWLEDGEMENTS

Firstly, I would like to express my deep gratitude to my advisor, Assoc. Prof. Soorathep Kheawhom for giving me the opportunity and for his invaluable guidance and support. I would especially like to thank each member of my dissertation committee, Asst. Prof. Pornchai Bumroongsri, Asst. Prof. Amornchai Arpornwichanop, Asst. Prof. Prakorn Ramakul, Dr. Chalida Klaysom and Dr. Palang Bumroongsakulsawat for their constructive suggestions on my research work.

I would also like to extend my warm thanks to Dr. Kittima Ngamsai who not only changed my mind to move forward but who is also stand beside me always. Her friendship and assistance meant a lot to me. My sincere thanks to Dr. Pawinee Sintarako for providing support whenever needed.

Thank you to members of my research group who helped from time to time with my research.

My deepest gratitude goes to my beloved family for their whole hearted love and constant support. To my parents who supported me in all my pursuits. To my elder brother who provided assistance in numerous ways. To my husband who encouraged me throughout the time of my research. To my little girl Chuenjai, who provides me with unending inspiration. I thank all of you for your patience.

This dissertation is particularly dedicated to my deceased father. Thank you for everything you did for me.

## CONTENTS

|  | Page |
|--|------|
| THAI ABSTRACT .....                          | iv   |
| ENGLISH ABSTRACT.....                        | v    |
| ACKNOWLEDGEMENTS .....                       | vi   |
| CONTENTS.....                                | vii  |
| LIST OF TABLES .....                         | x    |
| LIST OF FIGURES .....                        | xi   |
| CHAPTER I INTRODUCTION.....                  | 1    |
| 1.1 Introduction.....                        | 1    |
| 1.2 Research objective .....                 | 2    |
| 1.3 Scope of research .....                  | 2    |
| 1.4 Expected benefits .....                  | 3    |
| 1.5 Dissertation overview .....              | 3    |
| CHAPTER II LITERATURE REVIEWS .....          | 5    |
| 2.1 Screen printing technique .....          | 5    |
| 2.2 Problem of zinc anode .....              | 6    |
| 2.2.1 Passivation of zinc .....              | 6    |
| 2.2.2 Dissolution of zinc .....              | 7    |
| 2.3 Development of electrolyte.....          | 8    |
| 2.3.1 Aqueous electrolytes.....              | 9    |
| 2.3.2 Non-aqueous electrolyte .....          | 13   |
| 2.3.2.1 Solid polymer electrolytes.....      | 13   |
| 2.3.2.2 Room temperature ionic liquids ..... | 15   |
| 2.3.3 Hybrid electrolytes.....               | 16   |
| CHAPTER III THEORY AND PRINCIPLE .....       | 19   |
| 3.1 Zinc-air battery.....                    | 19   |
| 3.2 Electrochemical cell.....                | 20   |
| 3.3 Actual cell potential .....              | 22   |
| 3.3.1 Activation losses .....                | 23   |

|   | Page |
|---|------|
| 3.3.2 Ohmic losses .....  | 25   |
| 3.3.3 Mass-transport losses .....                                   | 25   |
| 3.4 Fundamental of electricity .....                                | 27   |
| 3.5 Surfactant .....  | 28   |
| 3.5.1 Basic theory .....  | 28   |
| 3.5.2 Molecular structure of surfactants .....                      | 30   |
| 3.5.3 Surface activity .....  | 32   |
| 3.5.3.1 Surface tension .....                                       | 32   |
| 3.5.3.2 Interfacial tension .....                                   | 33   |
| 3.5.3.3 Surface and interfacial tension reduction .....             | 34   |
| 3.5.4 Self-assembled surfactant aggregates .....                    | 37   |
| 3.5.4.1 Micelles and critical micelle concentration .....           | 38   |
| 3.5.4.2 Aggregate structures and shapes .....                       | 40   |
| 3.5.5 Adsorption of surfactants at surfaces .....                   | 43   |
| 3.5.5.1 Adsorption at liquid–gas and liquid–liquid interfaces ..... | 43   |
| 3.5.5.2 Adsorption at liquid–solid interface .....                  | 46   |
| 3.5.6 Anionic surfactant .....                                      | 50   |
| CHAPTER IV EXPERIMENT .....   | 52   |
| 4.1 Materials and Chemicals .....                                   | 52   |
| 4.2 Experimental methodology .....                                  | 53   |
| 4.3 Preparation of functional ink .....                             | 53   |
| 4.3.1 Zinc –based functional ink .....                              | 53   |
| 4.3.2 Gas diffusion ink .....                                       | 54   |
| 4.4 Preparation of aqueous electrolyte .....                        | 54   |
| 4.4.1 Potassium hydroxide .....                                     | 54   |
| 4.4.2 Potassium hydroxide with surfactant .....                     | 54   |
| 4.4.3 Potassium hydroxide with surfactant and ethanol .....         | 54   |
| 4.5 Preparation of flexible substrate and separator .....           | 55   |
| 4.5.1 Polyethylene terephthalate (PET) substrate .....              | 55   |



|  | Page |
|--|------|
| 4.5.2 Polytetrafluoroethylene (PTFE) substrate .....       | 55   |
| 4.5.3 Polypropylene (PP) membrane .....                    | 55   |
| 4.6 Preparation of anode electrode.....                    | 55   |
| 4.7 Preparation of cathode electrode.....                  | 56   |
| 4.8 Fabrication of flexible printed zinc-air battery ..... | 56   |
| 4.9 Characterizations.....                                 | 57   |
| CHAPTER V RESULTS AND DISCUSSIONS.....                     | 58   |
| 5.1 Effect of potassium hydroxide concentration .....      | 58   |
| 5.2 Effect of surfactants .....                            | 62   |
| 5.2.1 Sodium dodecyl benzene sulfonate .....               | 63   |
| 5.2.2 Sodium dodecyl sulfate.....                          | 68   |
| 5.2.3 Comparison between SDBS and SDS .....                | 73   |
| 5.3 Effect of ethanol on surfactant role.....              | 77   |
| 5.4 Morphological analysis .....                           | 84   |
| 5.5 All effects summary .....                              | 87   |
| 5.6 Electrochemical impedance investigation.....           | 89   |
| CHAPTER VI CONCLUSIONS .....                               | 96   |
| 6.1 Conclusions.....                                       | 96   |
| 6.2 Recommendations for the future work .....              | 97   |
| REFERENCES .....   | 98   |
| VITA.....  | 102  |

## LIST OF TABLES

|   | Page |
|---|------|
| Table 2.1 Composition and properties of SPEs used (potentially) for metal-air batteries [7]. .....                      | 14   |
| Table 3.1 Typical hydrophilic groups [12]. .....  | 29   |
| Table 3.2 Typical hydrophobic groups [12]. .....  | 30   |
| Table 3.3 Schematics of molecular surfactant structures and sample surfactants .  | 31   |
| Table 3.4 Structures of surfactant self-assemblies as a function of surfactant packing parameters and shape [12]. ..... | 42   |
| Table 4.1 List of the materials and the chemicals for electrolyte system improvement .....                              | 52   |
| Table 5.1 All impedances from equivalent circuit model of zinc-air battery. ....  | 90   |

## LIST OF FIGURES

|   | Page |
|---|------|
| Figure 1.1 Schematic diagram of the dissertation overview.....  | 4    |
| Figure 2.1 Schematic diagram of dissolution and oxide film formation in anodic oxidation of Zn. (a) Initial state. (b) Prepassive film formation. (c) Zinc oxide formation [11]. .....  | 7    |
| Figure 2.2 Correlation of mass % KOH and the conductivity [7].....  | 9    |
| Figure 3.1 The cross-sectional diagram of the zinc-air battery .....  | 19   |
| Figure 3.2 Correlation of cell voltage and current density which explain the loss behaviors in the cell [37].....   | 23   |
| Figure 3.3 Example of Tafel plot [37]. .....  | 24   |
| Figure 3.4 Simplified structure of surfactant [14]. .....   | 28   |
| Figure 3.5 Configuration of typical micelle [14].....   | 29   |
| Figure 3.6 Physical properties of aqueous surfactant solution as a function of surfactant concentration [14]. .....   | 38   |
| Figure 3.7 Four region isotherms of surfactant adsorption [14]. .....   | 48   |
| Figure 3.8 Surfactant adsorption on solid surfaces [14] .....   | 49   |
| Figure 4.1 Schematic diagram of electrolyte improvement.....  | 53   |
| Figure 4.2 Anode electrode pattern.....   | 56   |
| Figure 4.3 Cathode electrode pattern.....   | 56   |
| Figure 4.4 Layer by layer configuration of the zinc air battery.....  | 57   |
| Figure 5.1 Polarization curves of 5 mol L <sup>-1</sup> , 7 mol L <sup>-1</sup> and 9 mol L <sup>-1</sup> KOH electrolytes used in the flexible printed zinc-air battery with effective area of 1 cm <sup>2</sup> . .....   | 59   |
| Figure 5.2 Correlations of current density and cell power of 5 mol L <sup>-1</sup> , 7 mol L <sup>-1</sup> and 9 mol L <sup>-1</sup> KOH electrolytes used in the flexible printed zinc-air battery with effective area of 1 cm <sup>2</sup> . .....  | 60   |
| Figure 5.3 Correlations of discharging time and the cell voltage of 5 mol L <sup>-1</sup> , 7 mol L <sup>-1</sup> and 9 mol L <sup>-1</sup> KOH electrolytes used in the flexible printed zinc-air battery with effective area of 1 cm <sup>2</sup> by 1 mA cm <sup>-2</sup> constant current discharging.. | 61   |

|  | Page |
|--|------|
| Figure 5.4 Correlations of KOH concentration and capacity and energy of the flexible printed zinc-air battery with effective area of $1 \text{ cm}^2$ by $1 \text{ mA cm}^{-2}$ constant current discharging. ....   | 62   |
| Figure 5.5 Structural formula of sodium dodecyl benzene sulfonate. ....  | 63   |
| Figure 5.6 Polarization curve of $0.2 \text{ mmol L}^{-1}$ , $0.4 \text{ mmol L}^{-1}$ and $0.6 \text{ mmol L}^{-1}$ SDBS in $7 \text{ mol L}^{-1}$ KOH electrolytes used in the flexible printed zinc-air battery with effective area of $1 \text{ cm}^2$ . ....  | 64   |
| Figure 5.7 Correlations of current density and cell power of $0.2 \text{ mmol L}^{-1}$ , $0.4 \text{ mmol L}^{-1}$ and $0.6 \text{ mmol L}^{-1}$ SDBS in $7 \text{ mol L}^{-1}$ KOH electrolytes used in the flexible printed zinc-air battery with effective area of $1 \text{ cm}^2$ . ....  | 65   |
| Figure 5.8 Correlations of discharging time and cell voltage of $0.2 \text{ mmol L}^{-1}$ , $0.4 \text{ mmol L}^{-1}$ and $0.6 \text{ mmol L}^{-1}$ SDBS in $7 \text{ mol L}^{-1}$ KOH electrolytes used in the flexible printed zinc-air battery with effective area of $1 \text{ cm}^2$ by $1 \text{ mA cm}^{-2}$ constant current discharging. .... | 66   |
| Figure 5.9 Correlations of SDBS concentration in $7 \text{ mol L}^{-1}$ KOH and the capacity and the energy of the flexible printed zinc-air battery with effective area of $1 \text{ cm}^2$ by $1 \text{ mA cm}^{-2}$ constant current discharging. ....  | 68   |
| Figure 5.10 Structural formula of sodium dodecyl sulfate. ....   | 69   |
| Figure 5.11 Polarization curve of $0.2 \text{ mmol L}^{-1}$ , $0.4 \text{ mmol L}^{-1}$ and $0.6 \text{ mmol L}^{-1}$ SDS in $7 \text{ mol L}^{-1}$ KOH electrolytes used in the flexible printed zinc-air battery with effective area of $1 \text{ cm}^2$ . ....  | 70   |
| Figure 5.12 Correlations of current density and cell power of $0.2 \text{ mmol L}^{-1}$ , $0.4 \text{ mmol L}^{-1}$ and $0.6 \text{ mmol L}^{-1}$ SDS in $7 \text{ mol L}^{-1}$ KOH electrolytes used in the flexible printed zinc-air battery with effective area of $1 \text{ cm}^2$ . ....  | 71   |
| Figure 5.13 Correlations of discharging time and cell voltage of $0.2 \text{ mmol L}^{-1}$ , $0.4 \text{ mmol L}^{-1}$ and $0.6 \text{ mmol L}^{-1}$ SDS in $7 \text{ mol L}^{-1}$ KOH electrolytes used in the flexible printed zinc-air battery with effective area of $1 \text{ cm}^2$ by $1 \text{ mA cm}^{-2}$ constant current discharging. .... | 72   |
| Figure 5.14 Correlations of SDS concentration in $7 \text{ mol L}^{-1}$ KOH and the capacity and the energy of the flexible printed zinc-air battery with effective area of $1 \text{ cm}^2$ by $1 \text{ mA cm}^{-2}$ constant current discharging. ....  | 73   |
| Figure 5.15 Correlations of surfactant concentration in the electrolytes and maximum cell power for SDBS and SDS in $7 \text{ mol L}^{-1}$ KOH electrolytes comparing with $7 \text{ mol L}^{-1}$ KOH electrolyte. ....  | 75   |

|   | Page |
|---|------|
| Figure 5.16 Comparison of the capacities of the flexible printed zinc-air battery which employs various concentrations of SDBS and SDS in 7 mol L <sup>-1</sup> KOH electrolytes and 7 mol L <sup>-1</sup> KOH electrolyte by 1 mA cm <sup>-2</sup> constant current discharging.....   | 76   |
| Figure 5.17 Comparison of the energies of the flexible printed zinc-air battery which employs various concentrations of SDBS and SDS in 7 mol L <sup>-1</sup> KOH electrolytes and 7 mol L <sup>-1</sup> KOH electrolyte by 1 mA cm <sup>-2</sup> constant current discharging.....   | 77   |
| Figure 5.18 Polarization curve of 0.2 mmol L <sup>-1</sup> , 0.4 mmol L <sup>-1</sup> and 0.6 mmol L <sup>-1</sup> SDBS with 20 %v/v ethanol in 7 mol L <sup>-1</sup> KOH electrolytes used in the flexible printed zinc-air battery with effective area of 1 cm <sup>2</sup> .....   | 79   |
| Figure 5.19 Polarization curve of 0.2 mmol L <sup>-1</sup> , 0.4 mmol L <sup>-1</sup> and 0.6 mmol L <sup>-1</sup> SDS with 30 %v/v ethanol in 7 mol L <sup>-1</sup> KOH electrolytes used in the flexible printed zinc-air battery with effective area of 1 cm <sup>2</sup> .....  | 80   |
| Figure 5.20 Correlations of current density and cell power of 0.2 mmol L <sup>-1</sup> , 0.4 mmol L <sup>-1</sup> and 0.6 mmol L <sup>-1</sup> SDBS with 20 %v/v ethanol in 7 mol L <sup>-1</sup> KOH electrolytes used in the flexible printed zinc-air battery with effective area of 1 cm <sup>2</sup> . .....   | 81   |
| Figure 5.21 Correlations of current density and cell power of 0.2 mmol L <sup>-1</sup> , 0.4 mmol L <sup>-1</sup> and 0.6 mmol L <sup>-1</sup> SDS with 30%v/v ethanol in 7 mol L <sup>-1</sup> KOH electrolytes used in the flexible printed zinc-air battery with effective area of 1 cm <sup>2</sup> . .....   | 82   |
| Figure 5.22 Correlations of cell voltage and discharging time of 0.2 mmol L <sup>-1</sup> , 0.4 mmol L <sup>-1</sup> and 0.6 mmol L <sup>-1</sup> SDBS with 20 %v/v ethanol in 7 mol L <sup>-1</sup> KOH electrolytes used in the flexible printed zinc-air battery with effective area of 1 cm <sup>2</sup> by 1 mA cm <sup>-2</sup> constant current discharging..... | 83   |
| Figure 5.23 Correlations of cell voltage and discharging time of 0.2 mmol L <sup>-1</sup> , 0.4 mmol L <sup>-1</sup> and 0.6 mmol L <sup>-1</sup> SDS with 30 %v/v ethanol in 7 mol L <sup>-1</sup> KOH electrolytes used in the flexible printed zinc-air battery with effective area of 1 cm <sup>2</sup> by 1 mA cm <sup>-2</sup> constant current discharging.....  | 84   |

|   |    |
|---|----|
| Figure 5.24 Micrographs of zinc anode by scanning electron microscope: (a) Before discharge (b) The cell discharged in 7 mol L <sup>-1</sup> KOH electrolyte (c) The cell discharged in 7 mol L <sup>-1</sup> KOH + 0.4 mmol L <sup>-1</sup> SDBS electrolyte (d) The cell discharged in 7 mol L <sup>-1</sup> KOH + 0.4 mmol L <sup>-1</sup> SDS electrolyte (e) The cell discharged in 7 mol L <sup>-1</sup> KOH + 0.4 mmol L <sup>-1</sup> SDBS + 20 %v/v ethanol electrolyte (f) The cell discharged in 7 mol L <sup>-1</sup> KOH + 0.4 mmol L <sup>-1</sup> SDS + 30 %v/v ethanol electrolyte..... | 85 |
| Figure 5.25 Correlations of current density and capacity of all experiments by 1 mA cm <sup>-2</sup> constant current discharging. ....   | 87 |
| Figure 5.26 Correlations of current density and energy of all experiments by 1 mA cm <sup>-2</sup> constant current discharging. ....   | 88 |
| Figure 5.27 Equivalent circuit model of zinc-air battery.....   | 90 |
| Figure 5.28 The Nyquist plots of the flexible printed zinc-air battery using 0.2 mmol L <sup>-1</sup> , 0.4 mmol L <sup>-1</sup> and 0.6 mmol L <sup>-1</sup> SDBS in 7 mol L <sup>-1</sup> KOH electrolytes comparing with 7 mol L <sup>-1</sup> KOH electrolyte by 1 mA cm <sup>-2</sup> constant current discharging in frequency range of 0.1 Hz to 10 kHz. ....  | 91 |
| Figure 5.29 The Nyquist plots of the flexible printed zinc-air battery using 0.2 mmol L <sup>-1</sup> , 0.4 mmol L <sup>-1</sup> and 0.6 mmol L <sup>-1</sup> SDS in 7 mol L <sup>-1</sup> KOH electrolytes comparing with 7 mol L <sup>-1</sup> KOH electrolyte by 1 mA cm <sup>-2</sup> constant current discharging in frequency range of 0.1 Hz to 10 kHz. ....   | 92 |
| Figure 5.30 The Nyquist plots of the flexible printed zinc-air battery using 0.2 mmol L <sup>-1</sup> , 0.4 mmol L <sup>-1</sup> and 0.6 mmol L <sup>-1</sup> SDBS with 20 %v/v ethanol in 7 mol L <sup>-1</sup> KOH electrolytes comparing with 7 mol L <sup>-1</sup> KOH electrolyte by 1 mA cm <sup>-2</sup> constant current discharging in frequency range of 0.1 Hz to 10 kHz. ....   | 93 |
| Figure 5.31 The Nyquist plots of the flexible printed zinc-air battery using 0.2 mmol L <sup>-1</sup> , 0.4 mmol L <sup>-1</sup> and 0.6 mmol L <sup>-1</sup> SDS with 30 %v/v ethanol in 7 mol L <sup>-1</sup> KOH electrolytes comparing with 7 mol L <sup>-1</sup> KOH electrolyte by 1 mA cm <sup>-2</sup> constant current discharging in frequency range of 0.1 Hz to 10 kHz. ....  | 94 |

# CHAPTER I

## INTRODUCTION

### 1.1 Introduction

Recently, metal-air batteries have received increasing attention because of their high energy density [1, 2] as these batteries use oxygen from air, which is virtually unlimited, for their cathode half-cell. The most important metal-air batteries include lithium-air battery and zinc-air battery. However, lithium-air battery, which uses lithium as its anode, has high cost and high toxicity, although it exhibits higher energy density than zinc-air battery. In comparison, zinc-air battery shows comparatively lower energy density but it uses zinc which is relatively safe and cost effective, as its anode [3]. Moreover, zinc is environmentally friendly, abundant and has low toxicity [4]. Zinc-air battery is currently utilized in several devices such as hearing aids, navigation lights and rail-way signals [5]

One type of zinc-air battery which has been receiving an interest is a flexible printed zinc-air battery due to its simplicity, high throughput. Furthermore, the flexible printed zinc-air battery allows the manufacture of flexible and low cost devices [6-8].

In theory, zinc-air battery has specific energy of  $1350 \text{ Wh kg}^{-1}$ . Indeed,  $200 \text{ Wh kg}^{-1}$  of zinc air battery can only be utilized [5]. It can be calculated as around 15% of the theoretical specific energy which is quite low. This information indicates that the zinc in the battery is not fully utilized. Many reasons contribute to the difference between practical specific energy and theoretical specific energy such as passivation of zinc anode, zinc dissolution and shape change. Therefore, enhancement of zinc utilization is considerable. The resolutions of such problems are the ways to improve zinc utilization in the battery. In addition, the developments of the battery performance are also important, because the high-performance battery which is the low loss of the battery results in the high benefit. The development of electrolyte system will lead to comprehensively develop zinc-air battery.

There are many research groups which have developed and improved the performance of zinc-air battery by focusing on the electrolyte system. many types of the electrolyte systems, included of aqueous electrolyte, non-aqueous electrolyte and hybrid electrolyte, have been studied [9]. The purposes of the electrolyte system study are to minimize zinc passivation, zinc dissolution and shape change in zinc electrode during the operation of zinc-air battery. Furthermore, any undesirable effects should not be generated by the use of developed electrolyte system. For example, Wang et al. [10] suggested that the dendritic growth of zinc which is one type of shape change problem is greatly inhibited by synergistic effect of  $\text{Bi}^{3+}$  and TBAB at higher cathodic overpotential. These compositions were added in  $8 \text{ mol L}^{-1}$  KOH for acting as electrolyte. In addition, the adding both water and DMSO in 1-ethyl-3-methylimidazolium – Dicyanamide (EMI-DCA) which is one of RTILs can improve reversibility, cyclability and kinetics for the zinc redox reactions [11].

This work aims at enhancement of performance of a flexible printed zinc-air battery by improvement of ionic and electronic conductivity of electrolyte system using various additives. In order to improve the electrolyte system, sodium dodecylbenzenesulfonate (SDBS) and sodium dodecyl sulfate (SDS) are used as the additives with or without ethanol. The effects of these additives on characteristic and performance of the flexible printed zinc-air battery are studied.

## 1.2 Research objective

1. To enhance the performance of a flexible printed zinc-air battery.
2. To investigate the roles and effects of sodium dodecylbenzenesulfonate (SDBS) and sodium dodecyl sulfate (SDS) on the electrolyte of a flexible printed zinc-air battery.

## 1.3 Scope of research

1. A principle of flexible printed zinc-air battery is studied.
2. Zinc-air battery is fabricated by screen-printing technique.



3. Three concentrations (5 M, 7 M and 9 M) of potassium hydroxide solution are investigated to obtain the proper concentration for the best performance of flexible printed zinc-air battery.

4. 0.2 mM, 0.4 mM and 0.6 mM, sodium dodecylbenzene sulfonate and sodium dodecyl sulfate are added in potassium hydroxide solution which is a traditional aqueous electrolyte to enhance the performances of flexible printed zinc-air battery.

5. The effects of an ethanol on the surfactant function are examined to improve the zinc utilization.

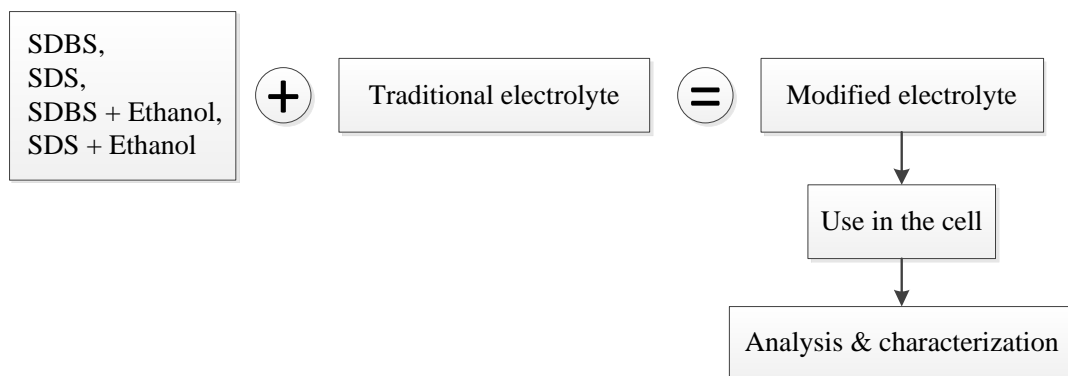
#### **1.4 Expected benefits**

1. The enhancing performance methods of the flexible printed zinc-air battery have been obtained.

2. The proper electrolyte system for the flexible printed zinc-air battery has been acquired.

#### **1.5 Dissertation overview**

One method to improve zinc utilization is improvement of electrolyte system [12, 13]. In this study, two types of surfactants were utilized to enhance zinc utilization. These surfactants consist of sodium dodecylbenzene sulfonate and sodium dodecyl sulfate. The two surfactants are anionic surfactant which has the typical critical micelle concentration (CMC) values at room temperature of  $10^{-3}$ – $10^{-2}$  M [14]. Since the CMC value is quite low for enhancing the zinc utilization in a zinc-air battery therefore, an ethanol is also employed for both surfactants in this studied to enhance the surfactant function. In addition, the effects of the surfactants and ethanol on characteristic and performance of the flexible printed zinc-air battery were studied. Overview of the dissertation is present in Figure 1.1.



**Figure 1.1** Schematic diagram of the dissertation overview.



## **CHAPTER II**

### **LITERATURE REVIEWS**

Flexible printed zinc-air battery has been studied in order to enhance the battery performance. In this study, the anode side (zinc electrode) and the electrolyte system have been studied. Therefore, in this chapter, Screen printing technique, problem of zinc anode, development of zinc electrode and development of electrolyte are reviewed as follows.

#### **2.1 Screen printing technique**

Lately, small electronic devices for articles of daily use are increasingly interesting resulting in increase in sales of these devices. Most small electronic devices need the energy storage capacities which should be thin, flexible and meet to the design needs. Screen printing technique is recently used in the fabrication of electronic devices and batteries for simplicity, scaled-up, high-throughput and environmental friendliness. Moreover, screen printing technique promises low-cost fabrication, light weight and flexibility. Various types of flexible batteries have been fabricated using screen printing technology e.g. lithium ion battery, zinc-silver battery, nickel metal hydride battery, and zinc-air battery [15].

The screen printing technique capacitates the sequential deposition of current collector, electrode and separator soaked with electrolyte onto a flexible substrate for a battery application. The capacity of a screen printing battery is determined by the amount and the layer thickness of screen print inks. This screen printing ink is rather easy to adjust for optimum performance. The particle size must relate to the attended printing technology. Generally, screen printing inks must have high viscosity in order to stabilize the large particles (tens of microns) dispersions. Commercially, the particle size of available zinc powder is higher than 60 microns. This size is suitable for screen printing inks. Flexible zinc-air battery using a screen-printing technique has been developed. Zinc/carbon/polymer composite is used as an anode. A poly(3,4-

ethylenedioxythiophene) (PEDOT) is used as cathode. Both materials are printed onto two sides of a photo quality paper. The effects of zinc/carbon combination and various electrolyte compositions are demonstrated [16]. Suren and Kheawhom [8] fabricated the flexible zinc air battery using an inexpensive screen-printing technique in order to improve an energy density. The result showed that the flexible zinc air battery had high energy density of  $682 \text{ Wh kg}^{-1}$ . Additionally, the voltage and the charging time of the flexible cell were not different in term of characteristic from non-flexible cell.

Furthermore, other types of batteries were fabricated. Flexible nickel metal hydride (Ni-MH) rechargeable battery was fabricated using screen printed thin technique. The capacity of the battery was 32 mAh [17]. Moreover, a flexible zinc-silver rechargeable battery was produced using screen-printing on tattoo paper. This appearance provided a maximum discharge capacity of  $2.1 \text{ mAh cm}^{-2}$  [18].

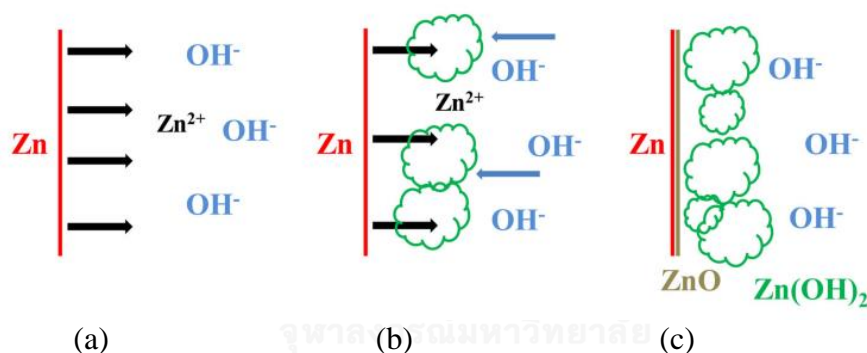
## **2.2 Problem of zinc anode**

### **2.2.1 Passivation of zinc**

The passivation of zinc electrode takes place when the concentration of hydroxide or salt in the electrolyte closed to the membrane is excess. The excessive concentration results of the dissolution of zinc. Then the excessive ions precipitate and form a compact film [13]. For zinc alkaline solutions, passive currents are found in the pH range of 10-13 [19]. The passive layers occur over the zinc electrode surface. There are two layers of the passive film including of 1) the external porous and white layer which is formed by the precipitation of saturated zincate ( $\text{Zn(OH)}_4^{2-}$ ) at the closer layer to the anode electrode and 2) the light gray to black and dense layer which is ZnO. The dense layer is favored by the lower pH. It takes place at the interface between the metal and the electrolyte and acts as diffusion barrier to  $\text{OH}^-$  ions [20]. The composition of passive film is  $\text{Zn(OH)}_2$  and ZnO [13]. The prepassive film results of intermediate species before the formation of zinc oxide. Furthermore, the passivation of the zinc anode accompanied by local drying also occurs because of electrolyte loss in the cell on charge [21].

In common alkaline electrolyte system, the energy and power densities of zinc electrode reduce significantly with the decrease of hydroxyl group concentration due to passivation of zinc surface. The use of very concentrated alkaline solution can reduce zinc passivation due to high solubility of the passive film in the concentrated solution. However, shape change can be taken place in too high alkaline concentration [13].

The additives such as silicate ( $\text{SiO}_3^{2-}$ ) which enhance the solubility of zinc are absorbed on ZnO leading to block the precipitation of other zinc ions [13]. Therefore, ZnO cannot coagulate at the zinc electrode surface. the passivation of the zinc surface can be minimized by adding sodium dodecyl benzene sulfonate (SDBS) in alkaline electrolyte. Furthermore, SDBS can improve the discharging capacity of zinc electrode [22], particularly in dilute alkaline solution [23]. The mechanism of zinc dissolution and the formation of oxide film are illustrated in Figure 2.1.



**Figure 2.1** Schematic diagram of dissolution and oxide film mechanisms in zinc anodic oxidation. (a) Initial state. (b) Prepassive film formation. (c) Zinc oxide formation [13].

### 2.2.2 Dissolution of zinc

The high solubility of zinc in the concentrated alkaline solution result from the formation of saturated or supersaturated zincate solution leading to the shape change of zinc electrode and dendritic growth process [13]. The system performance is also decreased and in worst case, internal short circuit occurs. The dissolution of zinc electrode in aqueous alkaline electrolyte takes place in two steps. Firstly, the oxidation of zinc to zincate occurs as shown in Equation (2.1). And then, when the zincate

saturated in such electrolyte, the precipitation of zinc oxide takes place (Equation (2.2)). Equation (2.3) expresses the overall reaction of zinc electrode.



In order to limit the solubility of zincate, there are three possible ways including of: 1) decrease the hydroxide ion concentration of the electrolyte, 2) add some species which lead to lowering of the solubility of the discharging product and 3) modify the electrolyte system [24].

### 2.3 Development of electrolyte

The selection of electrolyte system is particularly necessary to develop the performance of a zinc-air battery because the electrolyte is the electrochemical controller of such battery. The electrolyte determines the recharging capacity and the cell voltage as well as the obtaining energy of the battery. In addition, the transport properties of active species (zinc ion and oxygen) and power density also depend on the electrolyte.

The first primary zinc-air battery is commercialized in 1930s. Then there are significant efforts in order to develop secondary zinc air batteries or rechargeable zinc air batteries. The key of performance improvement is the selection of proper electrolyte system. An aqueous electrolyte is the preferable electrolyte. Many research groups have studied many electrolyte systems including aqueous electrolyte, non-aqueous electrolyte and hybrid electrolyte [9], in order to gain insight into future development of the electrolyte system. The details of these studied are shown as follows.

### 2.3.1 Aqueous electrolytes

Aqueous electrolytes which are alkaline electrolytes have been utilized in the first time.. Potassium hydroxide (KOH) is the most commonly used alkaline electrolyte due to high conductivity, high activity for both the air and zinc electrodes and good performance at low temperature. The correlation of KOH concentration and the conductivity is illustrated in Figure 2.1 [9].

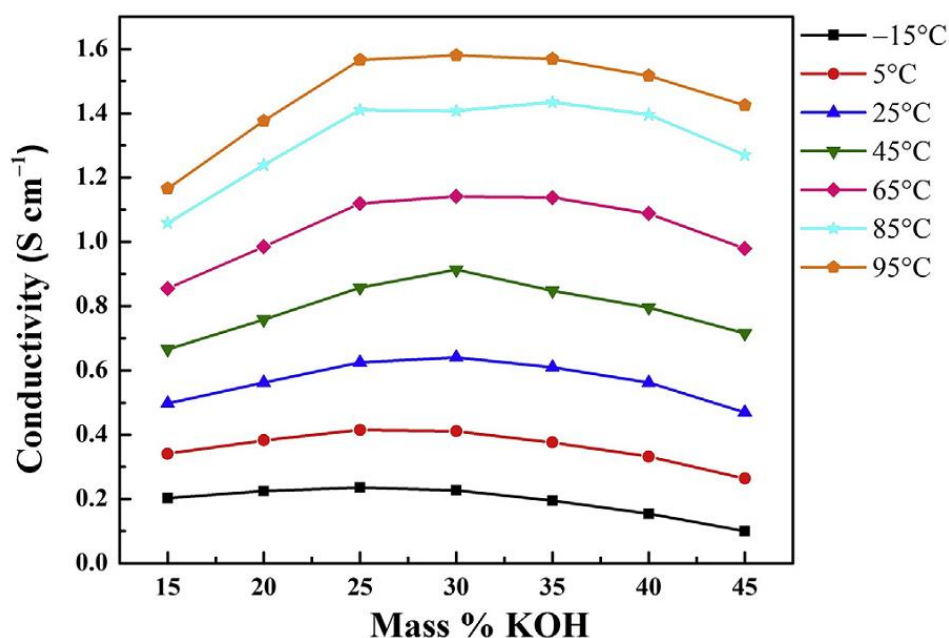
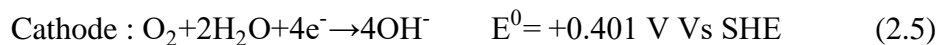
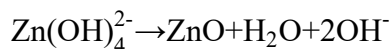
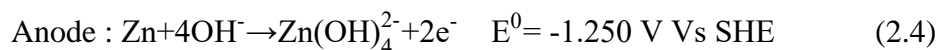


Figure 2.2 Correlation of mass % KOH and the conductivity [9]

Figure 2.2 shows that the highest conductivity is obtained at the KOH concentration of 30 wt% (7 M) and 25 °C (room temperature). The conductivity is higher with the operating temperature increase. However, 37 wt% KOH (9M) is widely employed in many modern alkaline batteries, because high conductivity and low corrosion gas are obtained at such concentration.

During discharging process, oxygen from surroundings diffused into the cathode. These oxygen species are reduced to hydroxyl ions. These ions move into the anode and react with zinc to form zincate ions ( $\text{Zn(OH)}_4^{2-}$ ). Then electrons are released. These electrons are transported to the air cathode. After reaching their equilibrium solubility level, ZnO occurs from the precipitation of zincate. These reactions can be expressed as Equations (2.4) – (2.6) [25].



From the occurring reaction, the water is used at the cathode. This water can be reused in Zincate ion decomposition. The ZnO is the overall product. Additionally, electrolyte dry out is another problem when having oxygen entering in the system for the reaction. Therefore, both Zn-electrode failure and poor air cathode performance diminish the battery's life.

For zinc-electrode failure, dendrite growth, passivation, self-discharge and shape change are the four main problems of poor cycle-life performance. The potential solutions of these problems are adding the additives in electrode and electrolyte (either inorganic [26] or organic [27]). These solutions have proven to be an effective way to minimize some of the problems. Furthermore, the use of a large electrolyte reservoir with sufficient OH<sup>-</sup> supply can prevent passivation well. However, the dissolution of zincate ion may be increased resulting in higher rates of dendrite formation and shape change. Moreover, when adding zincate solubility-reducing agent in electrolyte or electrode to depress dendrite growth and shape change, the additive concentration has to be controlled to avoid induced passivation [24]. In addition, the selection of the suitable additive with the passivation effect is also necessary to obtain desirable battery performance. The cycle life and capacity (material utilization) must be taken into account [9].

Furthermore, electrolytes based acid including both inorganic (e.g., sulfuric acid) and organic (e.g., methane sulfonic acid, polyvinyl sulfonic acid and polyvinyl sulfuric acid) have been developed to minimize dendrite formation. However, the zinc metal cannot stand in acid condition because it can be corroded by the acid. Therefore, the acidic electrolytes are not appropriate.

Many additives were added to aqueous electrolyte for various KOH concentrations in order to enhance the performance of zinc-air battery. For example, in



1990, [28] used Quaternary ammonium compounds included amphionic SFB, resistone QD, resistone TFR, tetramethylammonium bromide, tetraethylammonium bromide, tetrapropylammonium bromide, tetrabutylammonium bromide and benzyltrimethylammonium bromide in the 7 mol L<sup>-1</sup> KOH as electrolyte to enhance zinc electrodeposits. Simple current-time techniques were utilized, in order to screen potential alkyl groups and examine their effectiveness. Visual assessment and scanning electron microscopy were also employed to investigate the zinc electrodeposits. The results showed that a smoother relief and the reduction of dendritic growth were improved by improvement of deposit morphology using quaternary ammonium compounds. In addition, the various additives were added to 5.3 mol L<sup>-1</sup> KOH to improve the passivation. These additives consisted of Cd, Ca(OH)<sub>2</sub>, Mg(OH)<sub>2</sub>, Al<sub>2</sub>O<sub>3</sub>, sodium boroheptonate, potassium orthophosphate, potassium ferricyanide, potassium molybdate, potassium tungstate, potassium chromate, potassium tetraborate and boric acid. The galvanostatic passivation experiments were utilized to examine the passivation characteristics. The results showed that borate and chromate are the most effective of the passivants tested. In addition, Auger analysis of the passivated electrode surfaces implies that borate helps reducing the free hydroxyl species in solution leading to reducing zincate solubility whereas the cause of passivation in case of chromate was its strong oxidizing nature [24]. Furthermore, Bismuth ion and tetrabutylammonium bromide (TBAB) were added in 8 mol L<sup>-1</sup> KOH electrolyte as deposit-enhancing additives of zinc electrode. Current time technique, potentiodynamic polarization and scanning electron microscopy were utilized to investigate the dendritic growth of zinc. The results indicated that the addition of Bi<sup>3+</sup> suppresses the dendritic growth of zinc in the alkaline solution by substrate effect both at lower cathodic overpotential ( $\eta = -100$  mV) and at higher cathodic overpotential ( $\eta = -200$  mV). Moreover, the dendritic growth of zinc is greatly inhibited by synergistic effect of Bi<sup>3+</sup> and TBAB at higher cathodic overpotential [10]. Then, in 2004, Yang et al [22]. utilized sodium dodecyl benzene sulfonate (SDBS) which is an anionic surfactant in dilute alkaline electrolyte solution (20% KOH solution), In order to increase the capacity utilization of zinc anode. They employed the measurement of discharge capacity, passivation polarization curve, impedance spectra and scanning electron microscopy to investigate the anodic passivation behaviors of zinc electrode. The results found that the discharge capacity

of zinc anode increases up to 35% at moderate discharge rate of 40 mA/g. Furthermore, the passive layer formed on the zinc surface has a loose and porous structure rather than a dense and compact film by employing SDBS 2% in the dilute KOH solution. This porous structure film facilitates the diffusive exchange of the solution reactant and discharged product through the surface deposit layer. Therefore, anodic utilization of zinc anode is improved [22]. Additionally, different kinds of surfactant and deferent derivatives of benzene were studied to improve the performance of zinc batteries. The galvanostatic technique was used to prepare electrolytic zinc powders in 12 M KOH, 4 wt% zinc oxide solutions in the present of different kinds of surfactant and organic additive. The sweep voltammetry technique was employed to investigate the electrochemical behavior and the results showed that the maximum corrosion rate is found in zinc samples electrolyzed in the presence of cationic cetyl trimethyl ammonium bromide (Zn-CTAB). In addition, scanning electron microscopy was used to investigate the morphology and revealed that the zinc sample with cationic surfactant has the highest surface area. Moreover, the high dendritic and secondary growth is found by using zinc deposited with anionic surfactants, sodium dodecyl benzene sulfonate (SDBS) and sodium dodecyl sulfate (SDS). Furthermore, naphthalene can decrease corrosion rate and needle growth of zinc deposition. The addition of Triton X-100 in anode gel gave the maximum electrical capacity. Anionic (SDBS and SDS) surfactant additives resulted in higher electrical capacity than cationic [29]. Another research of the additive addition is the use of several tetra-alkyl ammonium hydroxides included tetramethyl ammonium hydroxide (TMAH), tetra-ethyl ammonium hydroxide (TEAH), tetrapropyl ammonium hydroxide (TPAH), tetrabutyl ammonium hydroxide (TBAH) and tributylmethyl ammonium hydroxide (TBMAH) in 6.6 mol L<sup>-1</sup> KOH electrolyte as novel inhibitors of Zn dendrite to replace the well-known tetraalkyl ammonium bromides. Current–time technique using potentiostatic electrodeposition, conductivity measurement, cycling test and scanning electron microscopy were utilized to assess the efficacy of these hydroxides. The results indicated that the size of alkyl groups and the added concentration affect the ability to inhibit Zn dendrite. The additives govern cathodic current profile and morphology of the deposits. The addition of these additives does not deteriorate conductivity of electrolyte. The inhibition ability of zinc dendrite was found to follow the sequence: 0.01 M TPAH > 0.001 M TBMAH

> 0.01 M TEAH. The addition of 0.1 M TEAH or 0.005 M TPAH into the blank solution highly improves rechargeability during high current charge-discharge. Because of comparing with those of known additives of tetra-alkyl ammonium bromides, the proposed TAAHs are environmentally cleaner and safer. Consequently, TAAHs used as inhibitors of Zn dendrite in Zn-based secondary batteries can be better alternatives to tetra-alkyl ammonium bromides. Etc.

Furthermore, the problem of zinc dissolution or corrosion is solved by adding ZnO or  $(\text{NH}_4)_2\text{CS}$  in an aqueous electrolyte. This method was proposed by [30]. In their study,  $\text{V}_2\text{O}_5$ , ZnO, PbO and  $(\text{NH}_4)_2\text{CS}$  were added in  $6 \text{ mol L}^{-1}$  KOH. Potentiodynamic polarization and triangular potential sweep voltammetric techniques were employed to examine. The results revealed that the proper additives for reduction of corrosion ZnO and  $(\text{NH}_4)_2\text{CS}$ . However, they need to be used as the optimum concentration.

### 2.3.2 Non-aqueous electrolyte

The purpose of non-aqueous electrolyte development is to solve electrode corrosion, dendrite formation, electrolyte drying out and air electrode flooding. These problems occur in aqueous electrolyte system. The non-aqueous electrolyte has 2 kinds including of solid polymer electrolyte (SPEs) and room temperature ionic liquids (RTILs). The details of 2 non-aqueous electrolytes are expressed as follows.

#### 2.3.2.1 Solid polymer electrolytes

Solid polymer electrolytes (SPEs) are ionically conductive solid formed by conducting salt(s) into polymer(s) [31]. The purpose of SPEs utilization is the elimination of air electrode flooding which exists in aqueous electrolyte system. Therefore, the battery life is enhanced. The electrode corrosion is also mitigated in SPEs because of low convection.

SPEs (based on polyethylene oxide ) were discovered by Wright et al.[9]. They exhibited extremely low conductivity ( $10^{-8}$  to  $10^{-7} \text{ S cm}^{-2}$ ), resulting in their application were limited. Consequently, the development of SPEs is concentrated on good ionic conductivity as well as good thermal and mechanical properties. The polymers that commonly used in alkaline SPEs are listed in Table 2.1 [9].

In 1983, there was the study of ionic motion in amorphous phase above the glass transition temperature ( $T_g$ ). The results show that a high fraction of amorphous phase gave higher conductivity than that of a crystalline phase. Therefore, the main method of enhancing the ionic conductivity of SPEs is the use of high fraction of amorphous phase in SPEs. In addition, the use of polyvinyl alcohol (PVA)/poly(acrylic acid) (PAA) membrane also provides the high conductivity. However, high PAA content reduces the mechanical strength of polymer membrane. Consequently, the enhanced ionic conductivity and the desirable mechanical strength need to be taken into account together.

**Table 2.1** Composition and properties of SPEs used (potentially) for metal-air batteries [9].

| Composition  | Conductivity<br>( $S\ cm^{-1}$ ) | Yield<br>stress<br>(MPa) | Cell performance   |
|--|----------------------------------|--------------------------|--|
| Poly(epichlorohydrin-co-ethylene oxide)+ KOH (aq)      | $10^{-3}$                        | -                        | Discharge up to 14 mA $cm^{-2}$ at 0.8 V (Zn-air primary cell)                   |
| Polyvinyl alcohol + poly(epichlorohydrin) + 32 wt% KOH | $10^{-3} - 10^{-2}$              | 57.8a                    | Reaches a discharge capacity of 1296 mAh at C/20 and 25 °C (Zn-air primary cell) |
| Polyethylene oxide + polyvinyl alcohol + KOH (aq)      | $10^{-2}$                        | -                        | Reaches a discharge capacity of 1431 mAh at C/20 and 25 °C (Zn-air primary cell) |
| Polyvinyl alcohol + poly(acrylic acid) + 32 wt% KOH    | $10^{-1}$                        | 3.47b                    | -  |

| Composition                      | Conductivity<br>(S cm <sup>-1</sup> ) | Yield<br>stress<br>(MPa) | Cell performance   |
|----------------------------------|---------------------------------------|--------------------------|--|
| Poly(acrylic acid) + KOH<br>(aq) | 10 <sup>-1</sup>                      | -                        | Reaches a discharge capacity of 1166 mAh/g at 52 mA cm <sup>-2</sup> (Al-air primary cell) |

All property values correspond to the optimal experimental condition.

<sup>a,b</sup>Measured at a pull rate of 200 mm min<sup>-1</sup>; film thickness 0.16 mm, width 10 mm.

### 2.3.2.2 Room temperature ionic liquids

Non-aqueous ionic liquids (ILs) have appeared as promising electrolyte candidates for rechargeable zinc-air batteries. Non-aqueous ionic liquids (composed of cations and anions) are salts which have low melting point approximately 100°C or below, they are thus called room temperature ionic liquids (RTILs). Different selections and combinations of cation and anion result in the diversity of RTILs. The advantages of RTIL over the aqueous electrolyte are 1) no volatility like aqueous electrolyte 2) being completely ionic (no solvent ions) of that salt, this ionic nature can be utilized in a wide electrochemical window. Generally, imidazolium (cation) is the key component in most traditional RTILs, because it has a low melting temperature and a desirable electrochemical stability [9]. There is the utilization of RTILs incorporated with ammonium cation to improve an electrochemical window (EW). And it found that EW is wider because an ammonium has better cathodic stability. Furthermore, pyrrolidinium cations and bis(trifluoromethanesulfonyl)imide (TFSI<sup>-</sup>) anion viscosity and conductivity is also improved [32].

For the zinc electrode side, there are many the researches which investigated aprotic RTILs (without dissociable H<sup>+</sup> and unable to donate hydrogen). These researches included 1-butyl-1-methylpyrrolidinium bis(trifluoromethanesulfonyl)imide (BMPTFSI), 1-ethyl-3-methylimidazolium bis(trifluoromethanesulfonyl)imide (EMI-TFSI), 1-butyl-1-methylpyrrolidinium dicyanamide (BMP-DCA) and 1-ethyl-3-methylimidazolium dicyanamide (EMIDCA). RTILs anions dominates the

electrochemical behavior of zinc which composed of reaction mechanism, reaction kinetics and Zn redox cyclability [9].

One advantage of aprotic RTILs utilization in zinc air battery is that zinc corrosion (resulting from hydrogen evolution and be eliminated. Moreover, the aprotic RTILs can also prevent zinc dendrite formation. Therefore, the use of RTILs-based electrolytes for zinc air battery shows promising leads to reducing of dendrite formation, avoiding electrolyte drying out and achieving reversible oxygen [9].

### 2.3.3 Hybrid electrolytes

Hybrid electrolytes are the combination of aqueous and non-aqueous electrolyte system. Because of different advantages in each type, this combination can enhance the performance of rechargeable zinc-air batteries. Since aqueous electrolytes have the benefit of high reaction kinetics and RTILs have the benefit of zinc morphology control, they are thus incorporated. There was adding RTILs in conventional alkaline aqueous electrolyte in order to depress zinc dendrite formation while maintain high electrode kinetic. One approach for the hybrid electrolytes is to mix non-aqueous RTILs with other solvents to improve electrolyte conductivity and guaranteeing good electrode kinetics for both the Zn and air sides. Because of the mobility of the ions, RTILs are considered to have capably high conductivities. However, RTILs are high viscosity which is their limitation [9]. Furthermore, the organic solvent (dimethyl sulfoxide; DMSO) facilitates the solvation of zinc ions. It is capable of stabilizing oxygen reduction reaction intermediate. Furthermore, a new electrolyte system composed of an alkaline solution (9 M KOH + 5 wt% ZnO) modified with a small amount (0.5 wt%) of room temperature ionic liquid 1-ethyl-3-methylimidazolium dicyanamide (EMI-DCA) was proposed in order to suppress the uneven deposition of Zn in the conventional alkaline electrolyte and prevent zinc dendritic growth. Cyclic voltammetry, chronoamperometry, electrochemical impedance spectroscopy (EIS) and scanning electron microscopy were utilized to study the mechanism for the modified Zn morphology in the EMI-DCA containing electrolyte [9]. The results indicated that the EMI-DCA containing electrolyte can suppress secondary nucleation process that leads to Zn dendrite formation. Particularly, the zinc deposit morphology was modified by

EMI-DCA. The two steps of the morphology change consist of 1) the zinc reduction process and 2) the zinc film/electrolyte interface. The former step is increase of the reduction overpotential, decrease of the reaction rate and narrowing the potential variation during electrodeposition. The latter step is a result of  $\text{EMI}^+$  cations being specifically adsorbed on the deposited Zn [9]. The use of many compositions in hybrid electrolyte increases the complexity of battery electrochemistry inevitably. Therefore, the interaction of any compositions occurring in the cell needs to be delicately studied.

Another electrolyte that is utilized to improve the performance of rechargeable zinc-air battery is a molten  $\text{Li}_{0.87}\text{Na}_{0.63}\text{K}_{0.50}\text{CO}_3$  eutectic electrolyte with added NaOH. A stable cycling performance through 110 cycles with a highest coulombic efficiency of 96%, and an average discharge potential of 1.04 V were obtained by using the molten salt electrolyte [33].

In addition, the effects of various types of electrolytes and conducting agents and the change in the additive contents to optimize the electrochemical performance were examined. Such electrolyte included sodium hydroxide (NaOH) solution, potassium hydroxide (KOH) solution, super-p, denka black, acetylene black, and ketjen black. Charge-discharge capacities and cycle efficiency was utilized to evaluate the electrochemical performance of the zinc anode. The results showed that the zinc anode with 6 M KOH indicated a higher first discharge capacity and good cycle ability than that with 6 mol L<sup>-1</sup> NaOH. Therefore, KOH was employed as the optimized electrolyte in further experiment. The zinc anode with the additives showed higher first discharge capacity and good cycle ability than pure zinc. The zinc anode containing super-p of 4% in 6 mol L<sup>-1</sup> KOH shows the highest performance [2].

Furthermore, there is the effort to fabricate a flexible solid-state electrolyte. This electrolyte needs to be utilized as both a solid electrolyte and a separator. Therefore, a nanoporous alkaline-exchange electrolyte membrane from natural cellulose nanofibres was invented. The advantages of the solid-state electrolyte are the superior hydroxide-ion conductive property, water retention within the nanoporous structure of the membrane, low anisotropic swelling boosted the specific capacity and improved the cycling stability of the battery compared to the commercial alkaline anion-exchange membrane. In addition, the use of natural cellulose nanofibres with high water retention

provides the development of high-performance, flexible, environmentally-friendly and cost-effective rechargeable zinc-air batteries [34] .





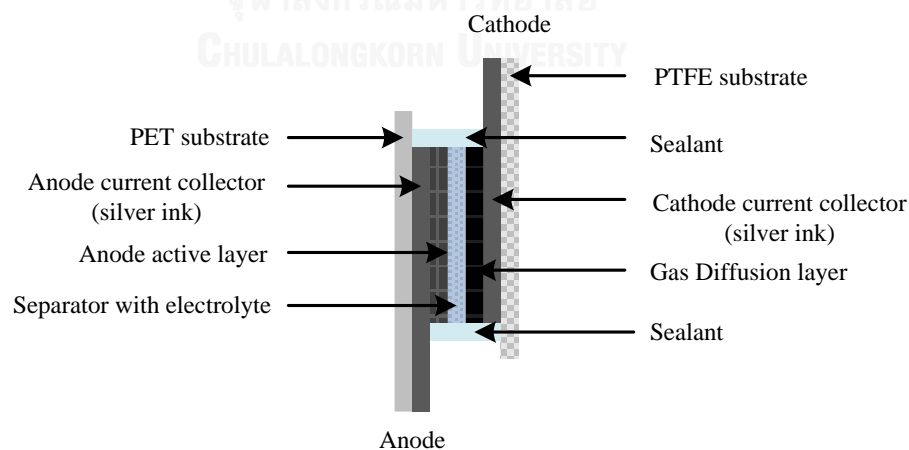
# CHAPTER III

## THEORY AND PRINCIPLE

Zinc-air battery uses the electrochemical principle in its operation. Therefore, in this chapter, principles of zinc-air battery and electrochemical cell are explained. In addition, an actual cell potential and fundamental of electricity are also described. Finally, because the surfactants are used to improve zinc utilization, theories of surfactants are explained. The details of all topics are present as follows

### 3.1 Zinc-air battery

Generally, zinc-air battery comprised of a zinc anode, an air as cathode with gas diffusion layer, a membrane separator, current collectors and an alkaline solution which is used as an electrolyte. The cross-sectional diagram of the zinc-air battery is present in Figure 3.1. In discharging process, the dissolution of zinc electrode involves two steps.

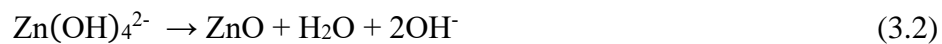


**Figure 3.1** The cross-sectional diagram of the zinc-air battery

The first steps is the oxidation of zinc to soluble zincate ion ( $\text{Zn}(\text{OH})_4^{2-}$ ) as shown in Equation (3.1).



Secondly, the dissolved  $\text{Zn}(\text{OH})_4^{2-}$  saturates in the electrolyte and reaches its solubility limit after that precipitation of zinc oxide ( $\text{ZnO}$ ) takes place as Equation (3.2).



At the anode, overall reaction consumes zinc and hydroxide ion ( $\text{OH}^-$ ) from the electrolyte,  $\text{ZnO}$  and water ( $\text{H}_2\text{O}$ ) are generated (Equation (3.3)).



Besides, the zinc anode an undesired reaction can occur by hydrogen evolution reaction (HER). The reaction consumes  $\text{Zn}$  and  $\text{H}_2\text{O}$  and produces  $\text{Zn}(\text{OH})_2$  and  $\text{H}_2$  on the surface of zinc particles that cause a self-corrosion and lower utilization of zinc as shown in Equation (3.4).



The oxygen reduction reaction (ORR) occurring at the cathode, the reaction consumes oxygen ( $\text{O}_2$ ) and  $\text{H}_2\text{O}$  and produces  $\text{OH}^-$  (Equation (3.5))



### 3.2 Electrochemical cell

An electrochemical cell concerns in both an electrical and a chemical energy. An electrochemical cell is therefore the device that is utilized to convert the energies from electrical energy to chemical energy or reversal. The oxidation and reduction reactions occur in the cell. These reactions are called redox reaction. An

electrochemical cell consists of two half-cells (anode and cathode) which separate by an ion exchange membrane. The half-cell of the oxidation reaction is anode whereas the half-cell of the reduction reaction is cathode. The connector between two half-cells may be a salt bridge or an ion exchange membrane in order to balance the charge in the cell [35].

According to the attribute of the energy changes, there are two types of the electrochemical cell: electrolytic and galvanic cells.

1) Electrolytic cell is the cell that is applied the different potential resulting in occurring redox reactions. These reactions are non-spontaneous.

2) Galvanic cell is the cell that redox reactions spontaneously occur and discharge the electrical energy. The operation of galvanic cell is contrary with the electrolysis cell. It can also be described that the electrical energy is generated from the chemical reaction in the cell.

In addition, the key of electrochemical cell is a standard potential of the redox reaction that explains the behavior of any half-cell. The standard potential is the measurement of any substances half-cell comparing with the standard hydrogen potential (SHE). The SHE has the potential of 0 volt [36]. Because electrons transport from low potential electrode to high potential electrode, the half-cell of receiving electron has higher potential than the half-cell of donating electron. The mobility of electron is reverse with the mobility of the electrical current. This current flows from high potential to low potential.

The cell operation is described by the standard potential of the cell. The negative standard potential indicates that the reactions in the cell are non-spontaneous. Therefore, the cell needs the additional energy to drive the reactions. This phenomenon is the electrolytic cell principle. On the other hand, the positive standard potential indicates that the reactions in the cell are spontaneous. Therefore the electrical energy is generated from the redox reaction. This phenomenon is the galvanic cell principle. The standard potential of electrochemical cell ( $E_{\text{cell}}^0$ ) can be explained by Equation (3.6)

$$E_{\text{cell}}^0 = E_{\text{Cathode}}^0 - E_{\text{Anode}}^0 \quad (3.6)$$

where  $E_{\text{cathode}}^0$  is standard potential of cathode half-cell and  $E_{\text{anode}}^0$  is standard potential of anode half-cell.

The primary zinc-air battery acts as only the galvanic cell that the redox reactions of zinc generate the electrical energy. The calculation of the standard potential of zinc-air cell can be expressed as follows.

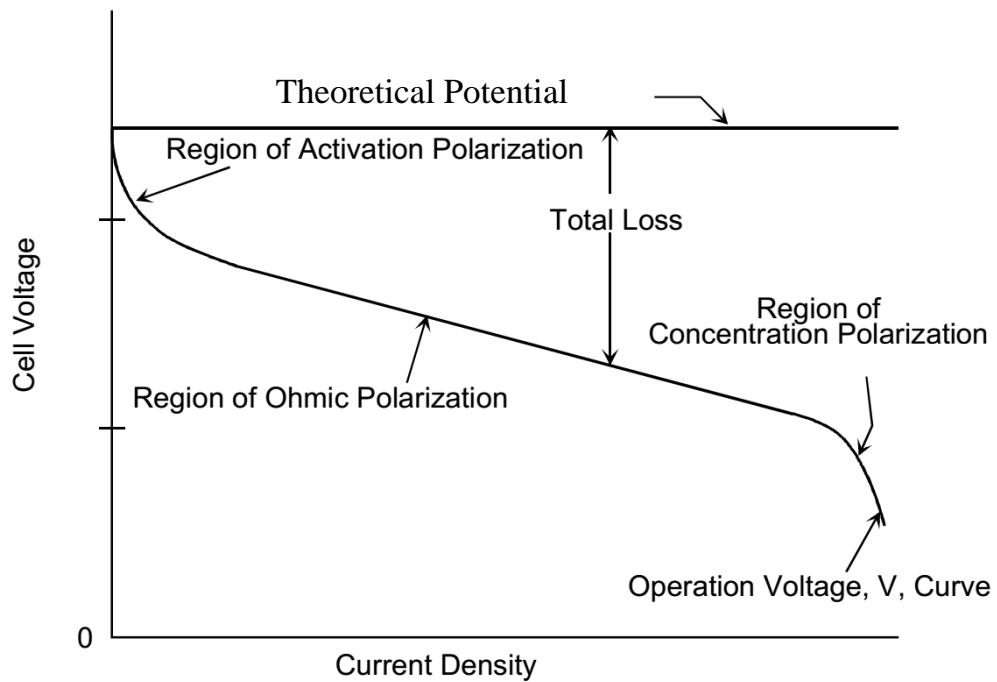
Consider in Chapter 2, Section 2.1, the reactions that occur during the zinc-air battery operation have been explained. The overall standard potential of zinc-air cell can be calculated as Equation (3.7).

$$E_{\text{cell}}^0 = 0.401 - (-1.250) = 1.651 \quad (3.7)$$

This potential is represented theoretical voltage of the zinc-air cell. In practical cell, the potential that closes to the standard potential is called open circuit potential (OCP). This potential can be measured when no electrical current passes through the cell. However, during cell operation, an electrical current must be passed through the cell. This current leads to many losses. Therefore, an actual cell potential which is the losses in the cell subtracts from the standard potential of the cell need to be understood. The details of an actual cell potential are described as follows.

### 3.3 Actual cell potential

The cell potential (or cell voltage) during the operation is the potential which has the effect of all losses. These losses are called polarization, overpotential or overvoltage. The losses consist of activation, ohmic and mass-transport losses. The correlation of cell voltage and current density that describe the losses is illustrated in Figure 3.2. The details of each loss are described as follows.



**Figure 3.2** Correlation of cell voltage and current density which explain the loss behaviors in the cell [37].

### 3.3.1 Activation losses

The inertia of the electrochemical reaction at electrode causes an activation losses ( $\eta_{act}$ ). This phenomenon concerns in the activation energy which the active species must overcome. Indeed, the result of complex surface electrochemical reaction steps is activation losses as well. However, in electrochemical reaction,  $\eta_{act} \geq 50-100$  mV. The voltage losses resulted from activation losses can be approximated by Tafel equation (Equation (3.8)) [37].

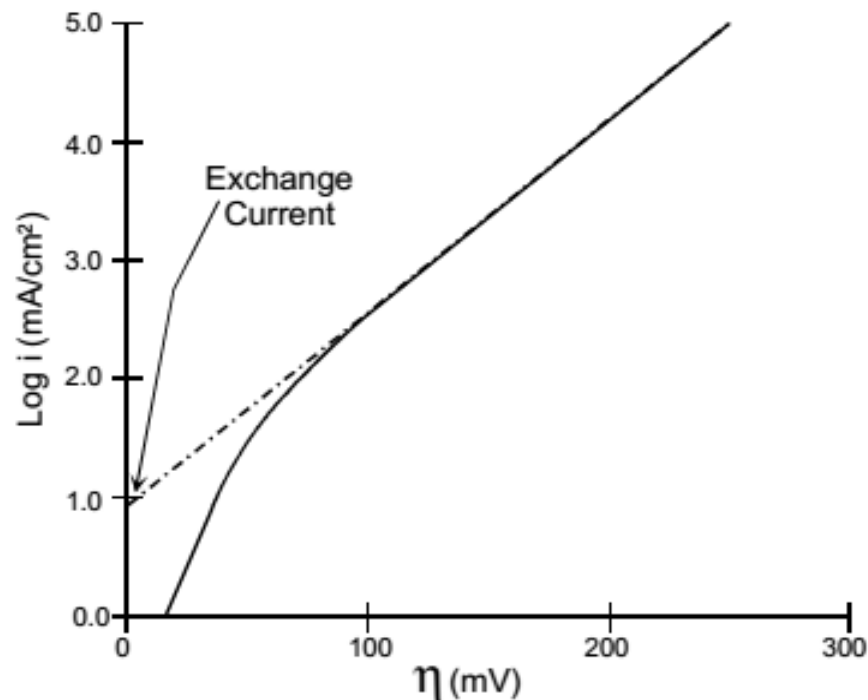
$$\eta_{act} = \frac{RT}{\alpha nF} \ln \frac{i}{i_0} \quad (3.8)$$

where  $\alpha$  is electron transfer coefficient of the reaction that occurs at the electrode,  $i_0$  is the exchange current density,  $i$  is current density

In order to determine exchange current density by Tafel plots, Equation (3.8) can be utilized. The plot is illustrated in Figure 3.3. The usual form of Tafel equation is rewritten and expressed in Equation (3.9). The extrapolated intercept at  $\eta_{\text{act}} = 0$  shows the exchange current density. It is a measurement of the maximum current that can be extracted at negligible polarization. The slope of this plot shows transfer coefficient.

$$\eta_{\text{act}} = a + b \ln i \quad (3.9)$$

Where  $a = (-RT / \alpha nF) \ln i_0$  and  $b = RT / \alpha nF$ . From Figure 3.4,  $a$  and  $b$  are obtained.  $b$  is determined from the Tafel slope then  $a$  can be calculated. Therefore,  $i_0$  can be obtained from the substitution of  $a$  and  $b$  in Equation (3.22).



**Figure 3.3** Example of Tafel plot [37].

### 3.3.2 Ohmic losses

Ohmic losses ( $\eta_{\text{ohm}}$ ) occur in both an electrolyte and an electrode. In an electrolyte, the losses result from the ions flow resistance. In addition, these losses in an electrode are the losses occurred from the electrons flow resistance which the electron transports through the electrode. The reduction of the electrode resistance and enhancement of the ionic conductivity of the electrolyte make the losses decrease. Since both the electrolyte and the electrodes obey Ohm's law. The ohmic losses can be explain by Equation (3.10) [37].

$$\eta_{\text{ohm}} = iR \quad (3.10)$$

where  $i$  is the current flowing through the cell, and  $R$  is the total cell resistance, which includes of electronic, ionic, and contact resistance. The total cell resistance can be determined by Equation (3.11).

$$R = R_{\text{electronic}} + R_{\text{ionic}} + R_{\text{contact}} \quad (3.11)$$

### 3.3.3 Mass-transport losses

The limitation of a reactant transfer rate generates mass-transport losses ( $\eta_{\text{conc}}$ ). These losses depend on, ability of a reactant in the reaction, a structure of electrode and the current density usage. The losses occur because of finite mass transport rate at the electrode limits the supply of fresh reactant and the evacuation of products [37].

The mass transport rate of active ions to an electrode surface can be explained by Fick's first law of diffusion as Equation (3.12).

$$i = \frac{nFD(C_B - C_S)}{\delta} \quad (3.12)$$

where  $C_B$  is its bulk concentration,  $C_S$  is its concentration at the electrode surface and  $\delta$  is the diffusion layer thickness.

The measurement of current at the maximum rate is the limiting current ( $i_L$ ). At this point, a reactant can be supplied to an electrode, and it occurs when  $C_S = 0$ . The limiting current can be determined by Equation (3.13).

$$i_L = \frac{nFDC_B}{\delta} \quad (3.13)$$

Equations (3.12) and (3.13) can be rewritten as Equation (3.14).

$$\frac{C_S}{C_B} = 1 - \frac{i}{i_L} \quad (3.14)$$

The Nernst equation for the reactant species at equilibrium conditions is presented in Equation (3.15).

$$E_{i=0} = E^0 + \frac{RT}{nF} \ln C_B \quad (3.15)$$

The surface concentration is less than the bulk concentration when the current is flowing, and the Nernst equation can be rewritten as Equation (3.16).

$$E = E^0 + \frac{RT}{nF} \ln C_S \quad (3.16)$$

The potential difference is generated by a concentration change at the electrodes leading to mass-transport losses. The losses can be calculated from Equation (3.17).

$$\Delta E = \eta_{\text{conc}} = \frac{RT}{nF} \ln \frac{C_S}{C_B} = \frac{RT}{nF} \ln \left( 1 - \frac{i}{i_L} \right) \quad (3.17)$$



### 3.4 Fundamental of electricity

Electricity can be divided into two major systems which consist of direct current (DC) and alternating current (AC). The direct current is utilized in zinc-air battery. The fundamental parameters of electricity which need to be known before study of the battery consist of:

1) Voltage (or potential;  $V$ ) is the level of potential energy at a point in electrical field. It is the energy that is used to move +1 charge from infinity or the 0 V point toward any points. The typical unit is volt (V). Additionally, voltage is also called electrical force or electromotive force. One volt of electrical force is the magnitude of force which is used to drive one ampere of current passed through one ohm of resistance.

2) Current ( $I$ ) is the electron current flow which has the typical unit as ampere. However, the direction of electron flow is opposite with the direction of electrical current flow.

3) Resistance ( $R$ ) is the characteristic of the conductor that allows the different quantity of current passes through. The typical unit of resistance is ohm ( $\Omega$ ). One ohm is the resistance of conductor which is connected with one volt and is passed by one ampere through the conductor. The resistance can be calculated from Equation (3.18) which is Ohm's law [38].

$$R = V / I \quad (3.18)$$

4) Power ( $P$ ) is the electrical energy which is employed within one time unit. The typical unit of power is watt (W) or joule per second. Power can also be calculated by multiplication of voltage and current. This calculation is presented in Equation (3.19).

$$P = I \cdot V \quad (3.19)$$

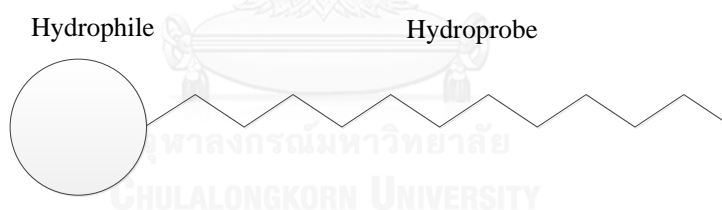
5) Electrical energy ( $E$ ) is the quantity of the power in a time period. The typical unit of the energy is watt multiply by time unit (such as watt hour etc.). The energy can be determined by Equation (3.20).

$$E = \int P \cdot dt \quad (3.20)$$

### 3.5 Surfactant

#### 3.5.1 Basic theory

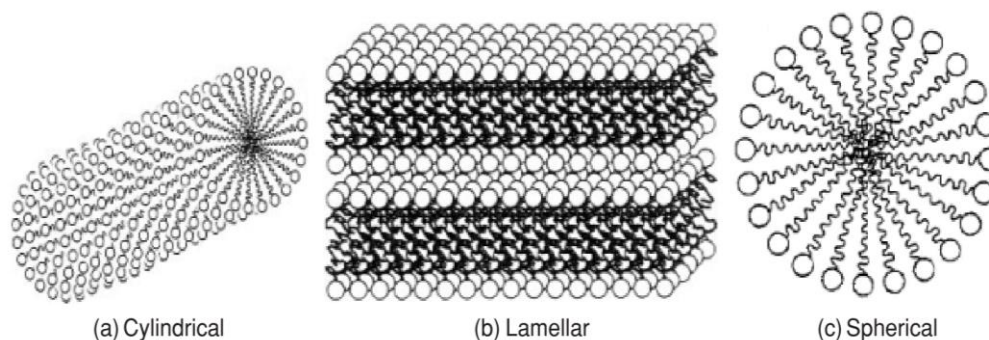
Surfactants or surface active agents are organic compounds which have at least one lyophilic (solvent-loving) group and one lyophobic (solvent-fearing) group in the molecule. Because water or aqueous solution is used as the solvent of surfactant, the respect terms ‘hydrophilic’ and ‘hydrophobic’ are used. In the simplest terms, a surfactant can define as it contains at least one non-polar group and one polar (or ionic) group. The simplified structure of surfactant is illustrated in Figure 3.4 [14].



**Figure 3.4** Simplified structure of surfactant [14].

An adsorption and an aggregation are two phenomena resulting from these opposing forces within the same molecule. The process of adsorption can be described that surfactant molecules will migrate to air/water and solid/water interfaces and orientate in such a fashion as to minimize, as much as possible, the contact between their hydrophobic groups and the water [14]. Similarly, an alternative way of the contact limitation between the hydrophobic groups and the water is the surfactant molecules aggregated in the bulk solution with the hydrophilic ‘head groups’ orientates towards the aqueous phase. The shape of these aggregations of surfactant molecules can vary depending on concentration and range in shape. The shape is from spherical to cylindrical to lamellar (sheets/layers) [14]. The aggregation process is called

‘micellisation’ and the aggregates are known as ‘micelles’. Micelles usually form at a distinct and frequently very low concentration known as the ‘critical micelle concentration’ or ‘CMC’. The various types of micelle are illustrated in Figure 3.5 [14].

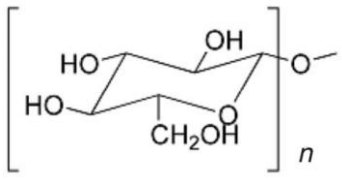


**Figure 3.5** Configuration of typical micelle [14]

The hydrophilic portion of a surfactant may bring a positive or negative charge, both positive and negative charges or no charge at all. These are classified as, cationic, anionic, amphoteric (or ‘zwitterionic’) or non-ionic surfactant, respectively. The typical hydrophilic groups are expressed in Table 3.1 [14].

**Table 3.1** Typical hydrophilic groups [14].

| Ionic type | Example             | Structure  |
|------------|---------------------|--|
| Anionic    | Sulphate            | $-\text{OSO}_2\text{O}^-$  |
|            | Sulphonate          | $-\text{SO}_2\text{O}^-$   |
|            | Ether sulphate      | $-(\text{OCH}_2\text{CH}_2)_n\text{OSO}_2\text{O}^-$                         |
|            | Ether phosphate     | $-(\text{CH}_2\text{CH}_2\text{O})_n\text{P}(\text{O})\text{O}^-$            |
|            | Ether carboxylate   | $-(\text{CH}_2\text{CH}_2\text{O})_n\text{CO}_2^-$                           |
|            | Carboxylate         | $-\text{C}(\text{O})\text{O}^-$  |
| Cationic   | Primary ammonium    | $-\text{N}^+\text{H}_3$  |
|            | Secondary ammonium  | $-\text{N}^+(\text{R})\text{H}_2$  |
|            | Tertiary ammonium   | $-\text{N}^+(\text{R})_2\text{H}$  |
|            | Quaternary ammonium | $-\text{N}^+(\text{R})_3$  |
| Amphoteric | Amine oxide         | $-\text{N}^+(\text{R})_3\text{O}^-$  |
|            | Betaine             | $-\text{N}^+(\text{R})_3(\text{CH}_2)_n\text{C}(\text{O})\text{O}^-$         |
|            | Aminocarboxylates   | $-\text{N}^+\text{H}(\text{R})_2(\text{CH}_2)_n\text{C}(\text{O})\text{O}^-$ |

| Ionic type | Example                           | Structure   |
|------------|-----------------------------------|---|
| Non-ionic  | Polyoxyethylene (an 'ethoxylate') | $-(\text{OCH}_2\text{CH}_2)_n\text{OH}$   |
|            | Acetylenic                        | $-\text{CH}(\text{OH})\text{C}\equiv\text{CH}(\text{OH})-$                          |
|            | Monoethanolamine                  | $-\text{NHCH}_2\text{CH}_2\text{OH}$  |
|            | Diethanolamine                    | $-\text{N}(\text{CH}_2\text{CH}_2\text{OH})_2$                                      |
|            | Polyglucoside                     |  |

There are many types of hydrophobe. Some of the common commercially available ones are illustrated in Table 3.2.

**Table 3.2** Typical hydrophobic groups [14].

| Group                                   | Example         | Structure  |
|---|-----------------|--|
| Alkylbenzene                            | Linear dodecyl- | $\text{CH}_3(\text{CH}_2)_5\text{CH}(\text{C}_6\text{H}_4)(\text{CH}_2)_4\text{CH}_3^{\text{a}}$ |
| Linear alkyl <sup>b</sup> (saturated)   | benzene         | $\text{CH}_3(\text{CH}_2)_{10}\text{CH}_2-$  |
| Branched alkyl <sup>b</sup> (saturated) | n-dodecyl       | $\text{CH}_3(\text{CH}_2)_3\text{CH}-\text{CH}_2-(\text{CH}_2\text{CH}_3)$                       |
|   | 2-ethyl hexyl   | $(\text{cis}-)\text{CH}_3(\text{CH}_2)_7=\text{CH}(\text{CH}_2)\text{CH}_2-$                     |
| Linear alkyl <sup>b</sup> (unsaturated) | Oleyl           | $\text{C}_9\text{H}_{19}(\text{branched isomers})\text{C}_6\text{H}_4-$                          |
|   | Nonylphenyl     | $-\text{[OCH}_2\text{CH}(\text{CH}_3)]_n-$   |
| Alkylphenyl (branched)                  |                 | $(\text{CH}_3)_3\text{Si}[\text{OSi}(\text{CH}_3)]_n\text{OSi}(\text{CH}_3)_3$                   |
| Polyoxypropylene                        |                 |  |
| Polysiloxane                            |                 |  |

<sup>a</sup>Alkylbenzene has a linear alkyl chain with, in the case of dodecyl, the phenyl group distributed between the second and sixth positions on the aliphatic chain. The C6 isomer is illustrated above.

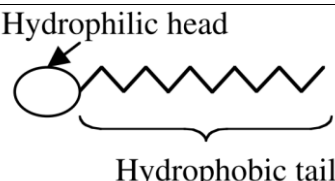


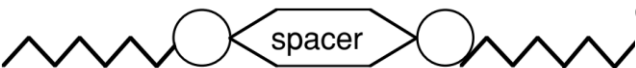
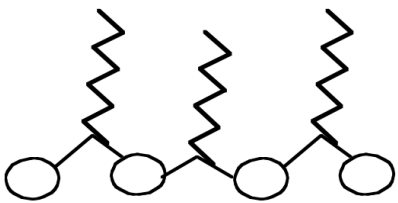
<sup>b</sup>Alkyl groups, whether linear, branched/saturated or unsaturated, are usually within the C8 to C18 chain length range.

### 3.5.2 Molecular structure of surfactants

The hydrophilic group makes the surfactant soluble in polar solvents such as water. The hydrophobic group makes the surfactant soluble in non-polar solvents. Many properties of a surfactant are determined by the relative sizes and shapes of the

hydrophobic and hydrophilic parts of the surfactant molecule [14]. Surfactant molecules can have one hydrophilic head and one hydrophobic tail, one hydrophilic head and two hydrophobic, one hydrophobic tail terminated at both ends by hydrophilic groups (bolaform surfactants or  $\alpha, \omega$  surfactants), hydrophilic heads of two surfactants are combined with a rigid spacer which is a linear or ring organic structure (gemini surfactants), and a number of hydrophilic (more than two) hydrophobic groups with both groups linked in the same molecule by covalent bonds (polymeric surfactants). These structures are expressed in Table 3.3 [14].

**Table 3.3** Schematics of molecular surfactant structures and sample surfactants [14].

| Schematic of surfactant structure   | Sample surfactants   |
|---|--|
|   | Soap (sodium salt of fatty acids)<br>Alkyltrimethylammonium salts<br>Polyoxyethylene alkyl ether<br>Alkyldimethylamine oxide |
|  | Alkylbenzene sulphonate<br>Phosphatidyl choline (phospholipids)<br>Alkyl secondary amines                                    |
|  | Bolaform quaternary  |
|  | Gemini phosphate esters  |
|  | Polymeric alkyl phenol ethoxylates<br>Silicone polymeric surfactants<br>Polyester surfactants                                |

The hydrophobic group is the major cost of the surfactant because the hydrophobic group is the largest part of the surfactant molecule. In the surfactant

structure, the hydrophobic group is made up of hydrocarbon chains, fluorocarbon chains, combination of fluorocarbon and hydrocarbon chains or silicone chains [14]. These hydrocarbon chains are synthesized from natural animal fats, natural vegetable oils or petrochemicals because their structures are built up from ethylene. The hydrocarbon chains can be linear or branched. These chains include polycyclic, saturated, unsaturated or polyoxypropylene structures. The linear structure is desirable due to its biodegradability [14]. Fluorocarbon and silicone chain surfactants in water and non-aqueous systems reduce the surface tension lower than the hydrocarbon chain surfactants. Both fluorocarbon and silicone chain surfactants have better chemical and thermal stability than hydrocarbons. Moreover, they provide excellent wetting for low-energy surfaces. However, their costs are higher than the hydrocarbon chain surfactants, so they are used in limited applications [39].

### **3.5.3 Surface activity**

The compound acted as a surfactant should exhibit surface activity. It means that when the compound is added to any liquid at low concentration, it should be able to adsorb on the surface or interface of the system. Additionally, the compound should reduce the surface or interfacial excess free energy as well. The surface is a boundary between air and liquid. The interface is a boundary between two immiscible phases (liquid–liquid, liquid–solid and solid–solid) [14]. Surfactant activities are at a maximum if the carbon atoms are between 10 and 18 at which level a surfactant has good but limited solubility in water. If the carbon atom is below 8, a surfactant is very soluble and if it is above 18, it is insoluble. Therefore, the solubility and practical surfactant properties are somewhat related [39]. In order to understand how surfactant reduces surface and interfacial tension, the concept of surface and interfacial tension need to be understood at first [14].

#### **3.5.3.1 Surface tension**

The attractive forces between molecules in the bulk liquid are uniform in all directions (zero net force). However, the molecules at the liquid surface cannot form uniform interaction because the molecules on the gas side are widely spaced. The

molecular interactions which are mainly between surface molecules and the subsurface liquid molecules (non-zero net force) are the other reasons of the non-uniform interaction [14]. Therefore, the molecules at the liquid surface have greater free potential energies than the molecules in the bulk liquid. This excess free energy per unit area that exists in the surface molecules is defined as surface tension ( $\gamma$ ). Surface tension is a thermodynamic property [14]. It can be measured under constant temperature and pressure. Furthermore, its value represents the amount of minimum work required per unit area to create a greater surface area. In addition, surface tension of the substances decreases with increasing temperature because increasing temperature reduces the cohesive energy between molecules. At the critical temperature, surface tension becomes zero [14].

### 3.5.3.2 Interfacial tension

Interfacial tension is the tension that exists at the interface of two immiscible phases. Generally, the value of interfacial tension is between the surface tension of two immiscible liquids [14]. The interfacial tension between phases A and B,  $\gamma_{AB}$ , is expressed by Equation (3.21):

$$\gamma_{AB} = \gamma_A + \gamma_B - 2\psi_{AB} \quad (3.21)$$

where  $\gamma_A$ ,  $\gamma_B$  and  $\psi_{AB}$  are surface tension of A, surface tension of B, and interaction energy between A and B per unit area, respectively.

The value of  $\gamma_{AB}$  also indicates how similar the molecules at the interface are. The interfacial tension ( $\gamma_{AB}$ ) will be small if the molecules of the two phases are similar (large  $\psi_{AB}$ ). The greater the similarity, the smaller the  $\gamma_{AB}$ . Therefore, the interface disappears ( $\gamma_{AB} = 0$ ) when the two phases become a single phase [14]. If one phase (phase B) is gas, the interface forms at the surface of the condensed phase (phase A) and the interfacial tension is equivalent to the surface tension of the condensed phase ( $\gamma_{AB} = \gamma_A$ ). Therefore, the tension produced by molecular interaction in the gas phase and gas phase–condensed molecules phase is negligible because the gas phase are widely spaced [14].

### 3.5.3.3 Surface and interfacial tension reduction

The movement of enough molecules from bulk to the interface results in the expansion of the interface by unit area. However, this move is hindered by the potential energy difference between the interface molecules and bulk molecules. In order to overcome this potential energy difference, a minimum amount of work is required [14].

The interfacial tension or interface free energy per unit area is a measurement of this work. When surfactant is used in such a system, the surfactant molecules transport towards the interface and the hydrophobic tail of the molecules either lie flat on the surface (few surfactant molecules at the interface). For another way, while the hydrophilic head orientates itself towards the polar phase, surfactant molecules align itself to the less polar liquid (adequate number of surfactant molecules at the interface) [14]. Then the cohesive forces between polar and non-polar molecules are destroyed by these surfactant molecules. The polar and non-polar molecules at the interface are also replaced. At the interface, the interaction of the molecules occurs between the hydrophilic head of the surfactant and the polar phase molecules. In addition, this interaction also occurs between the hydrophobic tail of surfactant and the non-polar phase molecules. In this phenomenon, the tension across the interface is lower because the newly developed interactions are stronger than the interaction between the non-polar and polar molecules [14]. The tension reduction at the interface is identified as surface tension reduction if one of the phases is gas or air. This reduction occurs because gas or air molecules are mainly non-polar. Low concentration surfactant has a tendency to adsorb at the surface or interface. This surfactant significantly reduces the amount of required work to expand those interfaces. The better surfactants are obtained with the stronger tendency. The denser surfactant packing at the interface results from the larger reduction in surface tension [14].

The surface activity of surfactant is one of the most commonly measured properties and can be quantified by the Gibbs adsorption equation:

$$d\gamma = -\sum_i \Gamma_i d\mu_i \quad (3.22)$$

where  $d\gamma$  is the change in surface or interfacial tension of the solution ( $\text{erg cm}^{-2} = \text{dyne cm}^{-1}$  or  $\text{mJ m}^{-2} = \text{mN m}^{-1}$ ),  $\Gamma_i$  is the excess surface concentration of solute per unit area



of surface or interface ( $\text{mol cm}^{-2}$  or  $\text{mmol m}^{-2}$ ) and  $d\mu_i$  is the change in chemical potential of the solute in the solution. At equilibrium between the interfacial and bulk phase concentrations,  $d\mu_i = RTd\ln a_i$  where  $R$  is the gas constant ( $8.314 \times 10^{-7} \text{erg mol}^{-1} \text{K}^{-1}$  or  $8.314 \text{J mol}^{-1} \text{K}^{-1}$ ),  $T$  is the absolute temperature and  $a_i$  is the activity of solute in the solution. Then, the Gibbs adsorption equation can be rewritten as equation (3.23) [14].

$$\begin{aligned} d\gamma &= - \sum_i \Gamma_i d\mu_i = -RT \sum_i \Gamma_i d\ln a_i = -RT \sum_i \Gamma_i d\ln(x_i f_i) \\ &= -RT \sum_i \Gamma_i d(\ln x_i + \ln f_i) \end{aligned} \quad (3.23)$$

where  $x_i$  is the mole fraction of solute in the bulk phase and  $f$  is the activity coefficient of solute in the bulk phase. For dilute solution containing only one type of non-ionic surfactant ( $10^{-2} \text{M}$  or less) and containing no other solutes, the activity coefficient of surfactant can be defined as constant and the mole fraction can be replaced by its molar concentration,  $C$  [14]. Thus Equation (3.23) becomes Equation (3.24).

$$d\gamma = - \sum_i \Gamma_i d\ln C \quad (3.24)$$

$\Gamma$  is positive (solute concentration at the solution surface is higher than that in the bulk liquid) when the surface or interfacial tension is decreased with the addition of a solute (surfactant).  $\Gamma$  is negative (solute concentration at the solution surface is lower than that in the bulk liquid) when the surface tension is elevated with the addition of a solute (such as  $\text{K}_2\text{CO}_3$ ) [14].

For one ionic surfactant with dilute solution ( $10^{-2} \text{M}$  or less) that completely dissociates ( $\text{A}^+\text{B}^-$ ), the Gibbs adsorption equation can be written as Equation (3.25).

$$d\gamma = -RT(\Gamma_A d\ln a_A + \Gamma_B d\ln a_B) \quad (3.25)$$

$\Gamma_A = \Gamma_B$  due to electroneutrality and  $a_A = a_B$ . Then Equation (3.25) can be rewritten as Equation (3.26) [14].

$$d\gamma = -2RT\Gamma_A d \ln C \quad (3.26)$$

The coefficient decreases from 2 to 1 with a decrease in the ionic surfactant concentration at the interface when the mixture of non-ionic and ionic surfactants in water with no electrolyte is employed. For the ionic surfactant solution in the presence of electrolyte such as NaCl, KCl, NaBr and KBr the Gibbs adsorption equation can express as Equation (3.27) [14].

$$d\gamma = -RT\Gamma d \ln C \quad (3.27)$$

Where  $y = 1 + \frac{C}{C+C_{NaCl}}$

In the presence of electrolyte containing non-surfactant counterion, for the ionic surfactant solution, the surface activity can be quantified with Equation 3.26 [16].

The surface concentration of surfactant or surface excess concentration ( $\Gamma$ ) can be determined by the representative Gibbs adsorption equation. The slope of a plot of  $\gamma$  versus  $\log[C]$  at constant temperature shows the  $\Gamma$  [14].

The critical micelle concentration (CMC) is represented by the CMC in the curve where the surfactant molecules start forming aggregates. This aggregate is known as micelles. Surfactant molecules are in monomeric form below CMC. At this point, the surface or interfacial tension decreases dramatically with increase in the surfactant concentration in the bulk. The slope of the curve below the CMC is constant. This value reaches its maximum value because the surface or interface is saturated with surfactant monomers [14].

The surface excess concentration expresses in Equation (3.28) for the dilute solution of non-ionic surfactant.

$$\Gamma = -\frac{1}{RT} (\text{Slope}/2.303) \quad (3.28)$$

The surface excess concentration expresses in Equation (3.29) for the dilute solutions of ionic surfactant.

$$\Gamma = -\frac{1}{2.303RT} (\text{Slope}) \quad (3.29)$$

The surface excess concentration expressed in Equation (3.30) for the ionic surfactant solution in the presence of electrolyte [14].

$$\Gamma = -\frac{1}{2.303RT} (\text{Slope}) \quad (3.30)$$

The area occupied per surfactant molecule ( $A$ ) at the surface or interface can be obtained from  $\Gamma$  by using Equation (3.31).

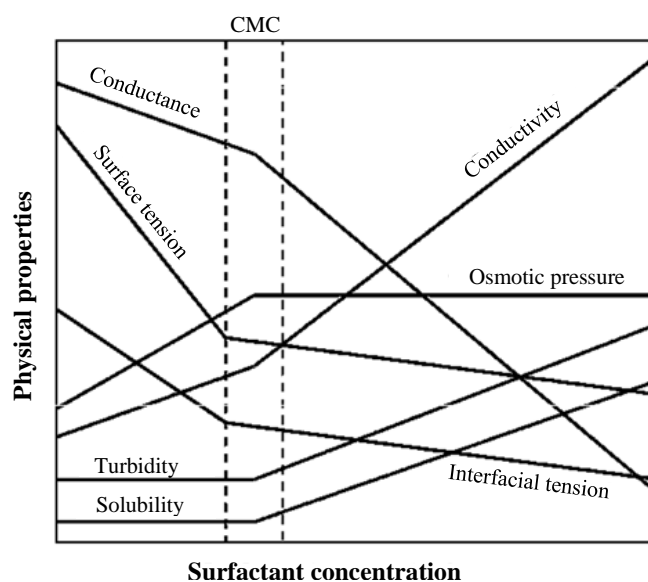
$$A = \frac{10^\alpha}{N\Gamma} \quad (3.31)$$

where  $\alpha$  is 16 for  $A$  in square angstrom and  $\Gamma$  in mol cm<sup>-2</sup>.  $N$  is Avogadro's number [14].

### 3.5.4 Self-assembled surfactant aggregates

In aqueous solution, at low concentration, a surfactant acts as monomers (free or unassociated surfactant molecules). At the interface, these monomers which collect together, form monolayer. They contribute to surface and interfacial tension lowering. However, this phenomenon is highly dynamic molecules. It shows that surfactant molecules arrive and leave the interface on a very rapid timescale. This phenomenon occurs at the interface interact with the neighbouring molecules very strongly which enables the rheological properties of the monolayer measurement [14]. Because the surfactant concentration increases, the available area at the surface for surfactant adsorption diminishes. Then surfactant monomers start accumulating in the solution. Nevertheless, the hydrophobic tail of the surfactant molecules has extremely small solubility in water and the hydrophilic head has extremely small solubility in non-polar solvents. Therefore, the hydrophobic effect will drive surfactant monomers to form self-assembled aggregates above certain aggregate concentration [14]. These aggregates are micelles, vesicles, liquid crystals and reverse micelles. The aggregates exist in

equilibrium with the surfactant monomers. All structures are dynamic in nature and surfactant molecules constantly join and leave the microstructure on a timescale of microseconds. However, the microstructures have a limited lifetime. Furthermore, the energy difference between various microstructures is small, thus the physical forces of the interaction become dominant. In addition, surfactant molecules can be transformed between several types of aggregates by small changes in temperature, concentration, pH or electrolyte strength [14]. Likewise, the properties of the solution show sharp changes around the critical aggregation concentration. The formation of self-assembled aggregates is evidenced by an increase in turbidity and organic dye solubility, a decrease in electrical conductivity (ionic surfactants only) and stability in surface tension, interfacial tension and osmotic pressure around the critical aggregation concentration as illustrated in Figure 3.6 [14].



**Figure 3.6** Physical properties of aqueous surfactant solution as a function of surfactant concentration [14].

#### 3.5.4.1 Micelles and critical micelle concentration

Surfactant monomers can form a closed aggregate (micelle) at a certain concentration, in which the hydrophobic tails are harbored from water while the hydrophilic heads face water. This concentration is called is called the critical micelle

concentration (CMC) which is the concentration of aggregation. The CMC is a characteristic of the surfactant. At this point, monolayer adsorption is complete and the surface active properties are at an optimum [14]. Above the CMC, the concentrations of monomers are approximately constant. Therefore, the surfactant properties of the solution do not significantly change because the monomers are the cause of the surface activity. There is no surface activity of micelles. In addition any increase in the surfactant concentration does not influence the number of monomers in the solution however it affects the structure of micelles [14].

The typical CMC values at room temperature are  $10^{-3}$ – $10^{-2}$  M for anionic surfactants,  $10^{-3}$ – $10^{-1}$  M for amphoteric and cationic surfactants and  $10^{-5}$ – $10^{-4}$  M for non-ionic surfactants. The CMC can be affected by the surfactant structure, the temperature, the presence of electrolyte, existence of organic compounds and the presence of a second liquid. The following factors contribute to CMC decrease [14]:

- (a) an increase in the number of carbon atoms in the hydrophobic tails
- (b) the existence of polyoxypropylene group
- (c) fluorocarbon structure
- (d) an increased degree of binding of the counterions
- (e) the addition of electrolyte to ionic surfactants
- (f) the existence of polar organic compounds (such as alcohols and amides)
- (g) the addition of xylose and fructose

The following factors contribute to CMC increase [14]:

- (a) branch hydrophobic structure
- (b) double bonds between carbon atoms
- (c) polar groups (O or OH) in hydrophobic tail
- (d) strongly ionised polar groups (sulphates and quaternaries)
- (e) hydrophilic groups placed in the surfactant molecule centre
- (f) increase in the number of hydrophilic head
- (g) trifluoromethyl groups
- (h) an increase in the effective size of hydrophilic head
- (i) an increase in the pH of weak acids (such as soap)

(j) a decrease in pH from isoelectric region and increase in pH from isoelectric region for amphoteric surfactants (low CMC at the isoelectric region and high CMC outside the isoelectric region)

(k) addition of urea, formamide, and guanidinium salts, dioxane, ethylene glycol and water soluble esters

The CMC is a useful tool which is utilized to select the surfactants for specific applications or properties. Measurement of the change in physical properties such as electrical conductivity, turbidity, surface tension, interfacial tension, solubilisation and auto diffusion can determine CMC. The CMC decreases with increase in temperature to a minimum and then increases with further increase in temperature [14]. For ionic surfactants, the minimum appears to be around 25 °C and for non-ionic surfactants 50°C. The electrolyte concentration also affects to the CMC. Generally, the CMC of ionic and non-ionic surfactants is higher in nonaqueous solvent than in water [14]. Most formulators use mixed surfactants to improve the properties of products. Additionally, commercial surfactants are mixtures because they are made from mixed chain length feedstock and they are mixtures of isomers and by-products depending on their synthesis. Purifying the surfactant to a great extent is not economically feasible [14].

#### 3.5.4.2 Aggregate structures and shapes

For a stable formation of a structure of surfactant aggregate in an aqueous system, the hydrophobic part of the surfactant molecule should exist in the internal section of the aggregate while the hydrophilic heads should exist at the surface of the aggregate. The hydrophilic heads in water, if ionic, will repel each other because of same charge repulsion. The larger charge results in the greater repulsion and the lower tendency to form aggregates [14]. The strong affinity for water is found at the hydrophilic heads which space out to allow water to solvate the head groups. On other sides, because of hydrophobic effect, hydrophobic tails can attract another one. Then the surfactant molecules pack together when the concentration of the surfactant is high enough. This phenomenon results of the interaction of the two opposing forces between the surfactant molecules. This aggregate has various shapes and sizes depended on the surfactant packing parameter which is the ratio of the hydrophobic group area ( $v/lc$ ) to the hydrophilic head area ( $ao$ ) as shown in Table 3.2 [14]. The  $v$  and  $lc$  are the volume

and length of the hydrophobic tail in the surfactant aggregate, respectively. The definition of  $v$  and  $l_c$  can be express as Equations (3.32) and (3.33), respectively [14].

$$v = 27.4 + 26.9 n \quad (3.32)$$




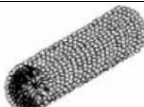
$$l_c \leq 1.5 + 1.265 n \quad (3.33)$$

where  $n$  is the total or one less than the total number of carbon atoms of the hydrophobic tail in the surfactant aggregate,  $v$  is in cubic Angstrom ( $\text{\AA}^3$ ) and  $l_c$  is in  $\text{\AA}$ .  $l_c$  is 80% of the fully extended chain for saturated straight chain [14].


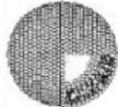

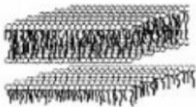



Table 3.4 shows structures of surfactant self-assemblies which are a function of surfactant packing parameters and shape. Firstly, spherical micelles are formed where the value of surfactant packing parameter is less than 1/3 (single chain surfactants with large head group areas such as anionic surfactants). The spherical aggregates are extremely small. The aggregate radius is approximately equal to the maximum stretched out length of the surfactant molecule [14]. And then when the surfactant packing parameter is between 1/3 and 1/2 (single chain surfactants with small head group areas such as non-ionic surfactants and ionic surfactants in high salt concentration), cylindrical micelles are formed. The aggregate size and shape will change from spherical to cylindrical form when the effective size of hydrophilic head groups is reduced by any change in solution properties. For example, the effective hydrophilic area of ionic surfactants is reduced by adding an electrolyte because the increased counterions reduce the repulsion between ionic polar head groups. In addition, the formation of cylindrical shape can also occur from addition of co-surfactant with a smaller head group size [14]. Furthermore, vesicles, liposomes and flexible bilayers are formed when the surfactant packing parameter is between 1/2 and 1 (double chain surfactants with large head group areas such as phospholipids, surfactants with bulky or branched tail groups and the mixture of anionic and cationic surfactants with single chain at nearly equimolar concentration). The surfactant shapes are truncated cone and cylinder, respectively [14]. Because the packing parameter approaches unity, the lamella becomes flat and planar (double chain anionic surfactants

in high salt concentration). Only the flexible lamellar bilayer bends around and joins in a sphere (vesicle). This structure keeps aqueous solution both inside and outside of the sphere. Liposomes which are concentric spheres of vesicles (layers of an onion arrangement) are formed by gentle shaking of surfactant in water. The size of the liposomes is more than a micrometer [14]. Moreover, the liposomes can easily be identified with a polarising light microscope due to the internal bilayer structures of the liposomes are optically active. Vesicles are formed from liposomes by ultrasonication, ultrafiltration or microfluidisation. The size of the vesicles is nanometre and can only be detected by electron microscopy. Vesicles are used as drug delivery agents, model components for cell membranes and cationic softeners in detergency [14]. Finally, inverted or reverse micelles are formed where the surfactant packing parameter is greater than 1 (surfactants with small head groups or large tail groups such as double tailed anionic surfactants). Their structures are formed in non-polar solvents. In the structures, head groups are clustered together and tails are extended towards the solvent. They can form water-in-oil microemulsions because they have the capacity to take water into their cores [14]. Therefore, hydrophilic materials can also be dissolved into the reverse micellar core (engine oil additives, hydraulic oils and cutting oils). In addition, inverse micelles are often used for the separation of biological molecules such as proteins [14].

**Table 3.4** Structures of surfactant self-assemblies as a function of surfactant packing parameters and shape [14].

| Surfactant shape  | Surfactant packing parameter ( $v/l_c a_0$ ) | Surfactant aggregates  |
|---|--|--|
| <br>Cone           | <1/3   | <br>Spherical micelle   |
| <br>Truncated cone | 1/3 – 1/2                                    | <br>Cylindrical micelle |



| Surfactant shape   | Surfactant packing parameter ( $v/l_c a_0$ ) | Surfactant aggregates   |
|--|--|---|
| <br>Truncated cone          | 1/2 - 1                                      | <br>Vesicle  |
| <br>Cylinder                | 1  | <br>Bilayer  |
| <br>Inverted truncated cone | >1   | <br>Reverse micelle<br><br>Reverse cylindrical micelle |

### 3.5.5 Adsorption of surfactants at surfaces

The adsorption mechanisms of surfactant consist of many processes such as dispersion, coating, emulsification, foaming and detergency. These interfaces are liquid–gas (foaming), liquid–liquid (emulsification) and liquid–solid (dispersion, coating and detergency). The details of the adsorption mechanisms are described as follows.

#### 3.5.5.1 Adsorption at liquid–gas and liquid–liquid interfaces

The surfactant concentration affects the adsorption of surfactants at interfaces. At very low concentration, surfactant molecules lie flat on the surface. An increase in surfactant concentration in the bulk increases surfactant molecules on the surface and surfactant tails start to orient towards gas or non-polar liquid because there is not enough space for the surfactant molecules to lie flat on the surface. These molecules

adsorb at the interface and form monolayer until the surface is occupied at which point the molecules start forming self-assembled structures in the liquid [14].

Adsorption can be measured by direct or indirect methods. The direct methods consist of surface microtome method, foam generation method and radio-labelled surfactant adsorption method. However, these methods have several disadvantages. Therefore, the amount of surfactant adsorbed per unit area of interface ( $\Gamma$ ) at surface saturation is mostly determined by indirect methods namely surface and interfacial tension measurements along with the application of Gibbs adsorption equations [14]. The  $\Gamma$  value is significantly affected by surfactant structure, presence of electrolyte, nature of non-polar liquid and temperature. Adsorption isotherms are used to relate the bulk surfactant concentration ( $C$ ) to  $\Gamma$ . The Langmuir adsorption isotherm generally represents surfactant solutions as shown in Equation (3.34) [14].

$$\Gamma = \Gamma_{\max} \frac{C}{C+a} \quad (3.34)$$

where  $\Gamma_{\max}$  is the maximum surfactant adsorption at infinite dilution in mol cm<sup>-2</sup> and  $a$  is a constant in mol cm<sup>-3</sup>.  $a$  is expressed as shown in Equation (3.35) [14].

$$a = \frac{\Gamma_{\max}}{\delta} \exp\left(\frac{\Delta G^0}{RT}\right) \quad (3.35)$$

where  $\delta$  is the thickness of the adsorption layer,  $G^0$  is the free energy of adsorption at infinite dilution,  $R$  is ideal gas constant and  $T$  is the absolute temperature [14]. Then Equation (3.34) can be rewritten in the linear form as expressed in Equation (3.36).

$$\frac{C}{\Gamma} = \frac{C}{\Gamma_{\max}} + \frac{a}{\Gamma_{\max}} \quad (3.36)$$

In case of the surfactant adsorption is of the Langmuir type, the plot of  $C/\Gamma$  versus  $C$  is a straight line. The values of  $\Gamma_{\max}$  and  $a$  can be then determined from the slope ( $1/\Gamma_{\max}$ ) and intercept ( $a/\Gamma_{\max}$ ) of this plot [14].

The Szyszkowski equation relates surface tension ( $\gamma$ ) to  $C$  as shown in Equation (3.37)

$$\pi = \gamma_0 - \gamma = RT\Gamma_{\max} \ln \left( \frac{C}{a} + 1 \right) \quad (3.37)$$

where  $\pi$  is the surface pressure of a solution,  $\gamma_0$  is the surface tension of pure solvent and  $\gamma$  is the surface tension of the surfactant solution. The Frumkin equation [14] derived from Equations (2.18) and (2.21) shows the relationship between  $\gamma$  and  $\Gamma_{\max}$  in Equation (3.38) [14].

$$\pi = \gamma_0 - \gamma = RT\Gamma_{\max} \ln \left( 1 - \frac{\Gamma}{\Gamma_{\max}} \right) \quad (3.38)$$

If the interaction between the adsorbed surfactant molecules and electrostatic charge of surfactant ions is incorporated in Equation 2.18, the Langmuir equation becomes Equation (3.39) [14].

$$\Gamma = (\Gamma_{\max} - \Gamma) \frac{C}{a \exp\left(-b\frac{\Gamma}{\Gamma_m}\right) \exp\left(\frac{Ze\psi_s}{kT}\right)} \quad (3.39)$$

where  $b$  is a constant representing the non-electrostatic interaction between adsorbed surfactant molecules,  $Z$  is the valence of surfactant ion (zero for non-ionic surfactant),  $e$  is the elementary charge,  $\psi_s$  is the surface electric potential and  $k$  is Boltzmann's constant [14].

The efficiency of surfactant adsorption is determined as a function of minimum bulk surfactant concentration,  $C$  that produces saturation adsorption ( $\Gamma_{\max}$ ) at the liquid–gas or liquid–liquid interface. This minimum concentration is defined as  $pC20$  which is  $(-\log C20)$  reducing the surface or interfacial tension by 20 dyne  $\text{cm}^{-1}$  ( $\pi = 20$  dyne  $\text{cm}^{-1}$ ). With  $C20$ ,  $\Gamma$  lies between 84 and 99.9% of  $\Gamma_{\max}$  [14]. The larger the  $pC20$  (smaller the  $C$ ), the more efficient the surfactant is in adsorbing at the interface and reducing the surface tension at liquid–gas or interfacial tension at liquid–liquid interfaces [14].

### 3.5.5.2 Adsorption at liquid–solid interface

Many interactions are used to adsorb any surfactants on any solid surfaces. These interactions include of the hydrophobic bonding, electrostatic interaction, acid–base interaction, polarization of  $\pi$  electrons and dispersion forces. Hydrophobic bonding occurs between the hydrophobic surfactant tail and the hydrophobic solid surface (tail down adsorption with monolayer structure) or between the hydrophobic tails of the surfactant adsorbed on the hydrophilic solid surface and the hydrophobic tails of the surfactant from the liquid phase (head down adsorption with bilayer structure) [14].

Electrostatic interactions occur between the ionic head groups of the surfactant and the oppositely charged solid surface (head down adsorption with monolayer structure). Acid–base interactions occur because of hydrogen bonding or Lewis acid–Lewis base reactions between solid surface and surfactant molecules (head down with monolayer structure). Polarization of  $\pi$  electrons occurs between the surfactant head group which has electron rich aromatic nuclei and the positively charged solid surface (head down with monolayer structure). Dispersion forces occur because of London–van der Waals forces between the surfactant molecules and the solid surface (hydrophobic tail lies flat on the hydrophobic solid surface while hydrophilic head orients towards polar liquid) [14].

The adsorption isotherms are generally be used to describe the adsorption of surfactants. A simple adsorption experiment at a constant temperature is set up to support this description. The known amounts of solid adsorbent are dispersed into a constant volume of dilute surfactant solution. The initial surfactant concentrations are varied. The mixture is then shaken until reaching to its equilibrium. For each solution, the moles of surfactant adsorbed per unit mass of the solid ( $N_s$ ) can be determined from Equation (3.40) [14].

$$N_s = \frac{(C_0 - C_e)V}{m} \quad (3.40)$$

where  $N_{s,max}$  is the initial concentration of surfactant in the liquid phase before adsorption,  $C_e$  is the concentration of surfactant in the liquid phase after the equilibrium is reached,  $V$  is the volume of liquid phase and  $m$  is the mass of the adsorbent. Then, the Langmuir adsorption isotherm can be expressed in linear form as Equation (3.41) [14].

$$\frac{C}{N_s} = \frac{C}{N_{s,max}} + \frac{a}{N_{s,max}} \quad (3.41)$$

Where  $N_{s,max}$  is the maximum moles of surfactant adsorbed per gram of adsorbent at equilibrium. The slope and intercept of a plot of  $C/N_s$  versus  $C$  are  $1/N_{s,max}$  and  $a/N_{s,max}$ , respectively. In addition, the surface concentration of surfactant on solid surface,  $\Gamma$  (mol/area), can be determined from Equation (3.42) [14]

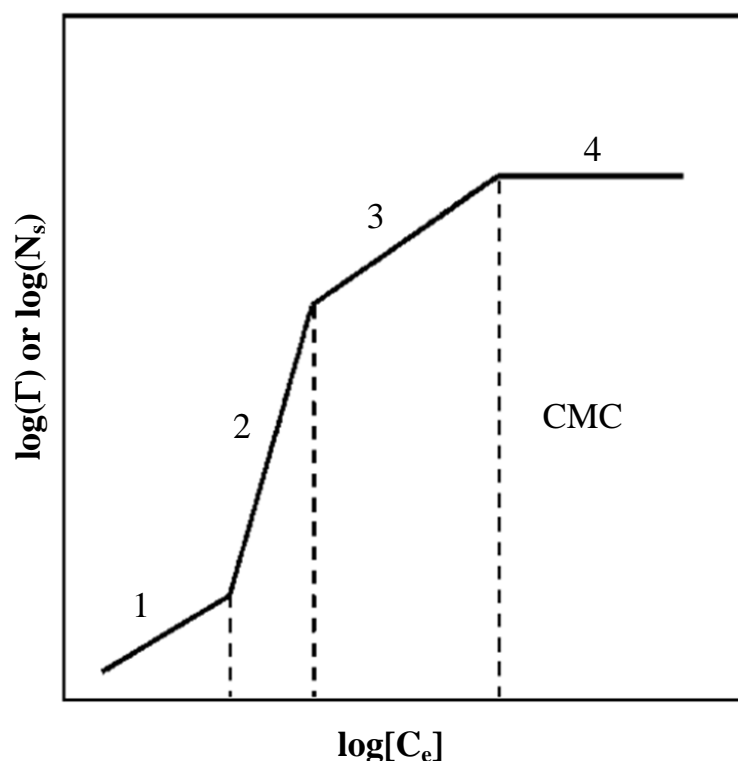
$$\Gamma = \frac{N_s}{A_s} = \frac{(C_0 - C_e)V}{A_s m} \quad (3.42)$$

where  $A_s$  is the surface area per unit mass of the solid adsorbent.

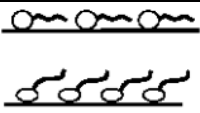

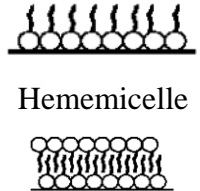
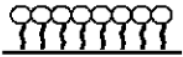


The  $\log N_s$  versus  $\log C_e$  (Equation (3.40)) or the  $\log \Gamma$  versus  $\log C_e$  (Equation (3.41)) is plotted to generally analyse characteristics of surfactant adsorption isotherm on solid surface. These plots have four region isotherms as shown in Figure 3.7. [14]

Region 1 represents the adsorption at low surfactant concentration. Linear adsorption isotherm exhibits a slope of 1 in this region, which can be explained by Henry's adsorption isotherm. And surfactant molecules adsorbed on the solid surface as seen in Figure 2.5 do not interact with each other and the zeta potential of the solid surface is unchanged. Hydrogen bonding (hydrophilic solid surface) or hydrophobic bonding (hydrophobic solid surface) is the interaction of non-ionic surfactant adsorbed on solid surface [14]. Electrostatic interaction (hydrophilic solid surface) or hydrophobic bonding (hydrophobic solid surface) is the interaction of ionic surfactants adsorbed on solid surface. In region 2, isotherm of adsorption shows an increase in a slope greater than 1. In the region 2 (Figures 3.7 and 3.8), surfactant molecules move toward the solid surface and form hemimicelle on the hydrophilic solid surface (head

down adsorption) or monolayer on the hydrophobic solid surface (tail down adsorption) [14]. Because of the bulk concentration increases, surfactant molecules interact with the previously adsorbed surfactant molecules by hydrophobic bonding and create surface aggregates (bilayer formation on solid surface known as admicelle) on the hydrophilic solid surface. The break between regions 1 and 2 represents the surfactant concentration where the first hemimicelle or admicelle is formed [14]. The concentration of the surfactant in region 2 is well below the CMC. The charge of the solid surface is neutralised by the adsorption of oppositely charged ionic surfactants in this region. In region 3, the slope of the isotherm decreases because the rate of bilayer formation decreases and the adsorption occurs on the least energetic part of the solid surface. In region 4, the plateau adsorption occurs due to micelle formation in the bulk liquid and slope of the isotherm levels off [14].



**Figure 3.7** Four region isotherms of surfactant adsorption [14].

| Surfactant concentration   | Water-hydrophilic surface  | Water-hydrophobic surface   |
|----------------------------|--|---|
| Well below CMC (region 1)  |   |                          |
| Below CMC (region 2 and 3) | Hemimicelle<br><br>Bilayer or admicelle | Monolayer<br>            |
| Above CMC (region 4)       | micelle<br><br>Bilayer or admicelle     | micelle<br><br>Monolayer |

**Figure 3.8** Surfactant adsorption on solid surfaces [14]

The amount of adsorbed surfactant at surface saturation can be reduced by an increase in the hydrophilic head group size. On the other hand, the surfactant adsorption may be increased, decreased or maintained by an increase in the hydrophobic tail length [14].

If the surfactant molecules are not closely packed, the surfactant adsorption on solid surfaces can be increased by an increase in the chain length of the tail. If the adsorption of surfactant on the solid surface is because of polarization of  $\pi$  electrons, the amount of surfactant adsorbed on the surface is reduced at surface saturation. If the adsorbed surfactants are closely packed on the solid surface, an increase in the chain length of the surfactant tail will have no effect on the surfactant adsorption [14].

The solid surface charge can change with the change in pH of the solution resulting in the adsorption of ionic surfactants on the charged solid surface changes. The increase in pH leads to more negative solid surface. The adsorption of anionic and cationic surfactants is also affected by the pH. When the pH increases, the adsorption of anionic surfactants will decrease whereas the adsorption of cationic surfactants will increase [14]. In addition, the change in pH also changes the ionic groups in the

amphoteric surfactant structure making it either positively or negatively charged or neutral [14].

For the temperature, the increase in temperature increases adsorption of non-ionic surfactants on solid surfaces because the solubility of non-ionic surfactants in water decreases with increased temperature. On the other hand, the increase in temperature decreases the adsorption of ionic surfactants on solid surfaces since the solubility of ionic surfactant increases with increased temperature. Moreover, the adsorption of ionic surfactants can increase with the presence of electrolytes in case of the solid surface has the same charge as the surfactant head groups [14].

### 3.5.6 Anionic surfactant

The surfactants that dissociate in water into a negatively charged ion and a positively charged ion are called anionic surfactants. The hydrophilic head of these surfactants is negatively charged (anion). Anionic surfactants are the most common and inexpensive surfactant. They are sold as alkali metal salts or ammonium salts. Anionic surfactants are the most commonly used class of surfactants in cleansing applications [14]. In addition, the ability of these surfactants is to emulsify oily soils into wash solutions. They can lift soils, including particulates, from surfaces because the negatively charged head group is repelled from most surfaces, which also tend to be slightly negatively charged. The reverse action to a cationic surfactant where the positively charged head group is adsorbed onto a surface gives an antistatic and conditioning effect [14].

The significant foaming will be generated by the great majority of anionic surfactants in solutions above their critical micelle concentration (CMC), which is a desirable attribute in most cleansing applications. However, this foam can restrict the use of anionic surfactants in areas where foam is a problem [14].

According to the polar group, anionics can be classified as follows [14].

-Sulphonates

Aromatic – alkylbenzene, alkyltoluene, alkylxylene, alkyl-naphthalene

Aliphatic –  $\alpha$ -olefin sulphonates, alkane sulphonates, sulphosuccinates

-Sulphates



Alkyl sulphates e.g. sodium lauryl sulphate (SLS)

Alkyl ethoxy sulphates e.g. sodium laureth sulphate

-Phosphate esters

-Carboxylates

-Soaps, isethionates, taurates



## CHAPTER IV

### EXPERIMENT

In order to enhance the battery performance, the electrolyte system was improved. The surfactants were used by adding to a traditional electrolyte which is potassium hydroxide solution in order to enhance the cell performance in term of zinc utilization. The surfactants can reduce passivation layer which results in the enhancement of zinc utilization. In this study, two anionic surfactants consisted of sodium dodecylbenzene sulfonate and sodium dodecyl sulfate were used. In addition, an ethanol was used to help enhancing surfactant functions. The details of the materials and chemicals and the methodology are present as follows.

#### 4.1 Materials and Chemicals

The materials and the chemicals which were employed in the electrolyte improvement are expressed in Table 4.1

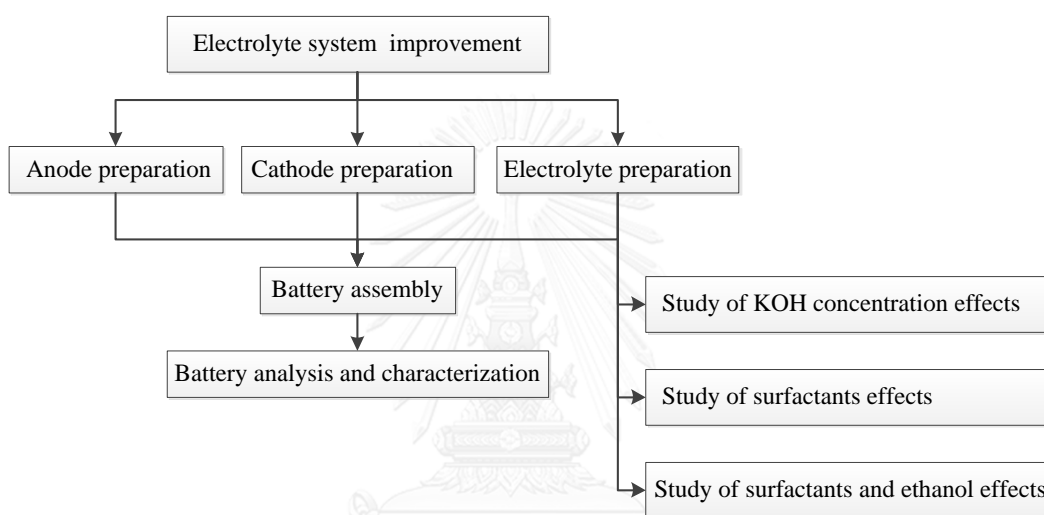
**Table 4.1** List of the materials and the chemicals for electrolyte system improvement

| <b>Material</b>                | <b>Molecular Formula</b>                           | <b>Company</b> |
|--------------------------------|--|----------------|
| Silver conductive ink          | Ag   | NovaCentrix    |
| Zinc powder                    | Zn   | Ajax Finechem  |
| Sodium silicate                | Na <sub>2</sub> SiO <sub>3</sub>                   | AppliChem      |
| Graphite                       | C  | Sigma Aldrich  |
| Poly(tetrafluoroethylene)      | (CF <sub>2</sub> CF <sub>2</sub> ) <sub>n</sub>    | Sigma Aldrich  |
| Potassium hydroxide            | KOH  | Ajax Finechem  |
| Sodium dodecylbenzenesulfonate | C <sub>18</sub> H <sub>29</sub> NaO <sub>3</sub> S | Sigma Aldrich  |

| Material               | Molecular Formula    | Company       |
|------------------------|----------------------|---------------|
| Sodium dodecyl sulfate | $C_{12}H_{25}NaO_4S$ | Sigma-Aldrich |
| Ethanol                | $C_2H_6O$            | QRëC™         |

## 4.2 Experimental methodology

The overview of electrolyte improvement is presented in Figure 4.1.



**Figure 4.1** Schematic diagram of electrolyte improvement.

## 4.3 Preparation of functional ink

The methods to prepare functional ink are shown below:

### 4.3.1 Zinc –based functional ink

The zinc-based functional ink or anode electrode was prepared by mixing 98% by weight of zinc powder (Ajax Finechem), 2% by weight of sodium silicate (AppliChem) used as a binder.

### **4.3.2 Gas diffusion ink**

The gas diffusion ink was prepared by mixing 78% by weight of graphite (20  $\mu\text{m}$ , Aldrich), 20% by weight of polytetrafluoroethylene (40  $\mu\text{m}$ , Sigma Aldrich) and 2% by weight of sodium silicate used as binder.

## **4.4 Preparation of aqueous electrolyte**

### **4.4.1 Potassium hydroxide**

Because the concentration of KOH affects the battery performance in both zinc utilization and the conductivity, the concentration effect was thus investigated. The electrolyte was prepared using potassium hydroxide (KOH) (Ajax Finechem). To study the effect of potassium hydroxide concentrations, three concentrations of KOH consisted of 5 mol L<sup>-1</sup>, 7 mol L<sup>-1</sup> and 9 mol L<sup>-1</sup> were studied. These KOH concentrations were employed as the battery electrolyte.

### **4.4.2 Potassium hydroxide with surfactant**

The proper concentration of KOH would be selected. The two surfactants, consisted of sodium dodecylbenzenesulfonate (SDBS) and sodium dodecyl sulfate (SDS), were employed. Three concentrations, consisted of 0.2 mmol L<sup>-1</sup>, 0.4 mmol L<sup>-1</sup> and 0.6 mmol L<sup>-1</sup>, of each surfactant were investigated. These concentrations are in the range of critical micelle concentration of the surfactants. Firstly, the surfactants were dissolved in deionized water. Then, the granular KOH was put in the surfactant solution and mixed together. The solution was left for cooling. Finally, the solution was used as the electrolyte for the fabrication of the battery.

### **4.4.3 Potassium hydroxide with surfactant and ethanol**

In order to study effect of ethanol, 95% ethanol was added to the all mixed solutions of KOH and the surfactants. In order to study SDBS effect, 20 v/v% ethanol was used. And 30 v/v% ethanol was used in the study of SDS effect. The amount of the ethanol addition depended on the white particle of the surfactants on the surface of the

mixed solution. Then, the mixed solutions, included ethanol, were used as the electrolyte for the fabrication of the battery.

## **4.5 Preparation of flexible substrate and separator**

### **4.5.1 Polyethylene terephthalate (PET) substrate**

A 3.0 x 3.0 cm<sup>2</sup> polyethylene terephthalate (PET) substrate was cut and used as anode substrate.

### **4.5.2 Polytetrafluoroethylene (PTFE) substrate**

A 3.0 x 3.0 cm<sup>2</sup> polytetrafluoroethylene (PTFE) substrate was cut and used as cathode substrate.

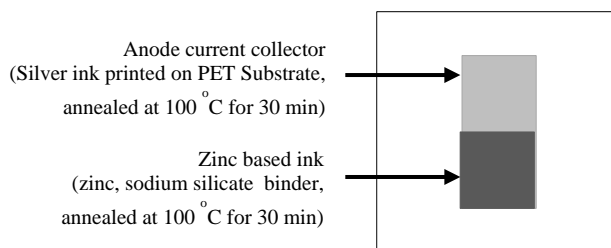
### **4.5.3 Polypropylene (PP) membrane**

A 1.5 x 1.5 cm<sup>2</sup> polypropylene (PP) membrane was cut and used as separator.

## **4.6 Preparation of anode electrode**

A commercial nano-silver conductive ink (NovaCentrix, 43%) was employed to fabricate the anode current collectors. A screen-printing technique was used in this step. The nano-silver ink was printed on PET substrate with the effective area of 1.0 x 2.0 cm<sup>2</sup>. Then, anode current collectors were annealed at 100°C for 30 minutes.

The zinc-based functional ink was then deposited onto the anode current collector using the screen-printing technique with the effective area of 1.0 x 1.0 cm<sup>2</sup> and annealed at 100 °C for 30 minutes. The zinc anode electrode pattern is illustrated in Figure 4.2.

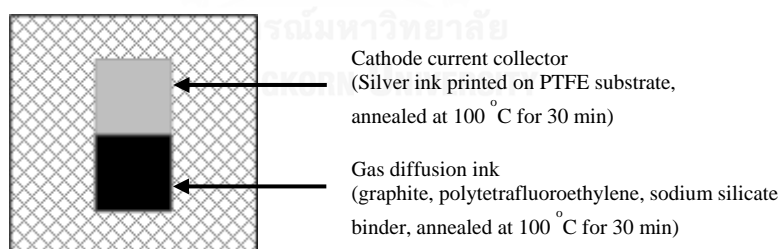


**Figure 4.2** Anode electrode pattern.

#### 4.7 Preparation of cathode electrode

A commercial nano-silver conductive ink (NovaCentrix, 43%) was employed to fabricate the cathode current collectors. A screen-printing technique was used in this step. The nano-silver ink was printed on PTFE substrate with the effective area of 1.0 x 2.0 cm<sup>2</sup>. Then, cathode current collectors were annealed at 100°C for 30 minutes.

The gas diffusion ink was then deposited onto the cathode current collector using the screen-printing technique with the effective area of 1.0 x 1.0 cm<sup>2</sup> and annealed at 100 °C for 30 minutes. The air cathode electrode pattern is illustrated in Figure 4.3.

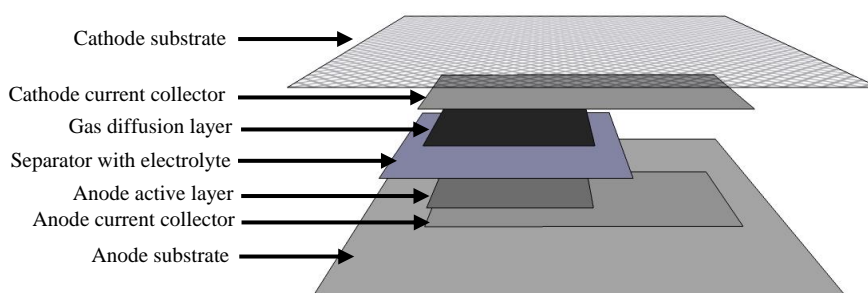


**Figure 4.3** Cathode electrode pattern.

#### 4.8 Fabrication of flexible printed zinc-air battery

The zinc-air cell was assembled layer by layer. First, one drop of electrolyte was dropped onto the anode and cathode. Then a 1.5 x 1.5 cm<sup>2</sup> polypropylene separator was soaked in electrolyte for 5 minutes and was hung on the air for 1 minute to reduce

droplets of electrolyte from the surface of separator. The same quantity of the all electrolyte experiments was thus maintained. Then the separator was placed on the anode. Next, the cathode was placed on top of the separator. The borders of the batteries were sealed by double sided tapes. The configuration of flexible printed zinc-air battery is illustrated in Figure 4.4.



**Figure 4.4** Layer by layer configuration of the zinc air battery.

## 4.9 Characterizations

The characteristic and the performance of the battery were investigated by battery analyzer (Battery Metric, MC2020). The polarization curve was obtained by varying the discharge current density, correlations of discharging time and the cell voltage, capacity and energy of the flexible printed zinc-air battery tested by  $1 \text{ mA cm}^{-2}$  constant current discharging.

Electrochemical impedance spectroscopy (EIS) measurement was performed using a potentiostat with impedance measurement unit (AMETEK, PAR VersaSTAT 3A) with the frequency range of 10 kHz to 0.1 Hz and the amplitude of 10 mV.

The morphologies of the anodes were analyzed by Scanning electron microscope (SEM (6400)).

## **CHAPTER V**

### **RESULTS AND DISCUSSIONS**

Enhancement of the battery performance can be done by several methods. One of the methods is modification of electrolyte system by the surfactant addition. SDBS and SDS are the candidates of this improvement. In this chapter, the results of SDBS and SDS addition were investigated. The cell performances of these additions were studied. The considerable parameters which were examined consist of polarization curve, cell power, capacity and energy. Effect of potassium hydroxide concentration, effect of surfactant and effect of ethanol on surfactant role were revealed in this chapter. Furthermore, in order to confirm the results, the morphology of zinc electrode was also investigated. All resulting details are shown as follows.

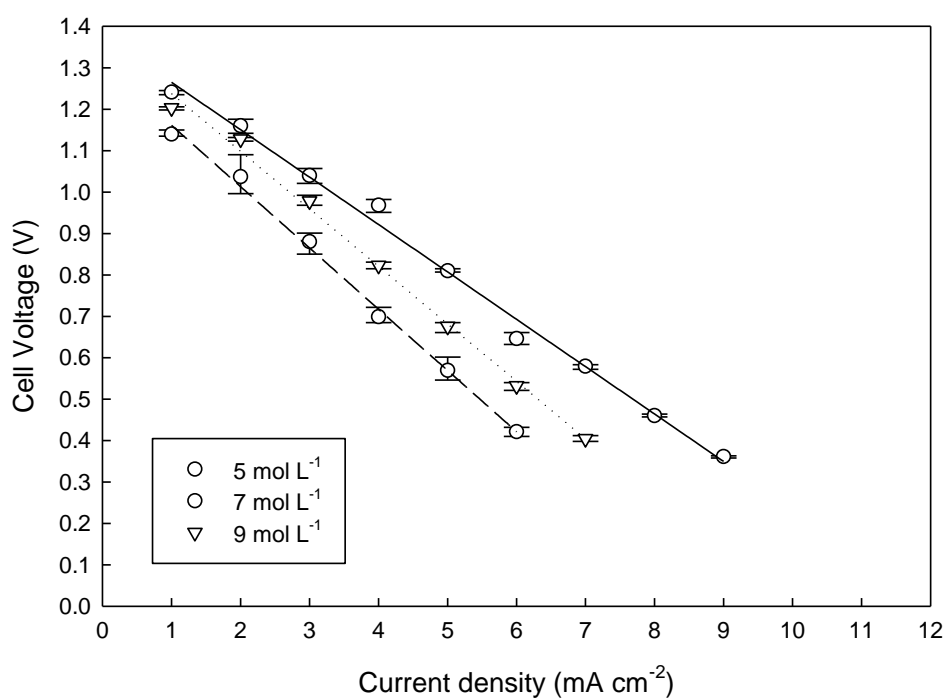
#### **5.1 Effect of potassium hydroxide concentration**

Potassium hydroxide is favored electrolyte for zinc-air battery due to a good conductivity [40]. However, the proper concentration needs to be taken into account. The use of high KOH concentration can reduce the passive film on the zinc surface because the passive film can be dissolved by high concentration of alkaline solution. On the other hand, too much dissolution results in the shape change [11] while the low concentration of KOH leads to higher passive film in the cell. Additionally, it also affects the conductivity of the cell to become lower. Therefore, the proper concentration of KOH is investigated by considering the zinc-air performance. Three KOH concentrations consisted of 5 mol L<sup>-1</sup>, 7 mol L<sup>-1</sup> and 9 mol L<sup>-1</sup> were studied. The results are present as follows.

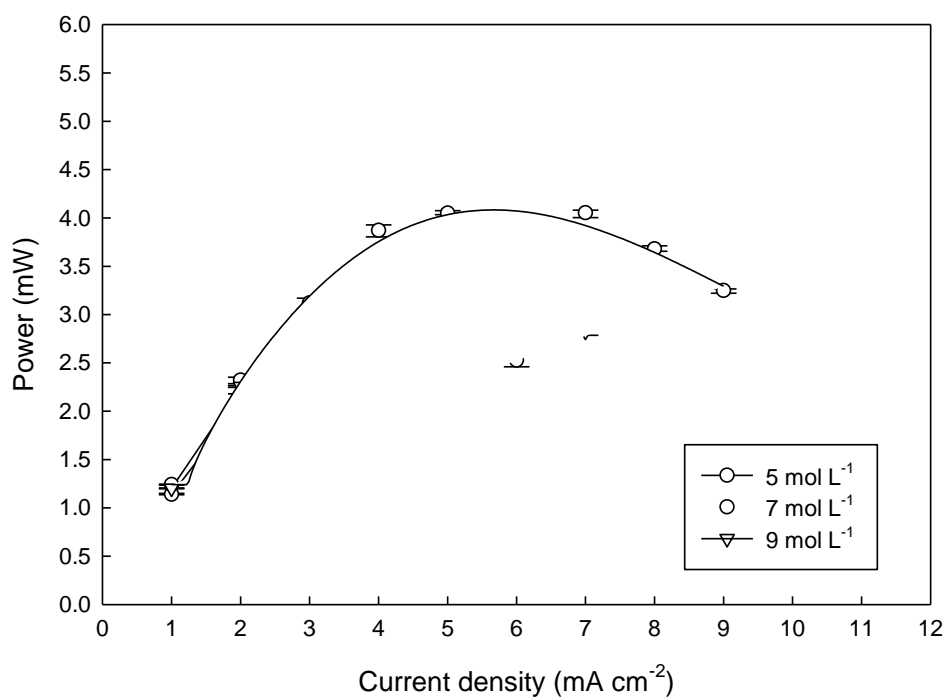
Firstly, the behaviors of the battery cell were studied by polarization curve (The correlations of cell voltage and current) as illustrated in Figure 5.1. The polarization curve shows the internal resistance of the cell. Normally, this curve has three regions of activation loss, ohmic loss and concentration loss. In this study, only ohmic loss was considered. In Figure 1, the lowest resistance is found with 7 mol L<sup>-1</sup> KOH. The higher



resistance is found with 9 mol L<sup>-1</sup> and 5 mol L<sup>-1</sup>, respectively. In order to obviously compare, this information has been used to calculate its power, then it is illustrated as the correlations of cell power and current density (Figure 5.2). The results showed that the cell power of 7 mol L<sup>-1</sup> is highest for every current density. Subsequently, the cell power of 9 mol L<sup>-1</sup> and 5 mol L<sup>-1</sup> are lower, respectively. Moreover, this information also expresses the maximum power of the cell. Additionally, the results showed that the maximum power is obtained at 5 mA current density for all KOH concentrations.

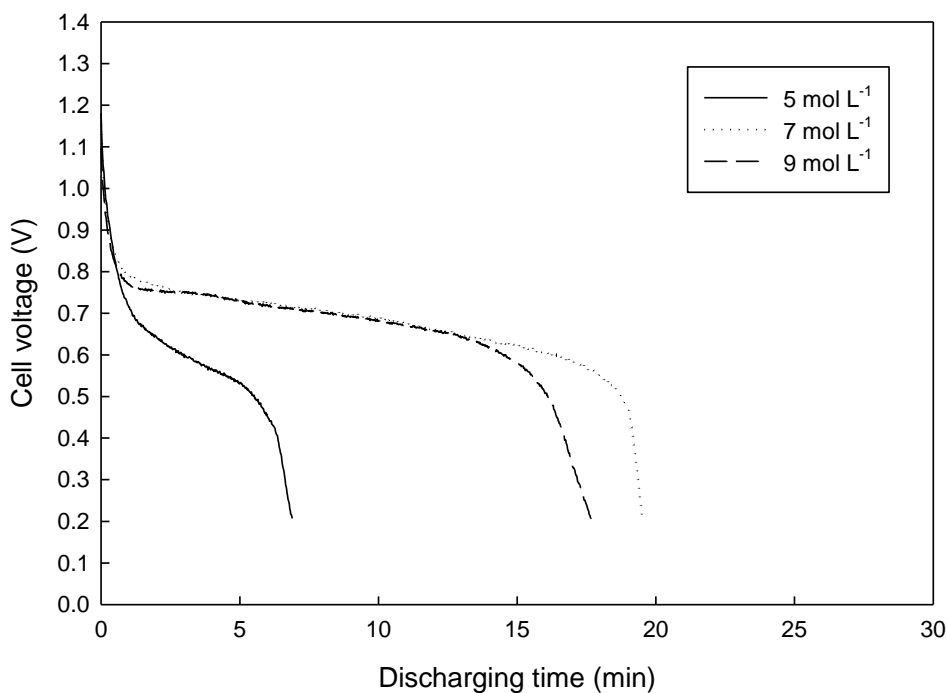


**Figure 5.1** Polarization curves of 5 mol L<sup>-1</sup>, 7 mol L<sup>-1</sup> and 9 mol L<sup>-1</sup> KOH electrolytes used in the flexible printed zinc-air battery with effective area of 1 cm<sup>2</sup>.



**Figure 5.2** Correlations of current density and cell power of 5 mol L<sup>-1</sup>, 7 mol L<sup>-1</sup> and 9 mol L<sup>-1</sup> KOH electrolytes used in the flexible printed zinc-air battery with effective area of 1 cm<sup>2</sup>.

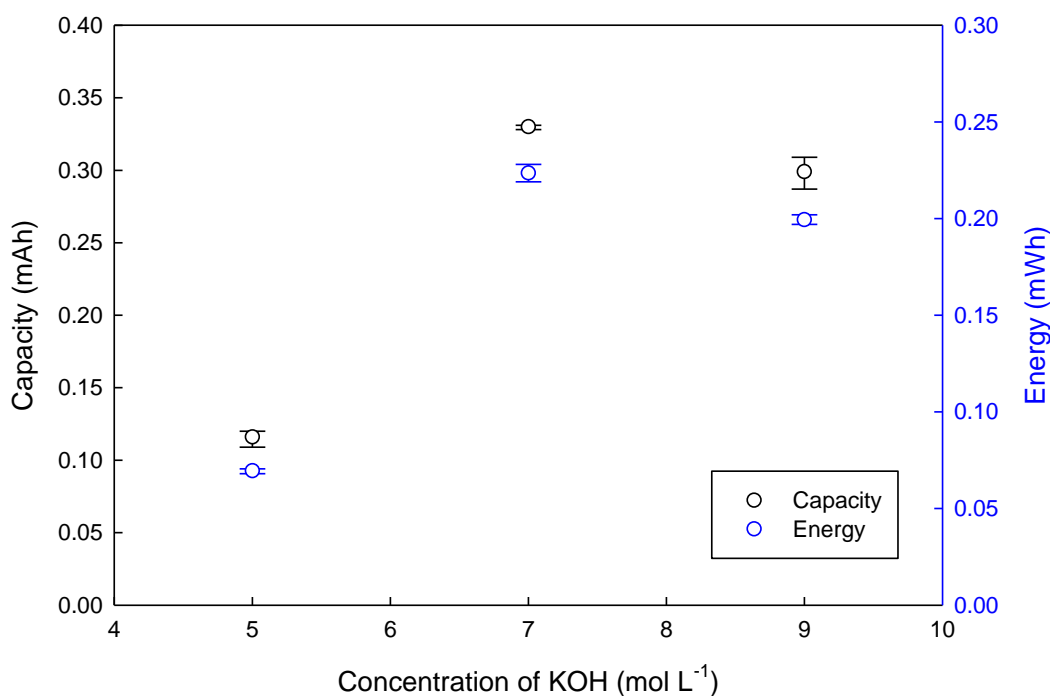
In addition, the cell power is not only considered, but the battery capacity (mA h) and energy (W h) are also taken into account in order to investigate the battery performance. In this study, constant current mode was used to test the battery capacity and energy. Therefore, the correlations of discharging time and cell voltage are obtained as shown in Figure 5.3.



**Figure 5.3** Correlations of discharging time and the cell voltage of 5 mol L<sup>-1</sup>, 7 mol L<sup>-1</sup> and 9 mol L<sup>-1</sup> KOH electrolytes used in the flexible printed zinc-air battery with effective area of 1 cm<sup>2</sup> by 1 mA cm<sup>-2</sup> constant current discharging.

The correlations in Figure 5.3 show that the cell voltages quickly decrease at the initial stage, particularly the cell voltage of 5 mol L<sup>-1</sup>. Then, the cell voltage of 5 mol L<sup>-1</sup> steadily decreases with the highest decreasing rate. The reason of this reduction is that the use of 5 mol L<sup>-1</sup> KOH has more passive film at the zinc surface than 7 mol L<sup>-1</sup> and 9 mol L<sup>-1</sup> during the discharging step. The use of high concentration KOH can dissolve more zinc oxide which is the main component of passive film [9]. Therefore, the use of 7 mol L<sup>-1</sup> or 9 mol L<sup>-1</sup> KOH results in higher zinc utilization in the battery. However, too much solubility of the passive film generates the shape change and the corrosion problems, leading to the reduction of battery capacity [13]. Furthermore, the cell voltages and the discharging times are utilized to calculate the capacity and the energy. The correlations of KOH concentration and the capacity and energy are illustrated in Figure 5.4. It shows that the highest capacity and energy are obtained with the use of 7 mol L<sup>-1</sup> KOH. It corresponds to the highest conductivity of the KOH solution which is obtained around 7 mol L<sup>-1</sup> at 25°C [9]. Subsequently, lower capacity

and energy are obtained with the use of 9 mol L<sup>-1</sup> and 5 mol L<sup>-1</sup> KOH, respectively. Consequently, the proper concentration of KOH is 7 mol L<sup>-1</sup>.



**Figure 5.4** Correlations of KOH concentration and capacity and energy of the flexible printed zinc-air battery with effective area of 1 cm<sup>2</sup> by 1 mA cm<sup>-2</sup> constant current discharging.

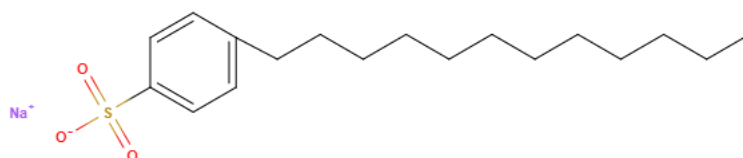
## 5.2 Effect of surfactants

In this study, surfactants consisting of sodium dodecyl benzene sulfonate and sodium dodecyl sulfate were investigated. Both surfactants are anionic surfactants. They were selected because anionic surfactant can improve the battery capacity in previous study [29]. The molecular structures of both surfactants are quite same. They have twelve carbon atoms of hydrophobic group and sulfur oxide acting as hydrophilic group. However, the difference of both surfactants is they have the different group between hydrophilic and hydrophobic groups in their molecules. SDBS has phenyl group while SDS has oxy group. This different molecular structure results in the

different properties in term of the stability of the molecule. The results of SDBS and SDS additives in the traditional electrolyte are present as follows.

### 5.2.1 Sodium dodecyl benzene sulfonate

Sodium dodecyl benzene sulfonate has a sulfonate acting as hydrophilic group and an alkylbenzene acting as hydrophobic group [39]. This structural formula is illustrated in Figure 5.5. SDBS is not easy to oxidation but is easy to compound with various additives. SDBS is a high content anionic surfactant with properties of dispersity. International security organizations have been recognized it as safe chemicals [14]. According to the results from section 5.1, 7 mol L<sup>-1</sup> KOH is the proper concentration. Therefore, SDBS was added in 7 mol L<sup>-1</sup> KOH. Then, the mixing solutions were employed as the electrolyte in flexible printed zinc-air battery. After that, the resulting analysis has been done. The results are shown as follows

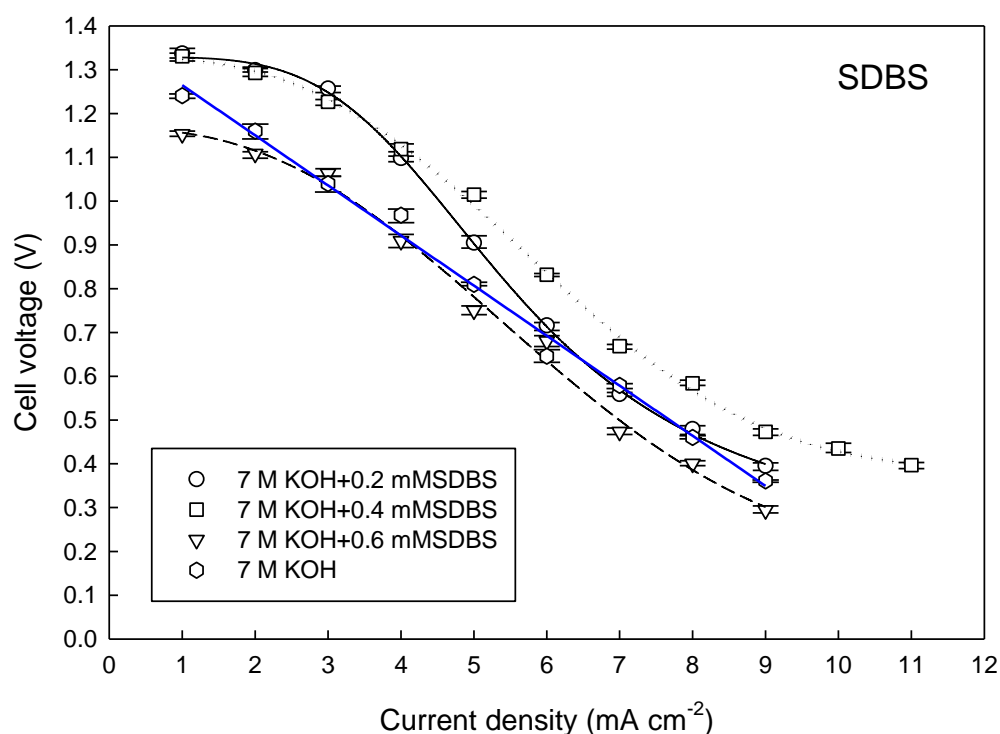


**Figure 5.5** Structural formula of sodium dodecyl benzene sulfonate.

Generally, characteristics of a battery are investigated by polarization curve and capacity and energy examinations. For capacity and energy examinations, constant current mode is favorably employed. Therefore, the results of these examinations are revealed as the correlations of discharging time and cell voltage. The details of these investigations are shown as follows.

The polarization curves of SDBS modified electrolyte in flexible printed zinc-air battery are illustrated in Figure 5.6. The results showed that polarization curves of all SDBS concentration are nonlinear, particularly at low and high current densities in ohmic loss region. Additionally, the lower slope is obtained at low and high current density and the higher slope is found at the middle current density. These curves indicate that SDBS help reducing the cell resistance. This phenomenon is the role of

surfactants which can be described as follows. Surfactants which adsorb on the solid by covering zinc surface to protect passive layer deposition. The zinc surface will be modified by surfactant to become more porosity. This phenomenon can improve the wettability of that solid [39]. Due to this property, the addition of SDBS which is a surfactant in traditional electrolyte can thus increase the penetrating capability of the electrolyte in zinc electrode, resulting in the improvement of active ion diffusion.

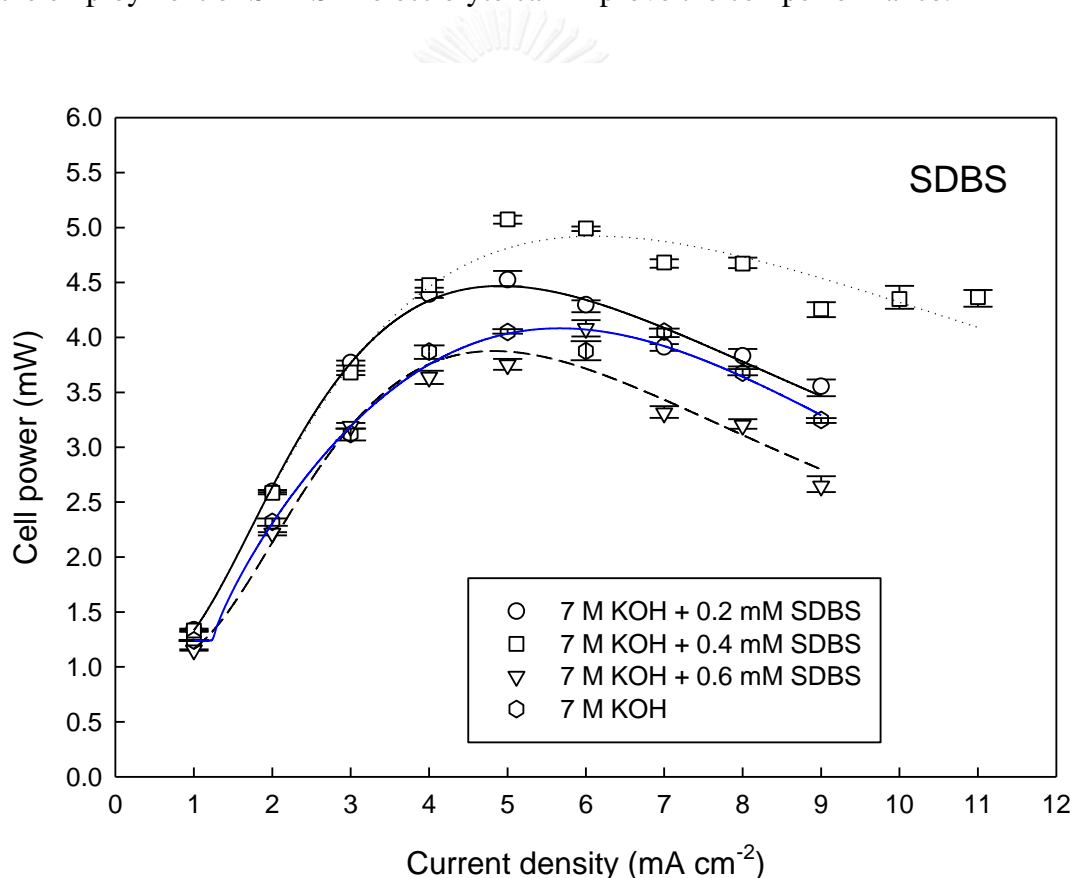


**Figure 5.6** Polarization curve of 0.2 mmol L<sup>-1</sup>, 0.4 mmol L<sup>-1</sup> and 0.6 mmol L<sup>-1</sup> SDBS in 7 mol L<sup>-1</sup> KOH electrolytes used in the flexible printed zinc-air battery with effective area of 1 cm<sup>2</sup>.

Consider Figure 5.6, it is found that the lowest internal resistance of the cell is obtained at 0.4 mmol L<sup>-1</sup> SDBS, owing to the lowest slope of the correlation. The higher internal resistances of the cell are found at 0.2 mmol L<sup>-1</sup> SDBS and 0.6 mmol L<sup>-1</sup> SDBS, respectively. The highest internal resistance is found at 0.6 mmol L<sup>-1</sup> SDBS because of self-aggregation of SDBS. This phenomenon will occur when the used surfactant concentration is higher than critical micelle concentration (CMC) of that surfactant. The aggregation can impede the diffusion of active ion. The supporting reason of this

effect can be observed from the correlation of 0.6 mmol L<sup>-1</sup>SDBS at high current density which is straight line and is significantly higher slope than 0.4 mmol L<sup>-1</sup> SDBS and 0.2 mmol L<sup>-1</sup> SDBS. The higher slope implies the higher resistance.

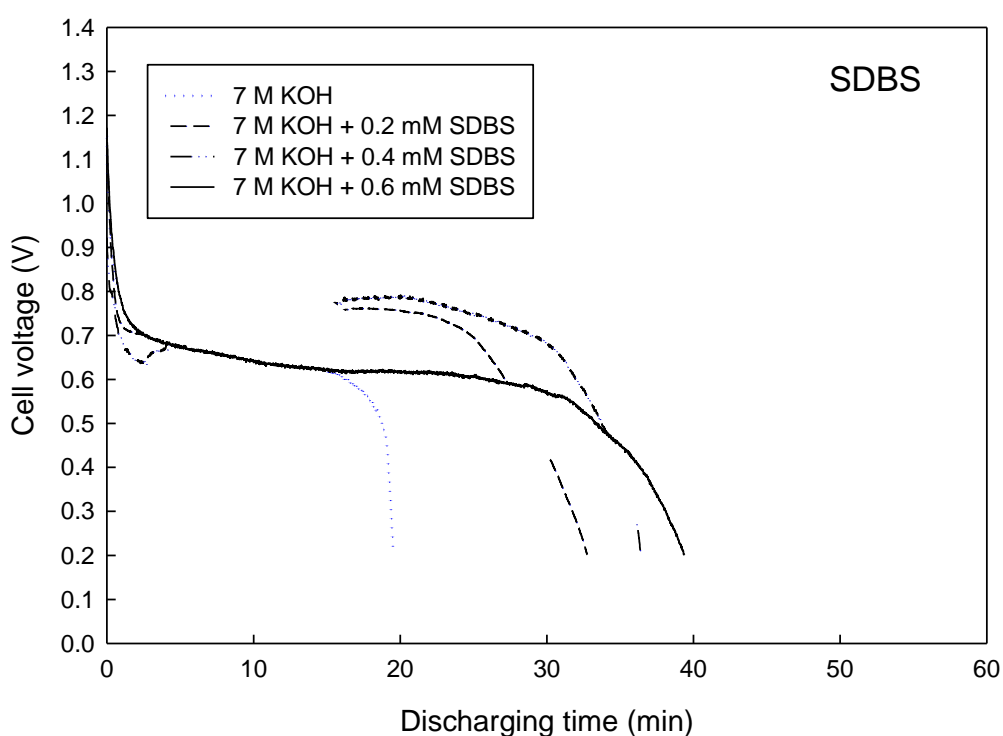
Another important parameter which has to be used to compare the cell performances is the cell power. The correlations of current density and cell power are illustrated in Figure 5.7. The correlations are inverted asymmetric parabola. The maximum power is obtained at current density of 5 mA cm<sup>-2</sup>. This result is similar to the result of traditional electrolyte. However, the powers of the cell with modified electrolyte are higher than that of the cell with traditionally electrolyte. Consequently, the employment of SDBS in electrolyte can improve the cell performance.



**Figure 5.7** Correlations of current density and cell power of 0.2 mmol L<sup>-1</sup>, 0.4 mmol L<sup>-1</sup> and 0.6 mmol L<sup>-1</sup> SDBS in 7 mol L<sup>-1</sup> KOH electrolytes used in the flexible printed zinc-air battery with effective area of 1 cm<sup>2</sup>.

Furthermore, two considerable parameters which need to be investigated are capacity and energy. Generally, the capacity of the battery is the amount of charges in

the battery which has the unit of milliampere hour (mA h). This capacity depends on the amount of active species in the battery and the battery efficiency (or the loss). Additionally, Energy of the battery does not only relate to the charge but it also concerns the cell voltage. Therefore, the unit of battery energy is watt hour (W h). In order to compare the performance of the batteries, capacity and energy are investigated. The correlations of cell voltage and discharging time are examined. These correlations of SDBS for various concentrations are illustrated in Figure 5.8.



**Figure 5.8** Correlations of discharging time and cell voltage of 0.2 mmol L<sup>-1</sup>, 0.4 mmol L<sup>-1</sup> and 0.6 mmol L<sup>-1</sup> SDBS in 7 mol L<sup>-1</sup> KOH electrolytes used in the flexible printed zinc-air battery with effective area of 1 cm<sup>2</sup> by 1 mA cm<sup>-2</sup> constant current discharging.

In Figure 5.8, the result of SDBS additive show that the highest cell voltage is obtained by using 0.4 mmol L<sup>-1</sup> SDBS. In addition, the cell voltage of 0.2 mmol L<sup>-1</sup> SDBS is close to 0.4 mmol L<sup>-1</sup> SDBS. These results agree with polarization curve at low current density which reveals that the cell voltages of 0.2 mmol L<sup>-1</sup> and 0.4 mmol L<sup>-1</sup> SDBS are close. However, the discharging time is lowest at 0.2 mmol L<sup>-1</sup> SDBS. It implies that the amount of SDBS in the electrolyte is insufficient to adsorb on whole



zinc. Therefore, the zinc is not completely utilized. Furthermore, the use of 0.6 mmol L<sup>-1</sup> SDBS results in the highest discharging time. It indicates that the amount of SDBS is sufficient for adsorbing on the zinc electrode. However, the lowest cell voltage is found by using 0.6 mmol L<sup>-1</sup> SDBS. The self-aggregation of SDBS which impedes the diffusion of active ion is the cause of the lowest voltage.

The capacity that is considered in this study is the discharging capacity which can be calculated from Equation (5.1). Similarly, the energy of the battery in this study is the discharging energy which can be calculated from Equation (5.2). The capacity and energy of the battery in this study for various SDBS concentrations is illustrated in Figure 5.9.

$$q = \int I dt \quad (5.1)$$

$$E = \int IV dt \quad (5.2)$$

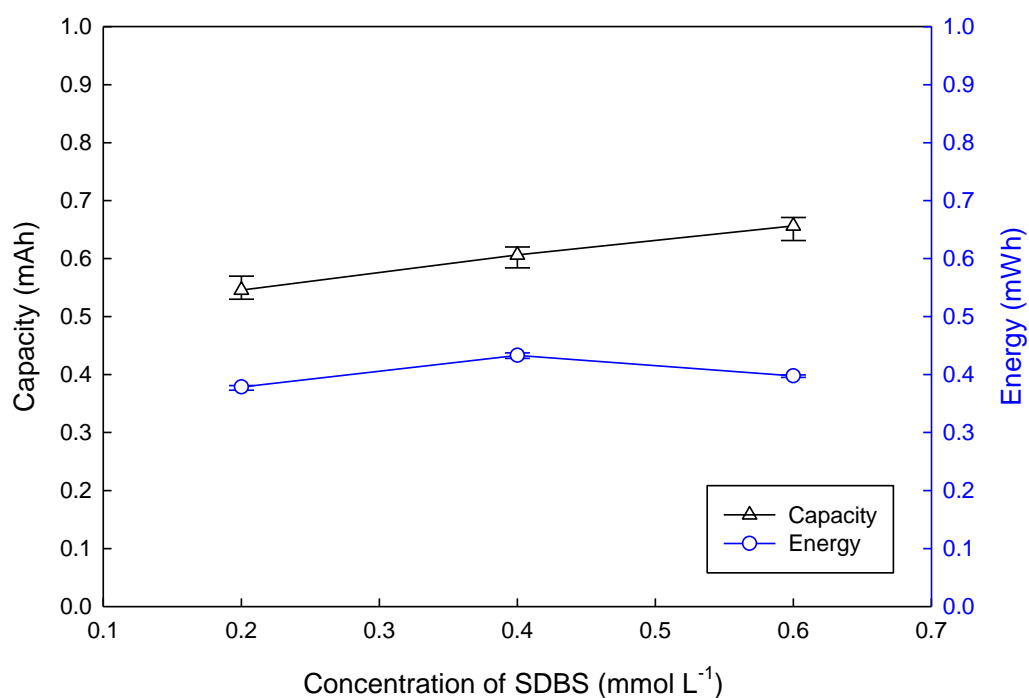
Where q is the discharging capacity

I is the electrical current

t is the time

E is the discharging energy

V is the cell voltage



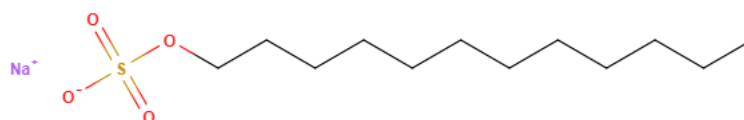
**Figure 5.9** Correlations of SDBS concentration in 7 mol L<sup>-1</sup> KOH and the capacity and the energy of the flexible printed zinc-air battery with effective area of 1 cm<sup>2</sup> by 1 mA cm<sup>-2</sup> constant current discharging.

Figure 5.9 shows that the capacity increases with increase of SDBS concentration. Therefore, the highest capacity is obtained with the use of 0.6 mmol L<sup>-1</sup> SDBS. Subsequently, the lower capacity is obtained with the use of 0.4 mmol L<sup>-1</sup> and the lowest capacity is obtained with the use of 0.2 mmol L<sup>-1</sup> SDBS. The reason of these results is explained as aforementioned. In addition, the highest energy is obtained at 0.4 mmol L<sup>-1</sup> SDBS. For 0.2 mmol L<sup>-1</sup> and 0.6 mmol L<sup>-1</sup> SDBSs, the energy of the battery reduces which the energy of 0.2 mmol L<sup>-1</sup> SDBS is slightly less than that of 0.6 mmol L<sup>-1</sup> SDBS. These results are affected from insufficient SDBS and self-aggregation of SDBS as aforementioned.

### 5.2.2 Sodium dodecyl sulfate

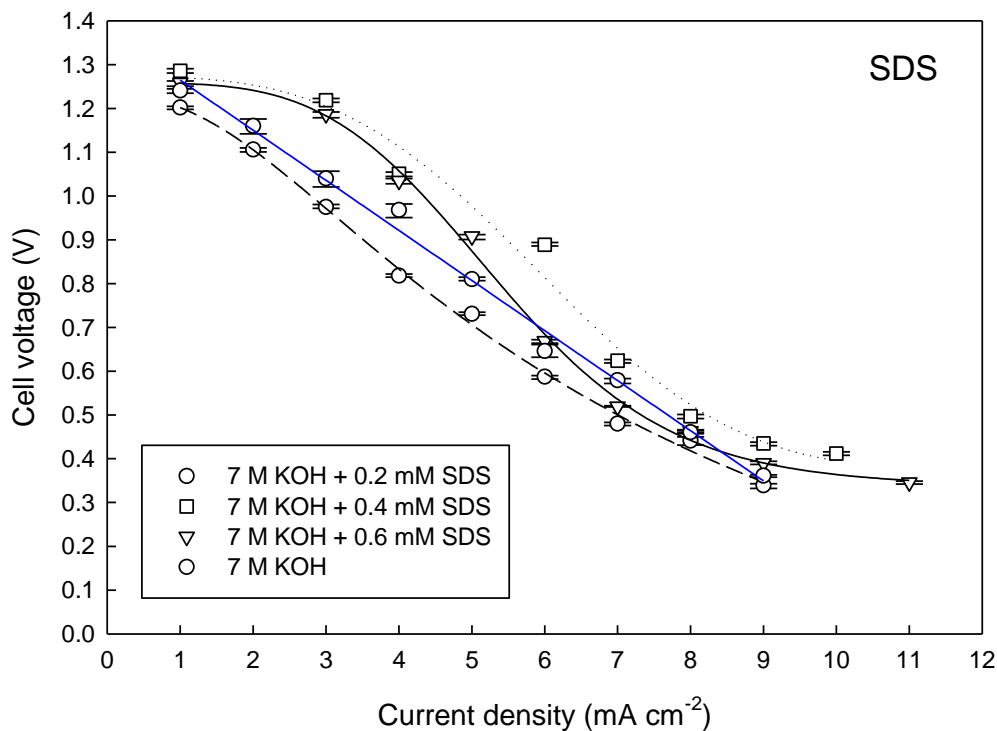
Sodium dodecyl sulfate has a sulfate acting as hydrophilic group and a dodecyl acting as hydrophobic group [39]. This structural formula is illustrated in Figure 5.10.

For the experiments, various concentrations of SDS were added to 7 mol L<sup>-1</sup> KOH which is the proper concentration from section 5.1. Then, this SDS modified electrolyte was used in flexible printed zinc-air battery in order to investigate the cell performance. The results of these experiments are shown in the same analysis as the use of SDBS. The details of these results are revealed as follows.



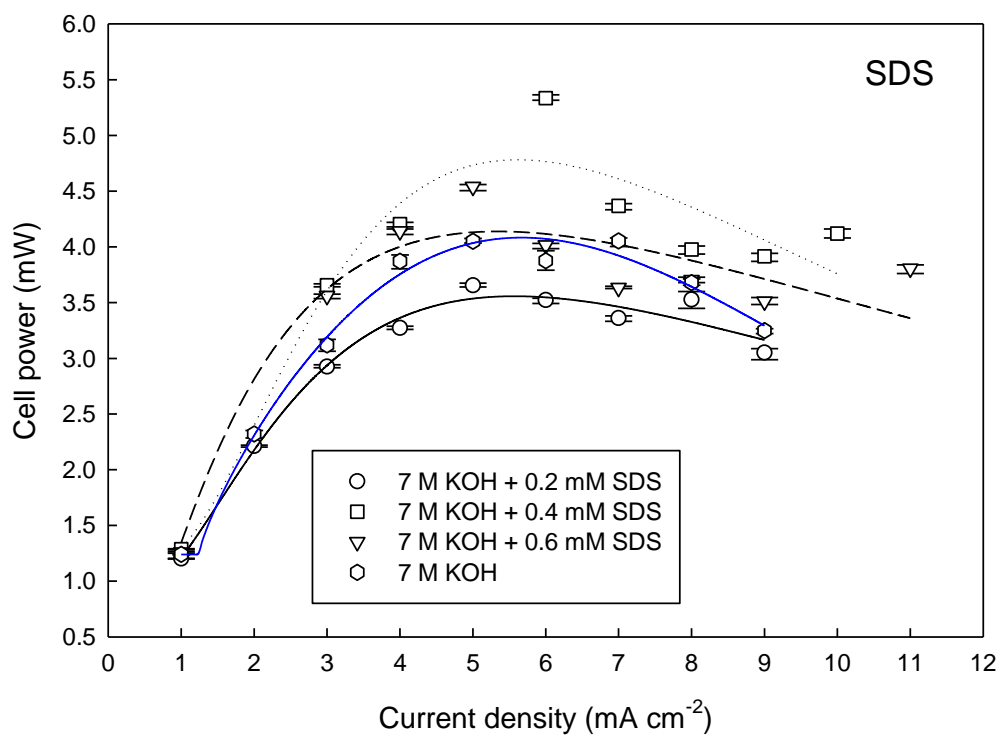
**Figure 5.10** Structural formula of sodium dodecyl sulfate.

Firstly, polarization curves of the cell using SDS modified electrolyte are illustrated in Figure 5.11. Characteristic of the curves are similar to polarization curve of SDBS modified electrolyte. Therefore, SDS also helps reducing the cell resistance by decreasing ohmic loss of the cell. SDS adsorbing on zinc electrode by covering zinc surface to protect passive layer deposition can improve the wettability of the zinc electrode, the penetrating capability of the electrolyte in zinc electrode thus increases, resulting in the improvement of active ion diffusion. However, the used concentration has to be sufficient for the amount of zinc electrode in the cell. Consider Figure 5.11, the correlations of 0.4 mmol L<sup>-1</sup> SDS and 0.6 mmol L<sup>-1</sup> SDS are not linear. It indicates that the amount of these SDS concentrations is sufficient for the zinc electrode, therefore, they can help improving the zinc utilization. Nevertheless, at 0.2 mmol L<sup>-1</sup> SDS, the amount of SDS is insufficient for the zinc electrode, thus, the correlation of 0.2 mmol L<sup>-1</sup> SDS is linear. Additionally, insufficient SDS is not only unimproved for the zinc utilization, but it can also increase the cell resistance. This phenomenon can be observed from the correlation of 0.2 mmol L<sup>-1</sup> SDS is lower curve level and higher slope than 0.4 mmol L<sup>-1</sup> SDS and 0.6 mmol L<sup>-1</sup> SDS. Moreover, the cell behavior with 0.4 mmol L<sup>-1</sup> SDS and 0.6 mmol L<sup>-1</sup> SDS are not much different because some of SDS molecule can self-aggregates at 0.6 mmol L<sup>-1</sup> SDS, thus the existing SDS can not fully perform.



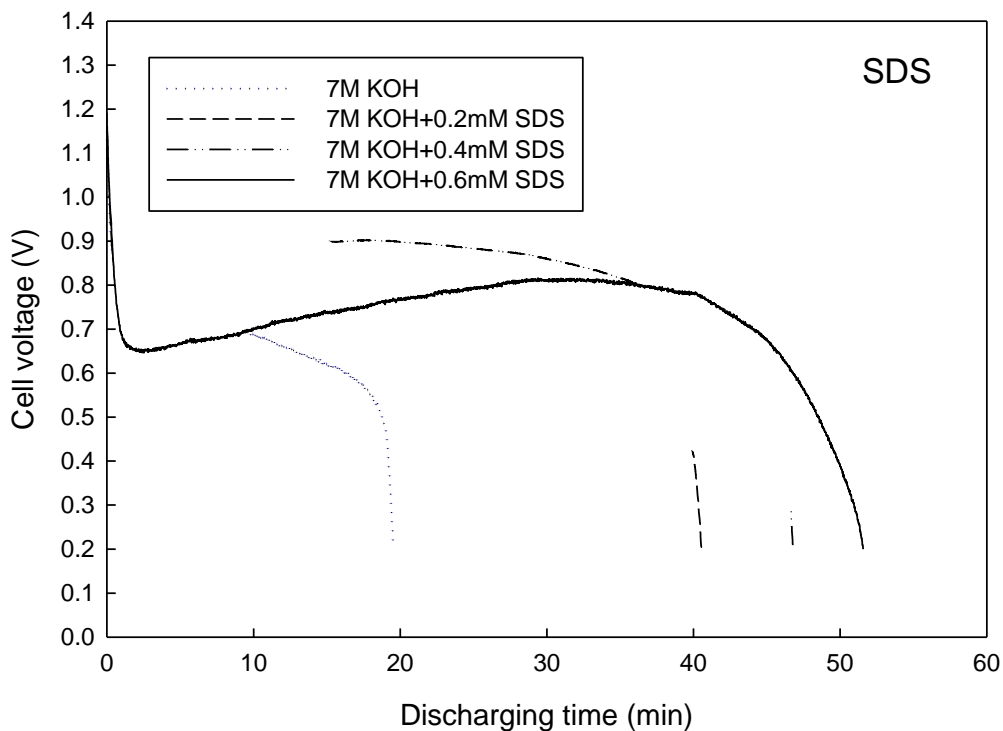
**Figure 5.11** Polarization curve of 0.2 mmol L<sup>-1</sup>, 0.4 mmol L<sup>-1</sup> and 0.6 mmol L<sup>-1</sup> SDS in 7 mol L<sup>-1</sup> KOH electrolytes used in the flexible printed zinc-air battery with effective area of 1 cm<sup>2</sup>.

Subsequently, the cell power of SDS modified electrolyte was investigated. The correlations of current density and cell power are also illustrated in Figure 5.12. The results showed that the maximum power is obtained around current density of 5 mA cm<sup>-2</sup>. At low current density, the cell powers of all concentrations are quite equal. However, at high current density, these cell powers are obviously different. The use of 0.4 mmol L<sup>-1</sup> SDS gives the highest cell power. The uses of 0.6 mmol L<sup>-1</sup> SDS and 0.2 mmol L<sup>-1</sup> SDS give the lower and the lowest cell powers, respectively. The cell powers of SDS modified electrolyte are higher than that of the cell with traditionally electrolyte. Therefore, the use of SDS in electrolyte can improve the cell performance.



**Figure 5.12** Correlations of current density and cell power of 0.2 mmol L<sup>-1</sup>, 0.4 mmol L<sup>-1</sup> and 0.6 mmol L<sup>-1</sup> SDS in 7 mol L<sup>-1</sup> KOH electrolytes used in the flexible printed zinc-air battery with effective area of 1 cm<sup>2</sup>.

Then, capacity and energy of the battery were investigated in order to compare the cell performance. The correlations of cell voltage and discharging time of SDS for various concentrations are illustrated in Figure 5.13.

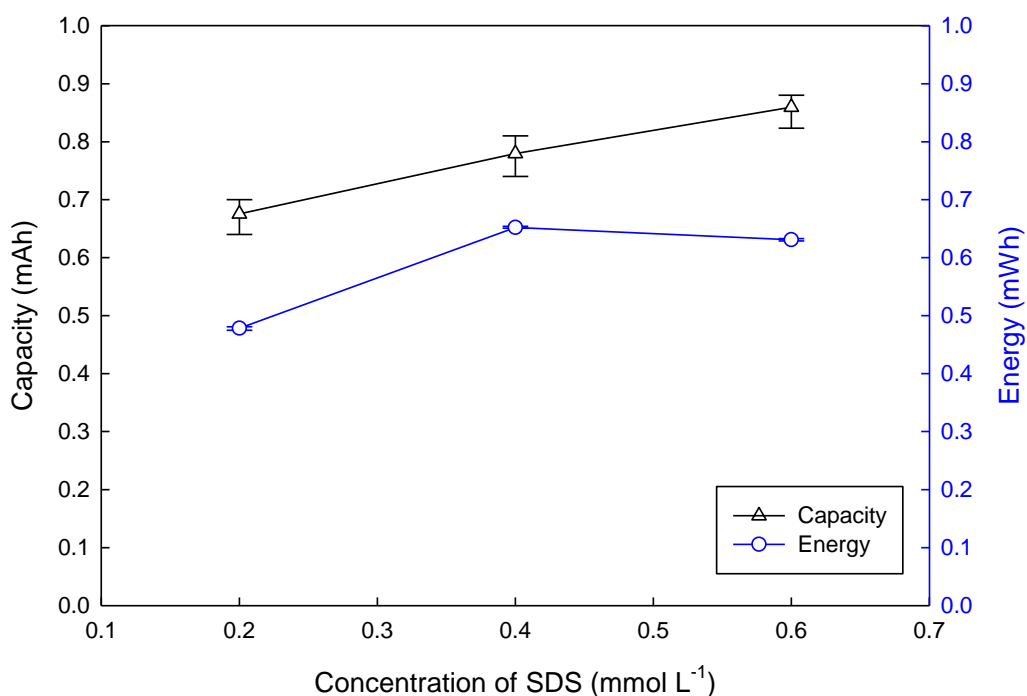


**Figure 5.13** Correlations of discharging time and cell voltage of 0.2 mmol L<sup>-1</sup>, 0.4 mmol L<sup>-1</sup> and 0.6 mmol L<sup>-1</sup> SDS in 7 mol L<sup>-1</sup> KOH electrolytes used in the flexible printed zinc-air battery with effective area of 1 cm<sup>2</sup> by 1 mA cm<sup>-2</sup> constant current discharging.

In Figure 5.13, the highest cell voltage is obtained at 0.4 mmol L<sup>-1</sup> of SDS because the self-aggregation of SDS does not occur at this concentration. Consider 0.6 mmol L<sup>-1</sup> SDS, the discharging time is higher than 0.4 mmol L<sup>-1</sup> SDS however, the cell voltage is lower. These results cause from the aggregation of some SDSs and the higher adsorption of SDS on the zinc electrode. For 0.2 mmol L<sup>-1</sup> SDS, both cell voltage and discharging time are lower than that of 0.4 mmol L<sup>-1</sup> SDS and 0.6 mmol L<sup>-1</sup> SDS because the amount of SDS is too little.

Subsequently, the capacity and energy of SDS are calculated using Equations (5.1) and (5.2), respectively. The capacity and the energy of various SDS concentrations are illustrated in Figure 5.14. The results showed that the higher capacity is obtained when the higher SDS concentration is employed. Because the use of higher SDS concentration results in more zinc electrode utilization, the capacity thus increases. For the energy, the highest energy is obtained at 0.4 mmol L<sup>-1</sup> SDS. The lower and the

lowest energies are obtained with using  $0.6 \text{ mmol L}^{-1}$  SDS and  $0.2 \text{ mmol L}^{-1}$  SDS, respectively. The reason of these results is described as aforementioned. Consequently, the parameters which affect to the cell performance include of characteristic of surfactant molecule, CMC of surfactants and the proper amount of surfactant.



**Figure 5.14** Correlations of SDS concentration in  $7 \text{ mol L}^{-1}$  KOH and the capacity and the energy of the flexible printed zinc-air battery with effective area of  $1 \text{ cm}^2$  by  $1 \text{ mA cm}^{-2}$  constant current discharging.

### 5.2.3 Comparison between SDBS and SDS

As aforementioned, the molecular structure of SDBS and SDS are quite same. Therefore, the capabilities of SDBS and SDS are compared. These comparisons will show polarization curve, cell power, capacity and energy of the cell. In this section, the similarity and the difference of the results are described as follows.

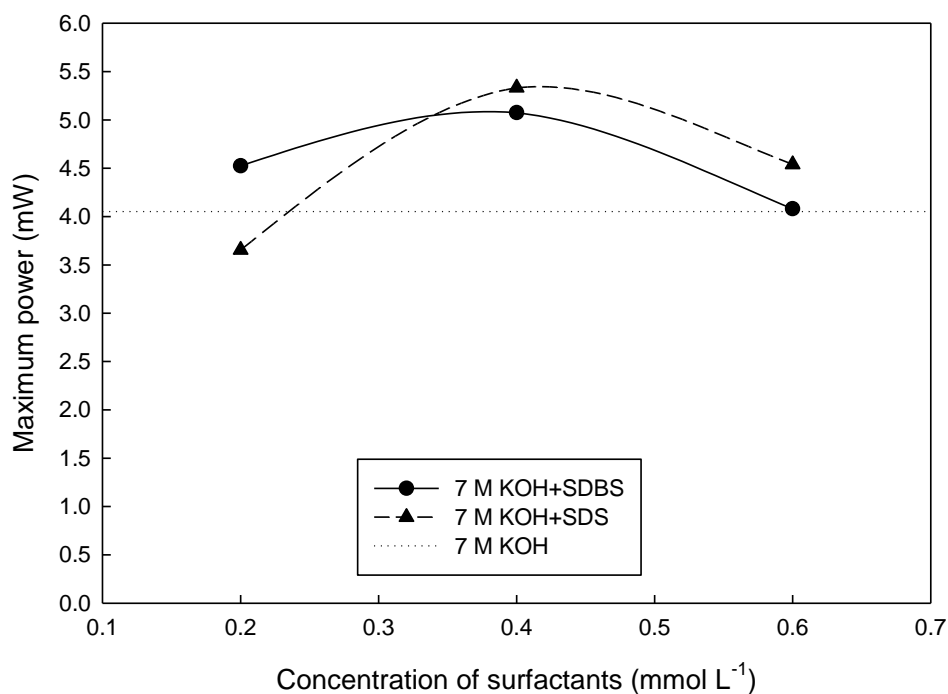
Firstly, polarization curve is discussed. The results from SDBS and SDS utilizations are the same. Polarization curves in ohmic loss region of both SDBS and SDS are nonlinear. The polarization curves of the SDBS and SDS modified electrolytes

reveal that at low and high current density, the slope is quite flat while at the middle current density, the slope is higher. These phenomena occur because SDBS and SDS can reduce the cell resistance. According to the role of surfactants, when surfactants adsorb on the solid by covering zinc surface to protect passive layer deposition. The zinc surface will be modified by surfactant to become more porosity. Then, the wettability of that solid can be improved. Then, the penetrating capability of the electrolyte in zinc electrode is also improved, resulting in the improvement of active ion diffusion. In Figures 5.6 and 5.11, both SDBS and SDS can improve the cell performance in this way except the use of  $0.2 \text{ mmol L}^{-1}$  SDS. Because  $0.2 \text{ mmol L}^{-1}$  SDS is too low concentration for the amount of zinc electrode in the cell, the cell performance was not improved. The comparison of  $0.2 \text{ mmol L}^{-1}$  between SDBS and SDS reveals that the cell behavior with each surfactant is different. It may cause from the CMC of that surfactants. The CMC of SDBS is lower than that of SDS [41]. These CMCs depend on temperature and the solvents [41]. The optimum surface active properties are obtained at the range of CMC point [39]. Therefore,  $0.2 \text{ mmol L}^{-1}$  of SDBS which is in its CMC range can be better surface active properties than  $0.2 \text{ mmol L}^{-1}$  of SDS which is in lower its CMC range. The CMC point is not only considerable parameter, the proper amount of the surfactant to the amount of zinc in the electrode is also important parameter which needs to be considered as well. The results in Figure 5.6 show that the correlation of  $0.4 \text{ mmol L}^{-1}$  SDBS is lower slope than that of  $0.2 \text{ mmol L}^{-1}$  SDBS. It indicates that the zinc electrode needs more SDBS in order to improve the cell performance. In addition,  $0.4 \text{ mmol L}^{-1}$  SDS and  $0.6 \text{ mmol L}^{-1}$  SDS which are in the CMC range can thus be better the cell performance than  $0.2 \text{ mmol L}^{-1}$  SDS.

Furthermore, the cell powers are considered. The results reveal that SDBS and SDS modified electrolytes can improve the cell power. The maximum powers of SDBS and SDS modified electrolytes are higher than that of traditional electrolyte except the use of  $0.2 \text{ mmol L}^{-1}$  SDS as illustrated in Figure 5.15. The maximum power of  $0.2 \text{ mmol L}^{-1}$  SDS is lower than that of  $7 \text{ mol L}^{-1}$  KOH because this concentration is lower than the CMC range of SDS. It indicates that the employment of surfactants in lower CMC range is not beneficial in this case. Moreover, the use of SDS modified electrolyte shows higher maximum power comparing with the use of SDBS modified electrolyte. The maximum powers of both surfactant additives are found at concentration of  $0.4$



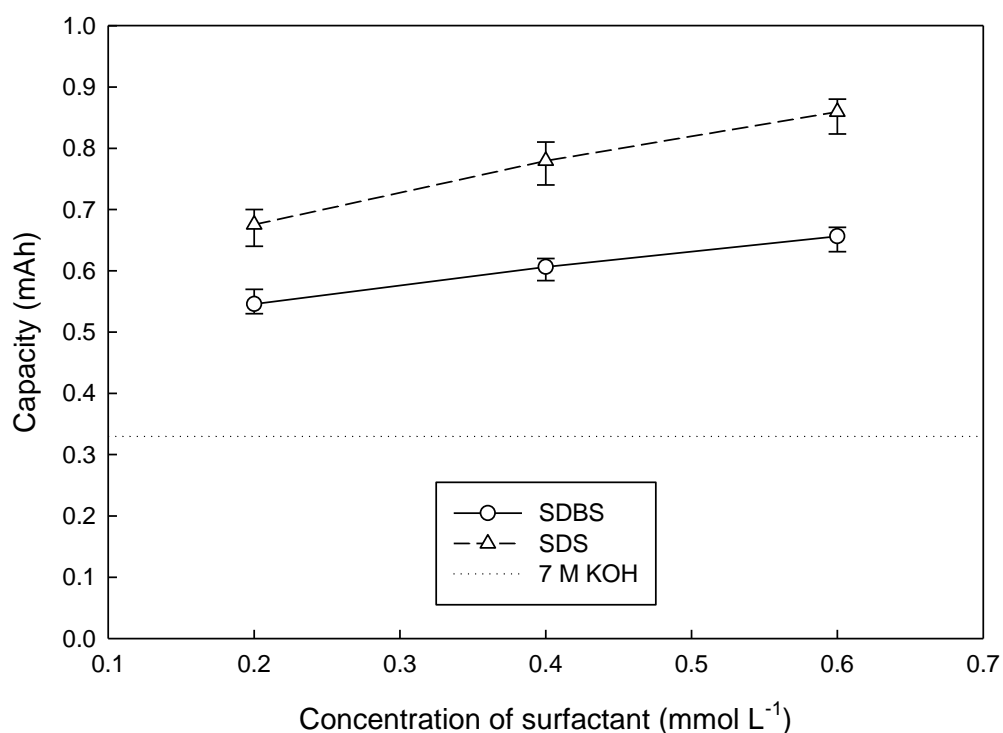
mmol L<sup>-1</sup>. It implies that 0.4 mmol L<sup>-1</sup> is the best concentration comparing with 0.2 mmol L<sup>-1</sup> and 0.6 mmol L<sup>-1</sup> for both surfactants.



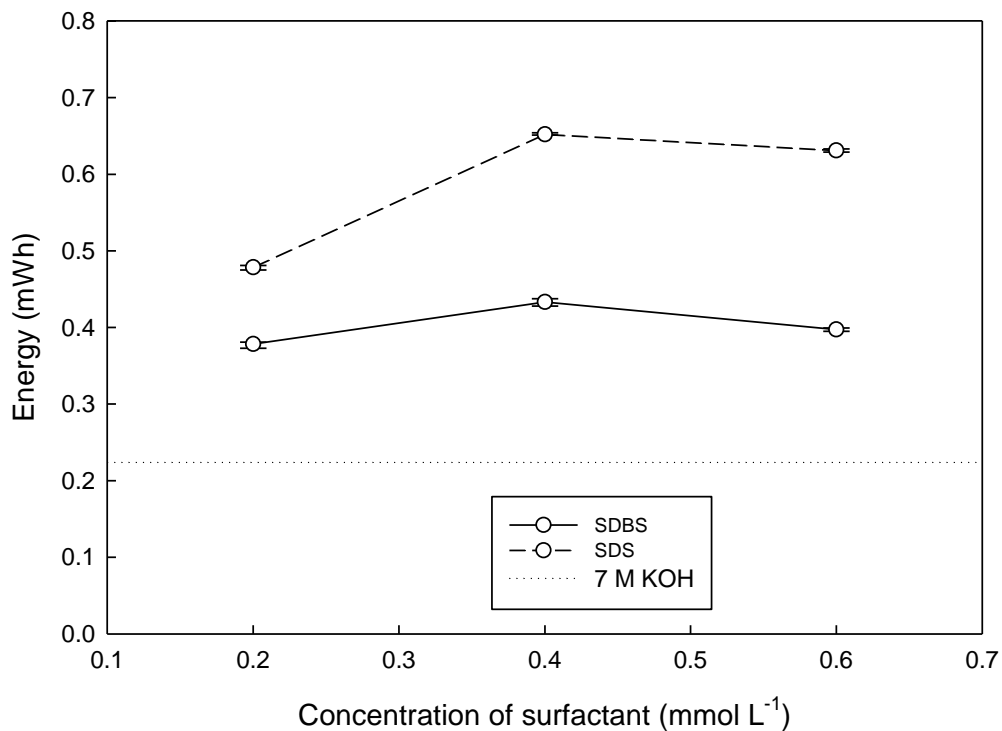
**Figure 5.15** Correlations of surfactant concentration in the electrolytes and maximum cell power for SDBS and SDS in 7 mol L<sup>-1</sup> KOH electrolytes comparing with 7 mol L<sup>-1</sup> KOH electrolyte.

Finally, the capacity and energy of SDBS and SDS are compared. The capacity of SDS modified electrolyte utilization is higher than that of SDBS modified electrolyte utilization for all concentrations. This comparison is illustrated in Figure 5.16. The capacity of both surfactants increases with increase of their concentrations. In addition, it is found that the use of SDBS and SDS modified electrolytes gives higher capacity comparing with 7 mol L<sup>-1</sup> KOH which is the traditional electrolyte (Figure 5.16). It indicates that these modified electrolytes can also enhance zinc utilization. Then, the energy of both modified electrolytes is compared. The results of this comparison are illustrated in Figure 5.17. The energy of SDS modified electrolyte utilization is also higher than that of SDBS modified electrolyte utilization for all concentrations. The reason of these results is SDS is smaller molecule than SDBS, leading to SDS can be

efficiently compacted. Therefore, the cell performance with SDS is better than that with SDBS. Additionally, the energy of both surfactants is higher than that of the traditional electrolyte. It also reveals that SDBS and SDS can help enhancing the battery performance. Moreover, the highest energy is obtained at  $0.4 \text{ mmol L}^{-1}$  for both SDBS and SDS. Therefore, concentration of  $0.4 \text{ mmol L}^{-1}$  is the best concentration comparing with  $0.2 \text{ mmol L}^{-1}$  and  $0.6 \text{ mmol L}^{-1}$  for both surfactants. A specific energy of the flexible printed zinc-air battery with traditional electrolyte is  $22.36 \text{ mWh g}^{-1}$  while specific energies of the batteries with  $0.4 \text{ mmol L}^{-1}$  SDBS and  $0.4 \text{ mmol L}^{-1}$  SDS are  $43.32 \text{ mWh g}^{-1}$  and  $65.21 \text{ mWh g}^{-1}$ , respectively.



**Figure 5.16** Comparison of the capacities of the flexible printed zinc-air battery which employs various concentrations of SDBS and SDS in  $7 \text{ mol L}^{-1}$  KOH electrolytes and  $7 \text{ mol L}^{-1}$  KOH electrolyte by  $1 \text{ mA cm}^{-2}$  constant current discharging.



**Figure 5.17** Comparison of the energies of the flexible printed zinc-air battery which employs various concentrations of SDBS and SDS in 7 mol L<sup>-1</sup> KOH electrolytes and 7 mol L<sup>-1</sup> KOH electrolyte by 1 mA cm<sup>-2</sup> constant current discharging.

### 5.3 Effect of ethanol on surfactant role

According to the results of effects of surfactants on the cell performance which show that the amount of surfactants should correspond to the amount of zinc electrode in the cell. This surfactant amount should be also in the range of its CMC in order to obtain the highest benefit. For example, 0.6 mmol L<sup>-1</sup> SDS in Figure 5.13 shows the highest discharging time which imply that the amount of SDS is sufficient, however, the cell voltage is lower. These phenomena imply that self-aggregation can occur in this concentration, because the concentration is higher than its CMC. Therefore, the addition of a substance to suppress the aggregation or shift CMC of the surfactants is one of the methods which can enhance zinc utilization. In this study, ethanol was selected to suppress the aggregation because it is a common solvent. In addition, the molecular structure of ethanol has both hydrophobic and hydrophilic groups thus it acts

as a surfactant as well. Ethanol was added in the modified electrolyte with the same amount. The results of the ethanol additions in term of polarization curve are illustrated in Figures 5.18 and 5.19.

The addition of ethanol in the modified electrolyte was utilized in the flexible printed zinc-air cells. Then the cells had been analyzed. The results which are illustrated in Figure 5.18 reveal that the use of KOH + SDBS + ethanol as electrolyte shows the same cell behavior as the use of KOH + SDBS. However, the cell voltage is lower than the use of traditional electrolyte in low current density. Because the conductivity of ethanol is poor, the conductivity of the cell reduces in low current density region. For the high current density, the effect of ethanol in term of change in surfactant CMC is presented. The amount of SDBS molecule is sufficient and the concentration also is in the CMC range therefore the cell voltage in this region is higher than that of traditional electrolyte. For SDS surfactant, the result of ethanol addition reveals that the polarization curves are linear for all concentrations as shown in Figure 5.19. In this Figure, the cell voltage of traditional electrolyte is higher than that of KOH + SDS + Ethanol electrolyte. This phenomenon occurs because the conductivity of ethanol is poor. Furthermore, ethanol also acts as a surfactant therefore it competes SDS to adsorb on the zinc surface layer. This competition makes the weak interaction between SDS and zinc surface [42] leading to some of SDS molecules are withdrawn from the zinc surface. Therefore, the addition of ethanol occurs as two mechanisms including of CMC region shifting (aggregation dispersing) and surfactant competing [42]. The conductivity of excess ethanol also needs to be considered.

Moreover, the cell powers of both SDBS and SDS are considered. The results showed that the cell powers of both surfactants are the same behavior. The maximum power is obtained with use of  $0.6 \text{ mmol L}^{-1}$  as illustrated in Figures 5.20 and 5.21. The lower power is obtained with the use of  $0.4 \text{ mmol L}^{-1}$  and  $0.2 \text{ mmol L}^{-1}$ , respectively. This phenomenon is the effect of ethanol conductivity which is rather poor. The same amount of ethanol was added to the modified electrolytes for the same surfactant. The ethanol amount was considered from the amount that can make the white particle on the surface of all modified electrolytes disappears. It results in the amount of the residual ethanol from the micelle dissolution for  $0.6 \text{ mmol L}^{-1}$  of both surfactants is smallest, leading to the internal resistance of the cell is lowest. However, the purpose

of the ethanol addition is to enhance surfactant role. Ethanol will help thoroughly dispersing surfactant aggregation to adsorb on the zinc electrode. Therefore, the addition of ethanol should improve surfactant capability particularly the cell capacity. In this study, constant current mode was used in discharging step. Consequently, the correlations of cell voltage and discharging time are examined as illustrated in Figures 5.22 and 5.23.

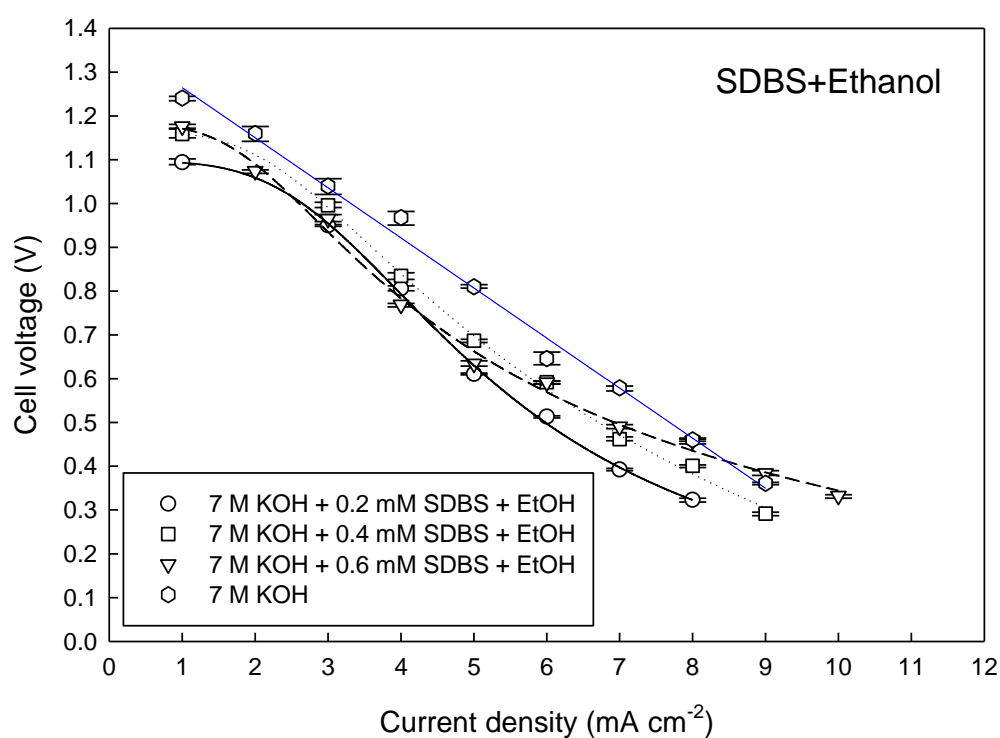


Figure 5.18 Polarization curve of 0.2 mmol L<sup>-1</sup>, 0.4 mmol L<sup>-1</sup> and 0.6 mmol L<sup>-1</sup> SDBS with 20 %v/v ethanol in 7 mol L<sup>-1</sup> KOH electrolytes used in the flexible printed zinc-air battery with effective area of 1 cm<sup>2</sup>.

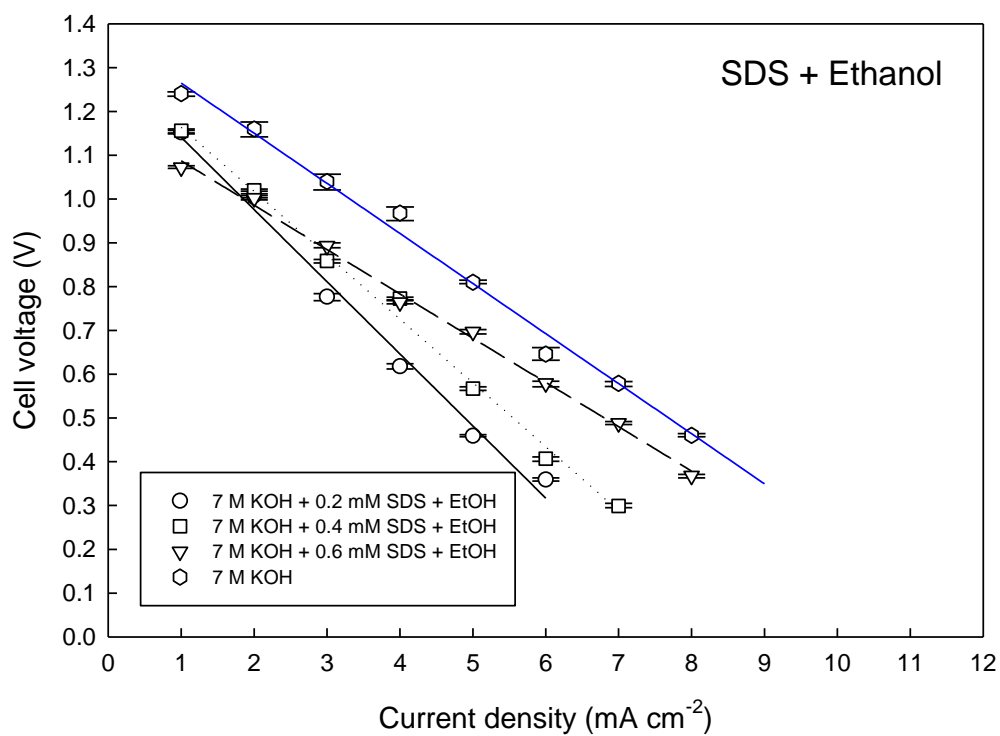
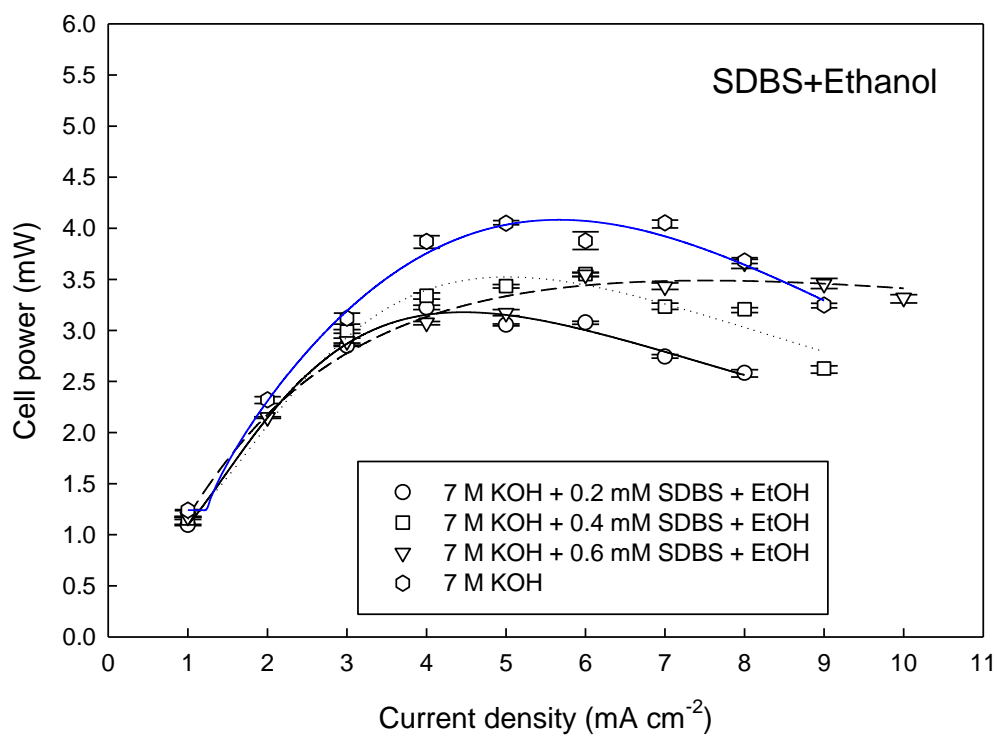
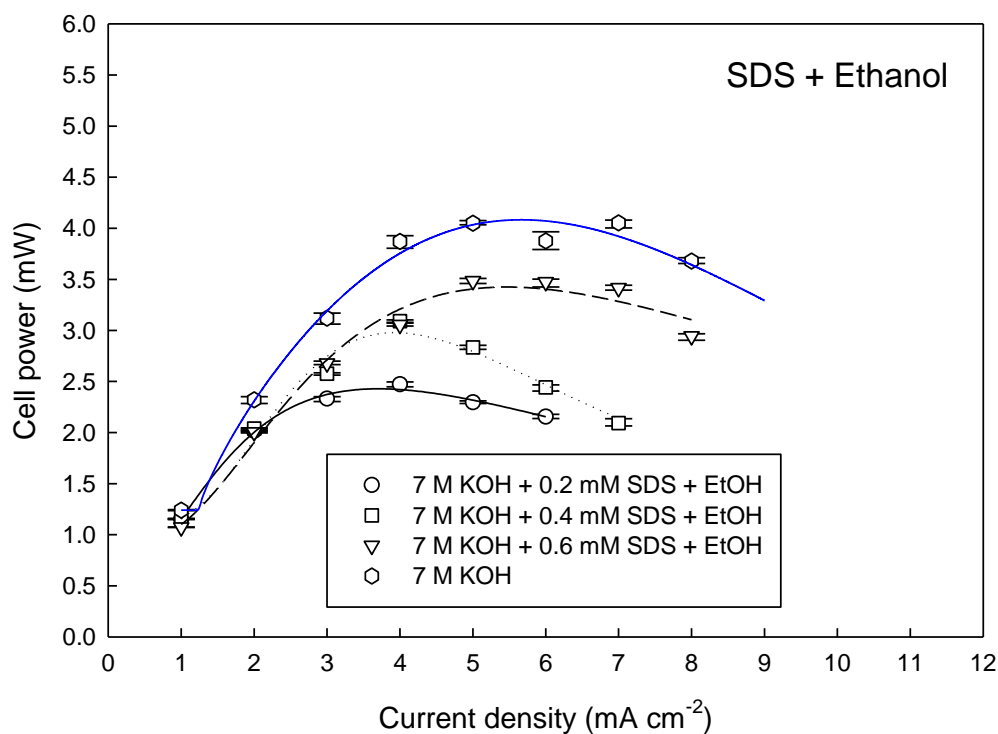


Figure 5.19 Polarization curve of 0.2 mmol L<sup>-1</sup>, 0.4 mmol L<sup>-1</sup> and 0.6 mmol L<sup>-1</sup> SDS with 30 %v/v ethanol in 7 mol L<sup>-1</sup> KOH electrolytes used in the flexible printed zinc-air battery with effective area of 1 cm<sup>2</sup>.



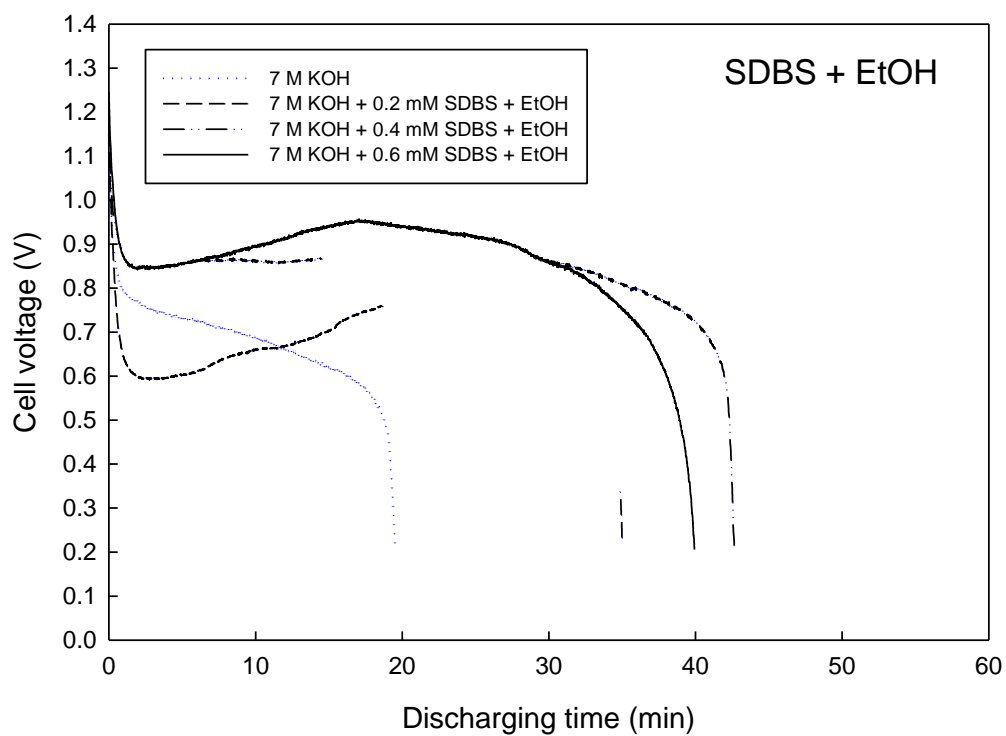
**Figure 5.20** Correlations of current density and cell power of 0.2 mmol L<sup>-1</sup>, 0.4 mmol L<sup>-1</sup> and 0.6 mmol L<sup>-1</sup> SDBS with 20 %v/v ethanol in 7 mol L<sup>-1</sup> KOH electrolytes used in the flexible printed zinc-air battery with effective area of 1 cm<sup>2</sup>.



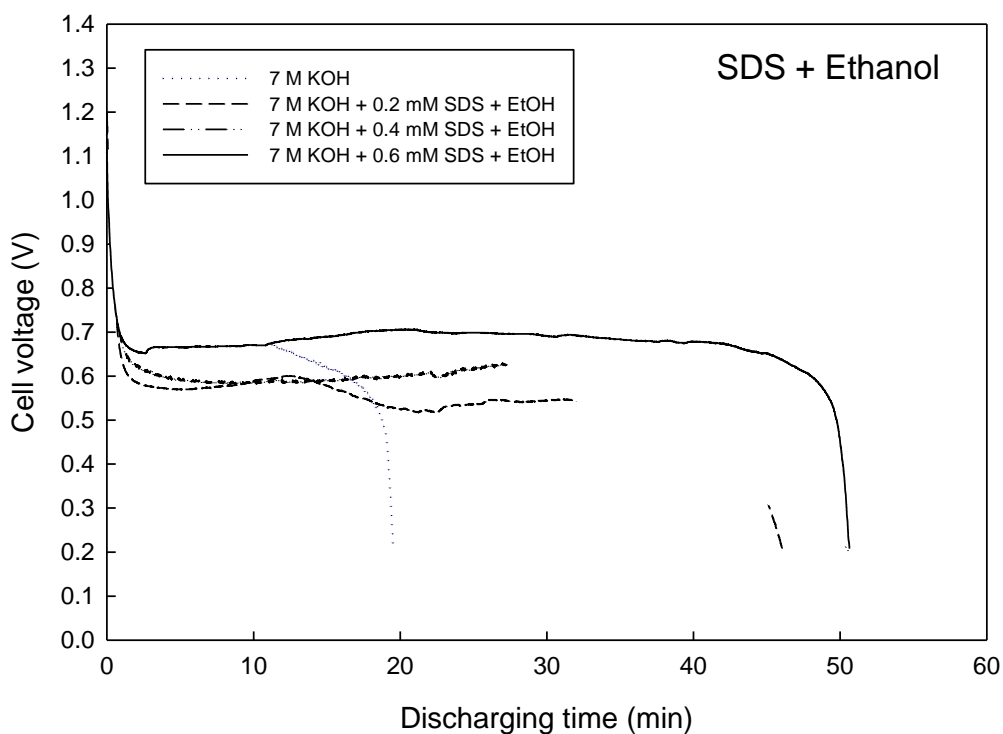
**Figure 5.21** Correlations of current density and cell power of 0.2 mmol L<sup>-1</sup>, 0.4 mmol L<sup>-1</sup> and 0.6 mmol L<sup>-1</sup> SDS with 30% v/v ethanol in 7 mol L<sup>-1</sup> KOH electrolytes used in the flexible printed zinc-air battery with effective area of 1 cm<sup>2</sup>.

Figure 5.22 and Figure 5.23 are compared and the result shows that the addition of ethanol in SDBS electrolyte improves both the cell voltage and discharging time because ethanol helps dispersing SDBS on zinc electrode. Thus, it can impede the micelle formation and can improve SDBS adsorption on the zinc electrode. Therefore, the zinc utilization is enhanced and the cell resistance is also reduced. On the other hand, the addition of ethanol in SDS electrolyte does not improve both the cell voltage and discharging time because ethanol acts as a surfactant in this case. Therefore, ethanol competes SDS to adsorb on zinc surface resulting in the weak interaction between SDS and zinc surface. Some of SDS molecules are withdrawn from the zinc surface. According to previous work, Huang et al. ([42]) presented that ethanol would shift the CMC region of surfactant if that surfactant had large molecular structure. On the other hand, ethanol would compete surfactant adsorption if that surfactant had small molecular structure. Therefore, ethanol affects to SDBS and SDS modified electrolytes in different mechanisms.





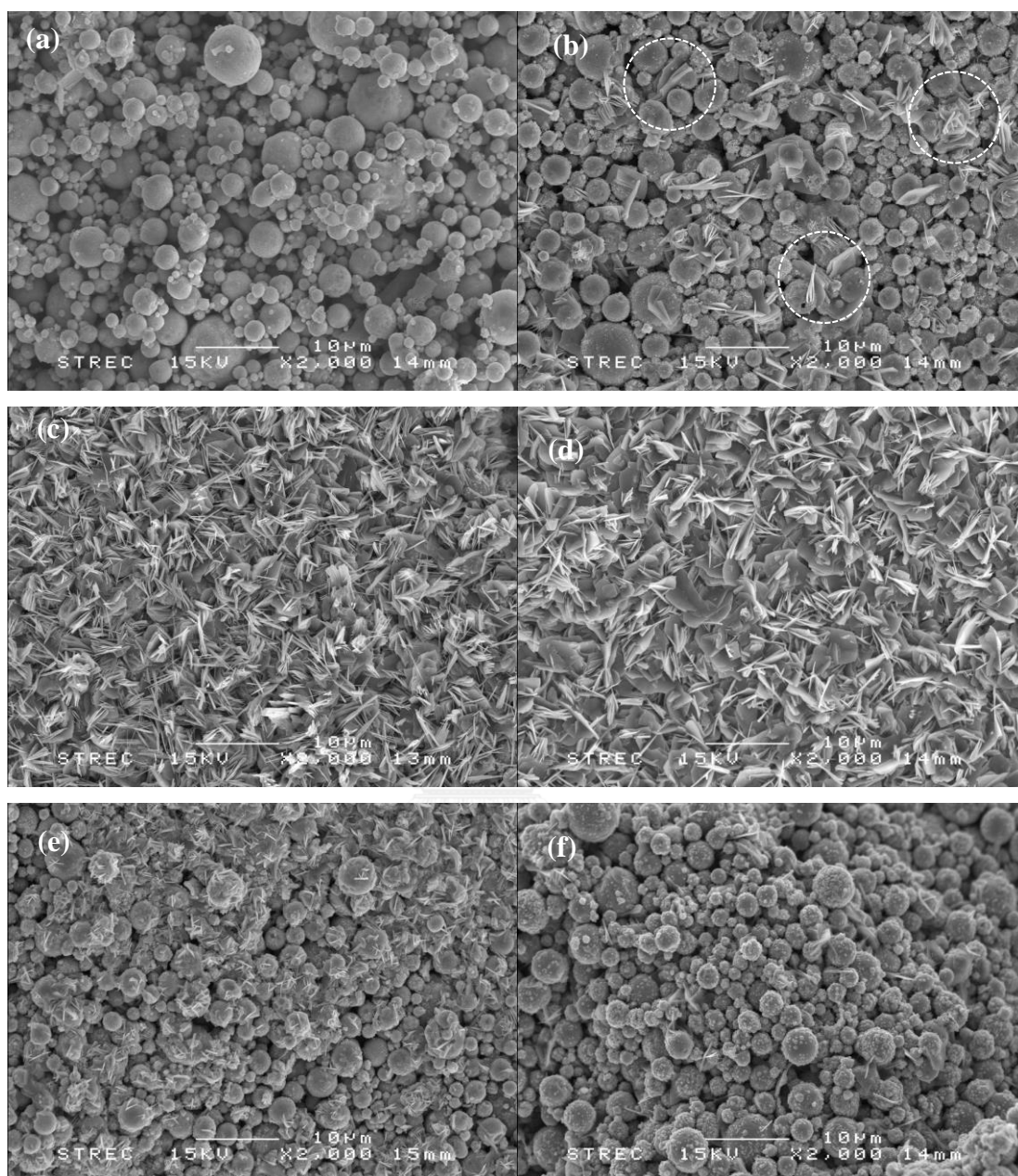
**Figure 5.22** Correlations of cell voltage and discharging time of 0.2 mmol L<sup>-1</sup>, 0.4 mmol L<sup>-1</sup> and 0.6 mmol L<sup>-1</sup> SDBS with 20 %v/v ethanol in 7 mol L<sup>-1</sup> KOH electrolytes used in the flexible printed zinc-air battery with effective area of 1 cm<sup>2</sup> by 1 mA cm<sup>-2</sup> constant current discharging.



**Figure 5.23** Correlations of cell voltage and discharging time of  $0.2 \text{ mmol L}^{-1}$ ,  $0.4 \text{ mmol L}^{-1}$  and  $0.6 \text{ mmol L}^{-1}$  SDS with 30 % v/v ethanol in  $7 \text{ mol L}^{-1}$  KOH electrolytes used in the flexible printed zinc-air battery with effective area of  $1 \text{ cm}^2$  by  $1 \text{ mA cm}^{-2}$  constant current discharging.

#### 5.4 Morphological analysis

In order to comprehend zinc surface electrode modification when the surfactants are added in the electrolyte, the morphology of zinc electrode is investigated. The zinc electrodes from the cell with various modified electrolytes which is completely discharged are analyzed by SEM. These samples consist of 1) zinc electrode before discharge 2) zinc electrode of  $7 \text{ mol L}^{-1}$  KOH electrolyte 3) zinc electrode of  $7 \text{ mol L}^{-1}$  KOH +  $0.4 \text{ mmol L}^{-1}$  SDBS electrolyte 4) zinc electrode of  $7 \text{ mol L}^{-1}$  KOH +  $0.4 \text{ mmol L}^{-1}$  SDS electrolyte 5) zinc electrode of  $7 \text{ mol L}^{-1}$  KOH +  $0.4 \text{ mmol L}^{-1}$  SDBS + ethanol electrolyte and 6) zinc electrode of  $7 \text{ mol L}^{-1}$  KOH +  $0.4 \text{ mmol L}^{-1}$  SDS + ethanol electrolyte. The micrographs of zinc electrodes for all samples are illustrated in Figure 5.24.

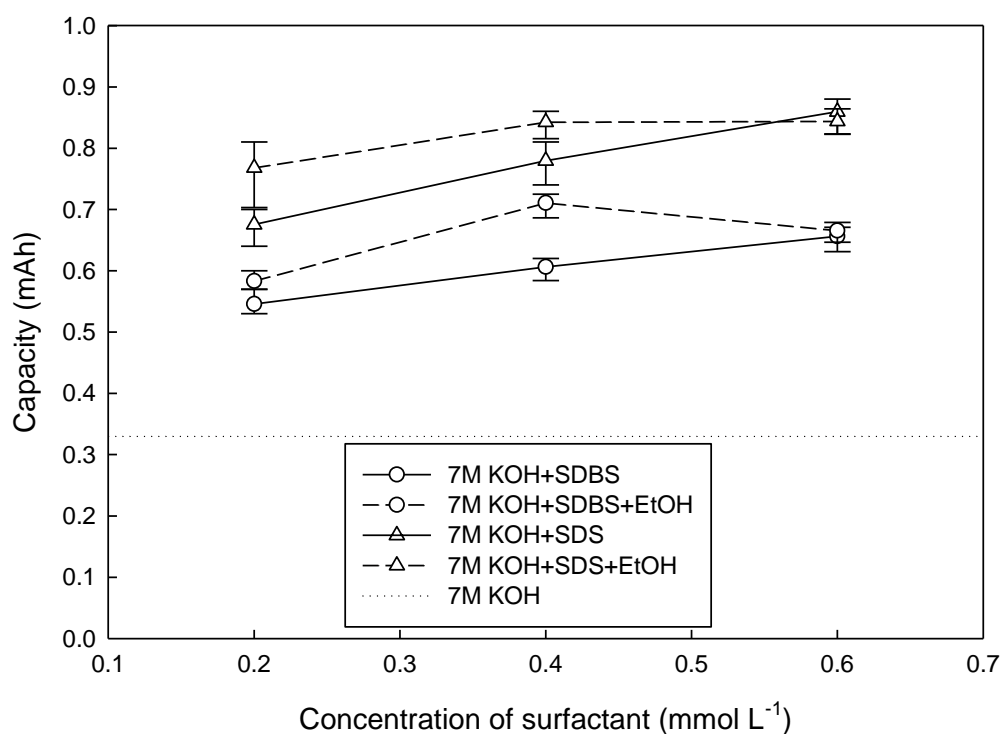


**Figure 5.24** Micrographs of zinc anode by scanning electron microscope: (a) Before discharge (b) The cell discharged in  $7 \text{ mol L}^{-1}$  KOH electrolyte (c) The cell discharged in  $7 \text{ mol L}^{-1}$  KOH +  $0.4 \text{ mmol L}^{-1}$  SDBS electrolyte (d) The cell discharged in  $7 \text{ mol L}^{-1}$  KOH +  $0.4 \text{ mmol L}^{-1}$  SDS electrolyte (e) The cell discharged in  $7 \text{ mol L}^{-1}$  KOH +  $0.4 \text{ mmol L}^{-1}$  SDBS + 20 %v/v ethanol electrolyte (f) The cell discharged in  $7 \text{ mol L}^{-1}$  KOH +  $0.4 \text{ mmol L}^{-1}$  SDS + 30 %v/v ethanol electrolyte.

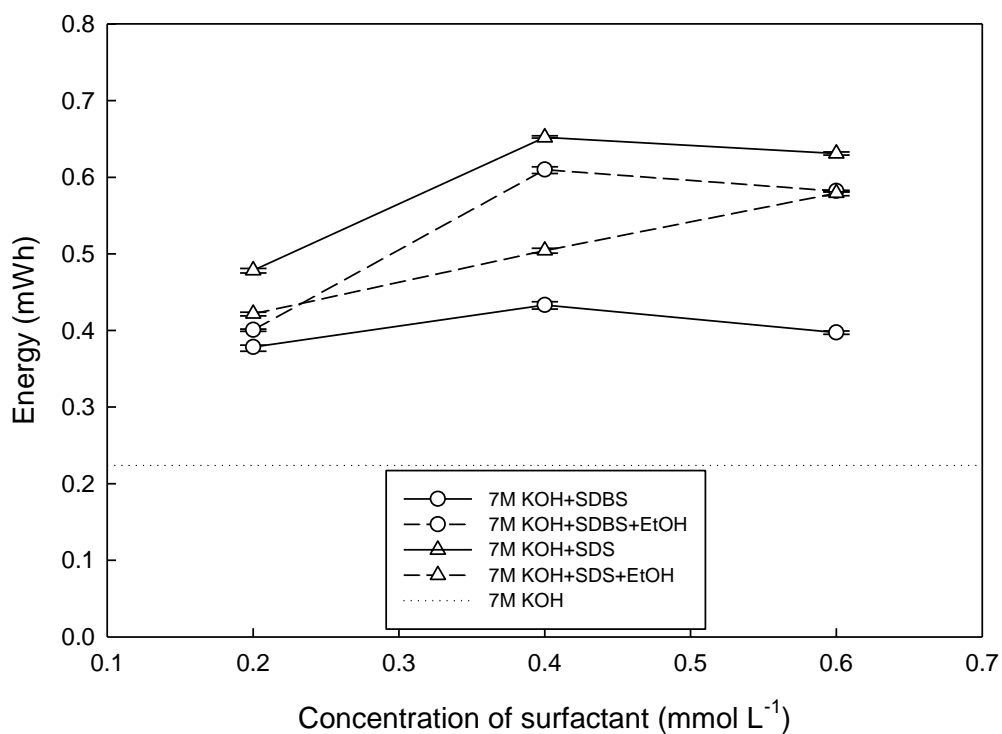
Figure 5.24(a) is a micrograph of zinc surface before discharge. It shows the surface of zinc granules. These granules have the smooth surface. When the cell with 7 mol L<sup>-1</sup> KOH electrolyte had been already discharged, the stacks of surface layers are found. These stacks are the dissolution of zinc which is normal reactions in discharging step as shown in the cycles of Figure 5.24(b). In addition, the partial zinc surface is also found that the porosity of the surface is decreased because the dark gray color is found at surface of the granules and small spots deposit on the granules. This appearance indicates that the zinc electrode is not completely utilized. For the zinc surface after discharging which uses surfactant and KOH as the electrolyte, the zinc surface is obviously modified. The granules of the normal zinc surface disappear. However, the stacks of surface layers which are the normal discharging appearance are thoroughly found in both SDBS (Figure 5.24(c)) and SDS utilizations (Figure 5.24 (d)). It indicates that SDBS and SDS can enhance zinc utilization. Furthermore, the needle-like crystallized structure is also found. This appearance agrees with previous research by Yang et al [22]. The zinc surface morphology is modified by SDBS and SDS resulting in higher porosity. The higher porosity of zinc electrode leads to more penetration of the electrolyte to the zinc electrode. Moreover, SDBS and SDS also suppress passive film because the small spots are not found on the zinc surface as illustrated in Figures 5.24(c) and 5.24(d), respectively. For the addition of ethanol in the SDBS modified electrolyte, the surface of zinc electrode which is completely discharged shows the granules of normal zinc surface. The porosity of the zinc surface is also close to the zinc surface before discharge. Additionally, the needle-like crystallized structure which is high porosity is also found as illustrated in Figure 5.24(e). It indicates that the addition of ethanol can improve SDBS capability. Finally, the addition of ethanol in the SDS modified electrolyte results in the surface of zinc electrode as illustrate in Figure 5.24(f). The zinc surface in Figure 5.24(f) shows that the granules of zinc are found. This appearance is the effect of SDS withdrawal resulted from the competition of ethanol to adsorb on zinc surface as aforementioned descriptions. Therefore, the morphology of zinc surface does not change.

## 5.5 All effects summary

In order to compare the battery performance, capacity and energy need to be considered. Therefore, capacity and energy of SDBS and SDS with and without ethanol for modifying electrolyte are taken into account. The correlations of surfactant concentration and capacity are illustrated in Figure 5.25. Also, the correlation of surfactant concentration and energy are illustrated in Figure 5.26.



**Figure 5.25** Correlations of current density and capacity of all experiments by 1 mA cm<sup>-2</sup> constant current discharging.



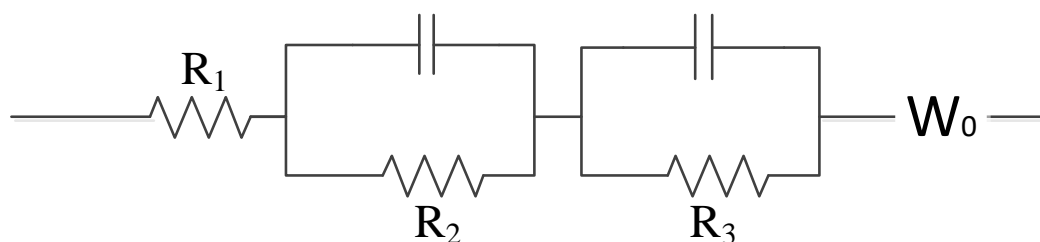
**Figure 5.26** Correlations of current density and energy of all experiments by 1 mA cm<sup>-2</sup> constant current discharging.

Figure 5.25 reveals that the addition of SDBS and SDS in traditional electrolyte significantly improves capacity of the battery. The capacity increases with increasing the surfactant concentration for the modified electrolyte without ethanol. In addition, the addition of SDS is higher capacity than that of SDBS. Furthermore, the capacity of SDBS modified electrolyte with ethanol is slightly higher than the modified electrolyte without ethanol. Similarly, the capacity of SDBS modified electrolyte with ethanol slightly increases except at 0.6 mmol L<sup>-1</sup> SDS. The energy of each surfactant with and without ethanol is considered in Figure 5.26. The results reveal that the addition of both SDBS and SDS in an electrolyte significantly improves the energy. The highest energy is obtained from the use of SDS without ethanol. The lower energy is obtained from the use of SDBS with ethanol, SDS with ethanol and SDBS without ethanol, respectively. Moreover, the proper concentration of surfactants for flexible printed zinc-air battery which fabricates electrode by print screen technique is 0.4 mmol L<sup>-1</sup>. The important parameters that affect the battery performance consist of 1) molecular structure of the

surfactant 2) amount of surfactant usage and its CMC. These parameters result in the self-aggregation of the surfactant and the amount of zinc electrode which surfactant will adsorb. In this study, because flexible printed zinc-air battery was used, the zinc electrode and the volume of electrolyte usage per effective area are quite constant. Therefore, the mole of surfactant is only defined as concentration. For the addition of ethanol, it will help improving the battery performance when the surfactant with the large molecular structure is employed.

## 5.6 Electrochemical impedance investigation

Electrochemical impedance spectroscopy (EIS) is employed to investigate the battery performance. In this study, the range of frequency which is employed is 10 kHz to 0.1 Hz with amplitude of 10 mV. For zinc air battery, the equivalent circuit model that shows in Figure 5.27 is used to explain the electrochemical cell configuration [43]. The term impedance of EIS is the frequency dependent resistance of current flow passed through circuit element (resistor, capacitor, inductor, etc.). Impedance assumes an AC current of specific frequency in Hertz which is cycles per second. In a zinc-air battery, zinc anode side is higher reaction rate than air cathode side therefore, zinc anode reaction effect is expressed in high frequency. From the equivalent circuit, the elements are described as follows.  $R_1$  represents the internal resistance of the cell which is total ohmic resistance of the cell [43, 44]. These internal resistances are shown at the real axis ( $Z'$ ) intercept of the impedance spectra at high frequency.  $R_2$  is associated with the anode reaction (redox reaction of zinc).  $R_3$  is associated with the cathode reaction (redox reaction of oxygen in the air) [44]. Warburg impedance ( $W_o$ ) represents the diffusion element in relatively low-frequency. In this study, the battery cell with various concentrations of SDBS and SDS modified electrolytes are investigated by EIS. The results of all parameters from equivalent circuit model are reveals in Table 5.1. In addition, the Nyquist plots of the cell with SDBS, SDS, SDBS+ethanol and SDS+ethanol are illustrated in Figures 5.28 -5.31, respectively.

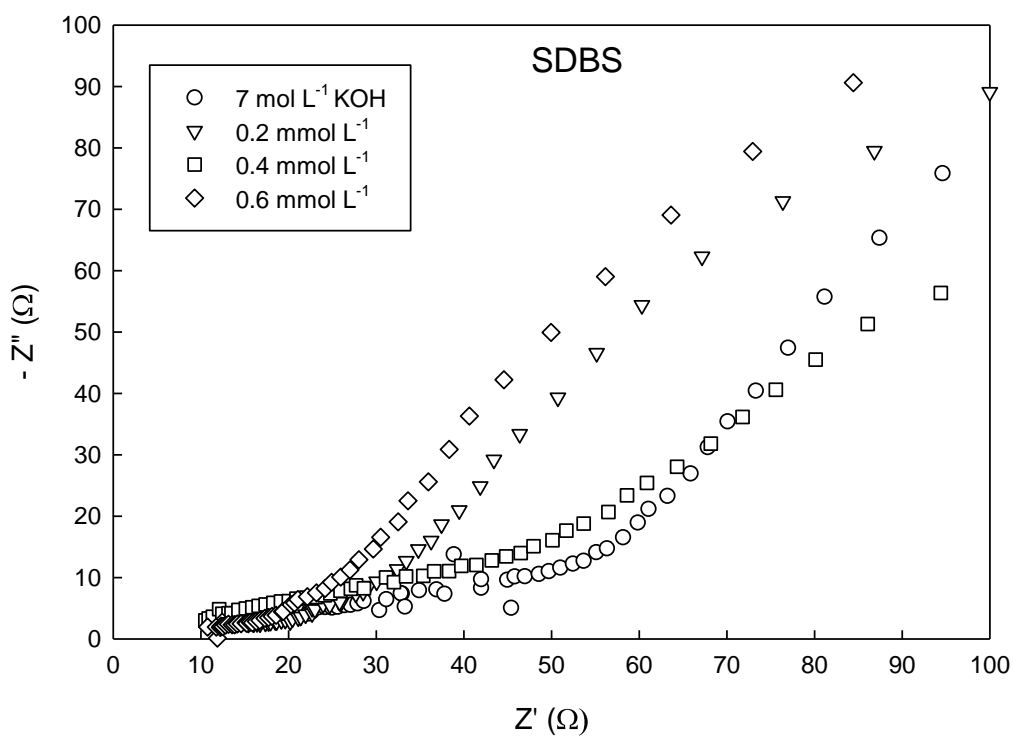


**Figure 5.27** Equivalent circuit model of zinc-air battery.

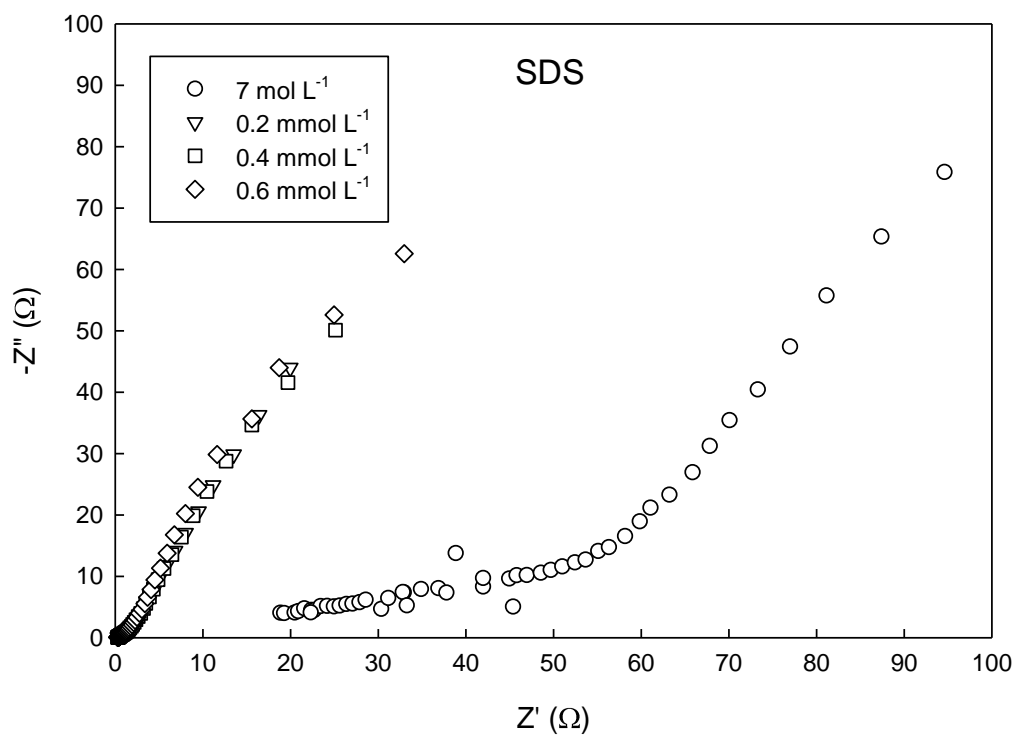
**Table 5.1** All impedances from equivalent circuit model of zinc-air battery.

| Substance         | Concentration<br>(mmol L <sup>-1</sup> ) | R <sub>1</sub><br>(Ω) | R <sub>2</sub><br>(Ω) | R <sub>3</sub><br>(Ω) | W <sub>0</sub><br>(S.sec <sup>5</sup> ) |
|-------------------|--|-----------------------|-----------------------|-----------------------|---|
| KOH               | 7 x 10 <sup>3</sup>                      | <b>17.9500</b>        | <b>12.5200</b>        | 8.7820                | 0.0125                                  |
|                   | 0.2                                      | <b>13.3600</b>        | <b>5.6710</b>         | 51.1900               | 0.0106                                  |
|                   | 0.4                                      | <b>10.1900</b>        | <b>4.0546</b>         | 13.7500               | 0.0118                                  |
| SDBS              | 0.6                                      | <b>11.3540</b>        | <b>4.1536</b>         | 100.2450              | 0.0123                                  |
|                   | 0.2                                      | <b>0.2805</b>         | <b>0.1955</b>         | 126.6000              | 0.0780                                  |
|                   | 0.4                                      | <b>0.2561</b>         | <b>0.1530</b>         | 125.0000              | 0.0716                                  |
| SDS               | 0.6                                      | <b>0.2531</b>         | <b>0.1646</b>         | 147.3000              | 0.0684                                  |
|                   | 0.2                                      | <b>1.2239</b>         | <b>0.9782</b>         | 2.3020                | 0.0329                                  |
|                   | 0.4                                      | <b>1.0130</b>         | <b>0.4341</b>         | 3.0730                | 0.0146                                  |
| SDBS +<br>Ethanol | 0.6                                      | <b>1.1690</b>         | <b>0.4786</b>         | 0.5860                | 0.0291                                  |
|                   | 0.2                                      | <b>5.1440</b>         | <b>4.1650</b>         | 29.8500               | 0.0281                                  |
|                   | 0.4                                      | <b>6.5570</b>         | <b>2.6550</b>         | 4.6670                | 0.0150                                  |
| SDS +<br>Ethanol  | 0.6                                      | <b>2.5650</b>         | <b>1.4420</b>         | 2.7050                | 0.0182                                  |

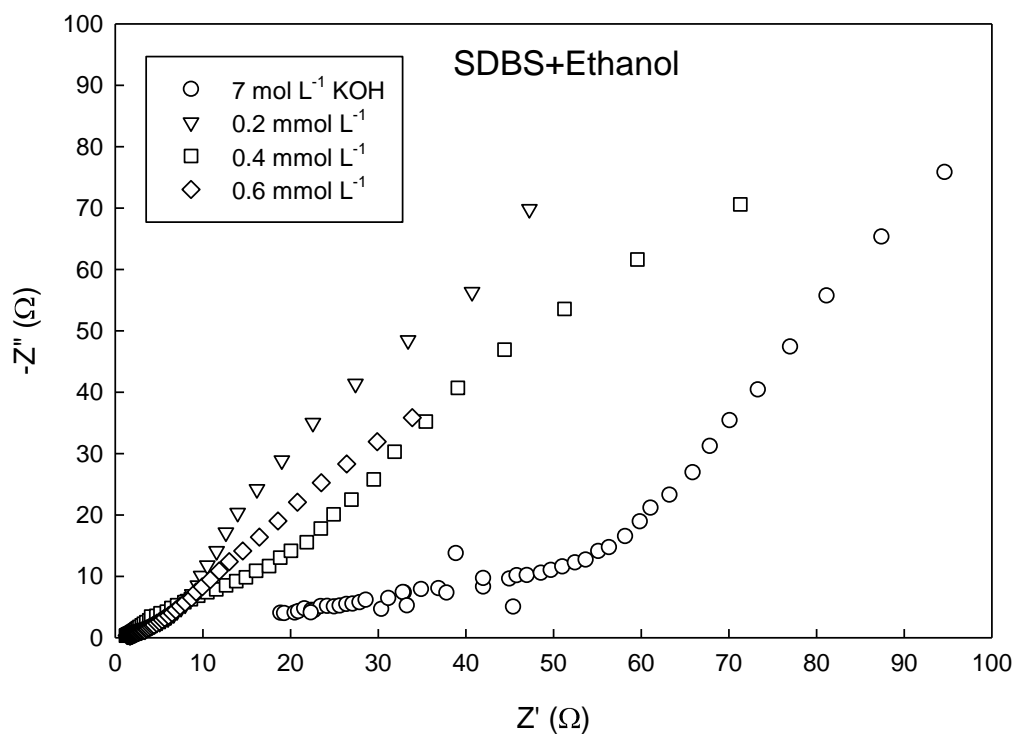




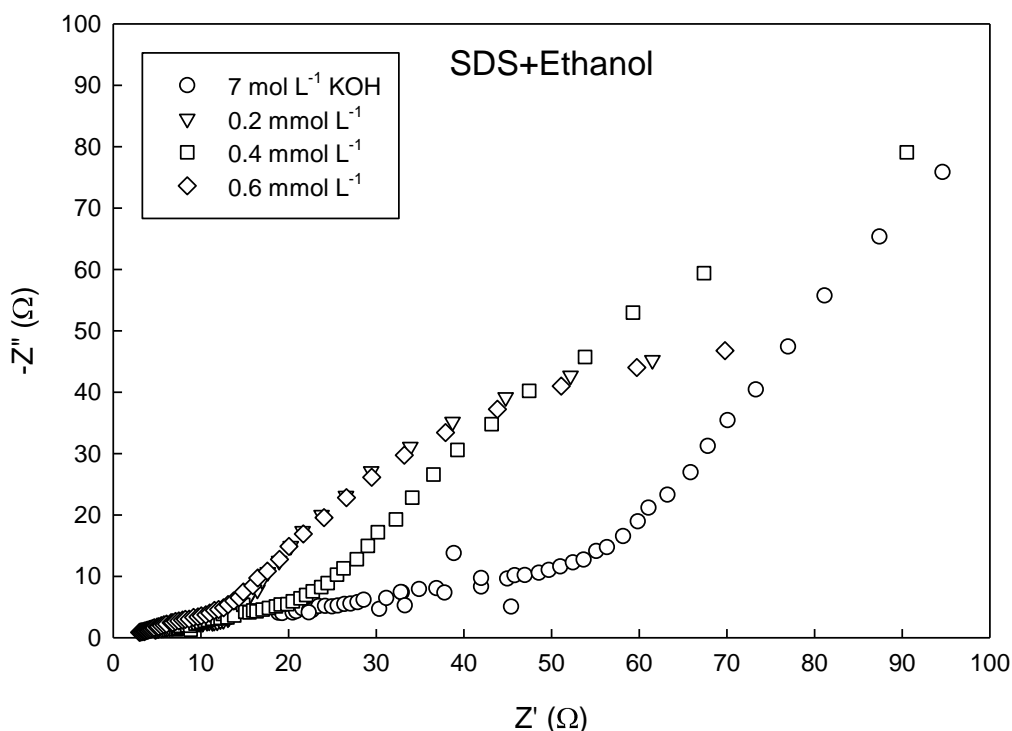
**Figure 5.28** The Nyquist plots of the flexible printed zinc-air battery using 0.2 mmol L<sup>-1</sup>, 0.4 mmol L<sup>-1</sup> and 0.6 mmol L<sup>-1</sup> SDBS in 7 mol L<sup>-1</sup> KOH electrolytes comparing with 7 mol L<sup>-1</sup> KOH electrolyte by 1 mA cm<sup>-2</sup> constant current discharging in frequency range of 0.1 Hz to 10 kHz.



**Figure 5.29** The Nyquist plots of the flexible printed zinc-air battery using 0.2 mmol L<sup>-1</sup>, 0.4 mmol L<sup>-1</sup> and 0.6 mmol L<sup>-1</sup> SDS in 7 mol L<sup>-1</sup> KOH electrolytes comparing with 7 mol L<sup>-1</sup> KOH electrolyte by 1 mA cm<sup>-2</sup> constant current discharging in frequency range of 0.1 Hz to 10 kHz.



**Figure 5.30** The Nyquist plots of the flexible printed zinc-air battery using  $0.2 \text{ mmol L}^{-1}$ ,  $0.4 \text{ mmol L}^{-1}$  and  $0.6 \text{ mmol L}^{-1}$  SDBS with 20 %v/v ethanol in  $7 \text{ mol L}^{-1}$  KOH electrolytes comparing with  $7 \text{ mol L}^{-1}$  KOH electrolyte by  $1 \text{ mA cm}^{-2}$  constant current discharging in frequency range of 0.1 Hz to 10 kHz.



**Figure 5.31** The Nyquist plots of the flexible printed zinc-air battery using 0.2 mmol L<sup>-1</sup>, 0.4 mmol L<sup>-1</sup> and 0.6 mmol L<sup>-1</sup> SDS with 30 %v/v ethanol in 7 mol L<sup>-1</sup> KOH electrolytes comparing with 7 mol L<sup>-1</sup> KOH electrolyte by 1 mA cm<sup>-2</sup> constant current discharging in frequency range of 0.1 Hz to 10 kHz.

Consider Table 5.1, the parameter which denotes the redox reaction of zinc anode is  $R_1$  and  $R_2$ . Therefore,  $R_1$  and  $R_2$  are focused in this consideration. The results show that  $R_1$  corresponds with  $R_2$ . The tendency of  $R_1$  is similar to that of  $R_2$ . The highest  $R_1$  and  $R_2$  are found when the cell with 7 mol L<sup>-1</sup> KOH is examined. It indicates that the passive film occurs, resulting in performance degradation of zinc anode. Subsequently, the cells with SDBS modified electrolytes have higher  $R_1$  and  $R_2$  than the others.  $R_1$  and  $R_2$  of the cell with 0.2 mmol L<sup>-1</sup> SDBS modified electrolyte is higher than that of the cells with 0.4 mmol L<sup>-1</sup> and 0.6 mmol L<sup>-1</sup> SDBS modified electrolyte which have quite similar  $R_1$  and  $R_2$ . These results are also illustrated in Figure 5.28. Then, the next lower  $R_1$  and  $R_2$  is  $R_1$  and  $R_2$  of SDS + ethanol modified electrolyte. The high concentration results in the low  $R_1$  and  $R_2$ . The Nyquist plot of the cell with SDS + ethanol modified electrolyte is illustrated in Figure 5.31 which corresponds with the results from section 5.3. The next lower  $R_1$  and  $R_2$  from SDS+ ethanol modified

electrolyte is SDBS + ethanol modified electrolyte. The Nyquist plot of the cell with SDBS + ethanol modified electrolyte (Figure 5.30) illustrates that all concentrations have nearly similar impedance. Finally, the lowest  $R_1$  and  $R_2$  are obtained with the cell using SDS modified electrolyte as shown in Table 5.1 and Figure 5.29. Consequently, the sequence of  $R_1$  and  $R_2$  from EIS is  $R_1$  and  $R_2$  of the cells with SDBS > SDS+ethanol > SDBS+ethanol > SDS. These results agree with the aforementioned results. However,  $R_3$  which is the resistance of cathode reactions need to be finely studied in order to clearly comprehend because the results in Table 5.1 show the effect of these modified electrolytes on  $R_3$ .



# CHAPTER VI

## CONCLUSIONS

### 6.1 Conclusions

In this research, electrolyte system of the zinc-air battery was studied in order to improve the battery performance. Due to the big difference between theoretical and practical capacity, enhancement of zinc utilization is focused. The flexible printed zinc-air battery was employed because of its simplicity, high throughput. Firstly, the effect of potassium hydroxide (KOH) concentration which is the traditional electrolyte on the cell performance was studied. The optimum KOH concentration would be obtained in this investigation and would be used in the electrolyte modification. Then the electrolyte was modified by adding the surfactants. These surfactants consist of sodium dodecylbenzenesulfonate (SDBS) and sodium dodecyl sulfate (SDS) which are anionic surfactants. In addition, an ethanol was employed to improve the surfactant role. For the battery analysis and characterization, battery analyzer and electrochemical impedance spectroscopy were used to analyze the battery performance. Scanning electron microscope was employed to analyze the morphology of zinc electrode.

The results of KOH concentration effect show that 5 mol L<sup>-1</sup> KOH is too low concentration because the lower capacity and energy is obtained. This phenomenon occurs because the low KOH concentration leads to high passive film. In addition, 9 mol L<sup>-1</sup> KOH is too high concentration which results in too much zinc dissolution. Therefore, 7 mol L<sup>-1</sup> KOH is the optimal concentration in term of both low passive film and high conductivity. The KOH concentration of 7 mol L<sup>-1</sup> KOH was thus used for electrolytes modification.

For the electrolyte modifications, the results show that the use of SDBS and SDS as the additives in traditional electrolyte enhances the zinc utilization because they improve the wettability of the zinc electrode. Therefore, the electrolyte can easily penetrate to the zinc electrode, leading to better diffusion of active species. Moreover, the morphology of the zinc electrode was modified by using both SDBS and SDS.

These modifications are increase in zinc porosity and passive film suppression. Furthermore the results reveal that SDBS and SDS double the capacity and energy compared with the traditional electrolyte. The best concentration of both SDBS and SDS is  $0.4 \text{ mmol L}^{-1}$  comparing with  $0.2 \text{ mmol L}^{-1}$  and  $0.6 \text{ mmol L}^{-1}$ . However, the amount of surfactants has to be sufficient for the zinc electrode. Additionally, because SDBS and SDS have low CMC, ethanol is employed to solve this limitation. The results show that ethanol can improve surfactant role when the surfactant concentration is higher than CMC and the surfactant molecule with the large molecular structure is employed. However, the addition of ethanol is not only ineffective but it also disturbs the battery when the surfactant molecule with the small molecular structure is employed. Finally, all the modified electrolytes are compared in term of the zinc anode resistance by using EIS. The results reveal that the zinc anode resistance with SDBS modified electrolytes is higher than that with SDS+ethanol modified electrolytes which is higher than that with SDBS+ethanol modified electrolytes. The lowest zinc anode resistance is obtained when the battery cell with SDS modified electrolytes are used. However, to appropriately select the surfactants, the cost of surfactant also needs to be considered.

## 6.2 Recommendations for the future work

1. The effects of all electrolyte modifications on the air electrode (cathode) need to be studied because the results from EIS show the effects of modified electrolyte on the cathode.
2. Modification of zinc electrode by the surfactants is interesting to study because it can also improve the zinc surface.
3. The effects of ethanol concentration in the modified electrolyte on the cell performance have to be studied.

## REFERENCES

- [1] Lee, J.-S., et al. Metal-Air Batteries with High Energy Density: Li-Air versus Zn-Air. Advanced Energy Materials 1(1) (2011): 34-50.
- [2] Lee, S.-H., Park, D.-J., Yang, W.-G., and Ryu, K.-S. Comparison of electrochemical performance for zinc anode via various electrolytes and conducting agents in Zn-air secondary batteries. Ionics (2017).
- [3] Li, Y. and Dai, H. Recent advances in zinc-air batteries. Chem Soc Rev 43(15) (2014): 5257-75.
- [4] Wang, K., Pei, P., Ma, Z., Xu, H., Li, P., and Wang, X. Morphology control of zinc regeneration for zinc-air fuel cell and battery. Journal of Power Sources 271 (2014): 65-75.
- [5] Pei, P., Wang, K., and Ma, Z. Technologies for extending zinc-air battery's cyclelife: A review. Applied Energy 128 (2014): 315-324.
- [6] Park, S., Vosguerichian, M., and Bao, Z. A review of fabrication and applications of carbon nanotube film-based flexible electronics. Nanoscale 5(5) (2013): 1727-52.
- [7] Grau, G., Cen, J., Kang, H., Kitsomboonloha, R., Scheideler, W.J., and Subramanian, V. Gravure-printed electronics: recent progress in tooling development, understanding of printing physics, and realization of printed devices. Flexible and Printed Electronics 1(2) (2016): 023002.
- [8] Suren, S. and Kheawhom, S. Development of a High Energy Density Flexible Zinc-Air Battery. Journal of The Electrochemical Society 163(6) (2016): A846-A850.
- [9] Xu, M., Ivey, D.G., Xie, Z., and Qu, W. Rechargeable Zn-air batteries: Progress in electrolyte development and cell configuration advancement. Journal of Power Sources 283 (2015): 358-371.
- [10] Wang, J.M., Zhang, L., Zhang, C., and Zhang, J.Q. Effects of bismuth ion and tetrabutylammonium bromide on the dendritic growth of zinc in alkaline zincate solutions. Journal of Power Sources 102 (2001): 139-143.
- [11] Xu, M., Ivey, D.G., Qu, W., and Xie, Z. Improved Zn/Zn(II) redox kinetics, reversibility and cyclability in 1-ethyl-3-methylimidazolium dicyanamide with water and dimethyl sulfoxide added. Journal of Power Sources 252 (2014): 327-332.
- [12] Bass, K., Mitchell, P.J., and Wilcox, G.D. Methods for the reduction of shape change and dendritic growth in zinc-based secondary cells. Journal of Power Sources 35 (1991): 333-351.
- [13] R. Mainar, A., et al. Alkaline aqueous electrolytes for secondary zinc-air batteries: an overview. International Journal of Energy Research 40(8) (2016): 1032-1049.
- [14] Farn, R.J. Chemistry and Technology of Surfactants. Oxford, United Kindom: Blackwell Publishing Ltd., 2006.
- [15] Tehrani, Z., et al. Ultra-thin flexible screen printed rechargeable polymer battery for wearable electronic applications. Organic Electronics 26 (2015): 386-394.
- [16] Hilder, M., Winther-Jensen, B., and Clark, N.B. Paper-based, printed zinc-air battery. Journal of Power Sources 194(2) (2009): 1135-1141.



- [17] Wendler, M., Hubner, G., and Krebs, M. Development of printed thin and flexible batteries [Online]. 2010. Available from: [https://www.hdm-stuttgart.de/international\\_circle/circular/issues/11\\_01/ICJ\\_04\\_32\\_wendler\\_huber\\_krebs.pdf](https://www.hdm-stuttgart.de/international_circle/circular/issues/11_01/ICJ_04_32_wendler_huber_krebs.pdf) [November 1, 2016]
- [18] Berchmans, S., Bandodkar, A.J., Jia, W., Ramírez, J., Meng, Y.S., and Wang, J. An epidermal alkaline rechargeable Ag–Zn printable tattoo battery for wearable electronics. J. Mater. Chem. A 2(38) (2014): 15788-15795.
- [19] Mokaddem, M., Volovitch, P., and Ogle, K. The anodic dissolution of zinc and zinc alloys in alkaline solution. I. Oxide formation on electrogalvanized steel. Electrochimica Acta 55(27) (2010): 7867-7875.
- [20] Macdonald, D.D. The history of the Point Defect Model for the passive state: A brief review of film growth aspects. Electrochimica Acta 56(4) (2011): 1761-1772.
- [21] Chakkaravarthy, C., Waheed, A.K.A., and Udupa, H.V.K. Zinc-air alkaline batteries-a review. Journal of Power Sources 6 (1981): 203-228.
- [22] Yang, H. Improved discharge capacity and suppressed surface passivation of zinc anode in dilute alkaline solution using surfactant additives. Journal of Power Sources 128(1) (2004): 97-101.
- [23] Ghavami, R.K., Rafiei, Z., and Tabatabaei, S.M. Effects of cationic CTAB and anionic SDBS surfactants on the performance of Zn–MnO<sub>2</sub> alkaline batteries. Journal of Power Sources 164(2) (2007): 934-946.
- [24] Bass, K. and Mitchell, P.J. The performance of secondary zinc electrodes in modified alkaline electrolytes I. Galvanostatic passivation studies in alkaline electrolyte. Journal of Power Sources 39 (1992): 237-284.
- [25] Huh, T., Savaskan, G., and EVANS, J.W. Further studies of a zinc-air cell employing a packed bed anode Part II: Regeneration of zinc particles and electrolyte by fluidized bed electrodeposition Journal of Applied Electrochemistry 22 (1992): 916-921.
- [26] Mcbreen, J. and Gannon, E. Bismuth oxide as an additive in pasted zinc electrodes. Journal of Power Sources 15 (1985): 169-177.
- [27] Sharmaa, Y., Azizb, M., Yusofb, J., and Kordeschc, K. Triethanolamine as an additive to the anode to improve the rechargeability of alkaline manganese dioxide batteries. Journal of Power Sources 94 (2001): 129-131.
- [28] Wilcox, G.D. and Mitchell, P.J. Electrolyte additives for zinc-anoded secondary cells II. quaternary ammonium compounds. Journal of Power Sources 32 (1990): 31-41.
- [29] Ghavami, R.K. and Rafiei, Z. Performance improvements of alkaline batteries by studying the effects of different kinds of surfactant and different derivatives of benzene on the electrochemical properties of electrolytic zinc. Journal of Power Sources 162(2) (2006): 893-899.
- [30] Shivkumar, R., Kalaignan, G.P., and Vasudevan, T. Effect of additives on zinc electrodes in alkaline battery system. Journal of Power Sources 55 (1995): 53-62.
- [31] Vassal, N., Salmon, E., and Fauvarque, J.-F. Electrochemical properties of an alkaline solid polymer electrolyte based on P(ECH-co-EO) Electrochimica Acta 45 (2000): 1527-1532.

- [32] Deng, M.-J., Chen, P.-Y., and Sun, I.W. Electrochemical study and electrodeposition of manganese in the hydrophobic butylmethylpyrrolidinium bis((trifluoromethyl)sulfonyl)imide room-temperature ionic liquid. Electrochimica Acta 53(4) (2007): 1931-1938.
- [33] Liu, S., et al. A novel rechargeable zinc-air battery with molten salt electrolyte. Journal of Power Sources 342 (2017): 435-441.
- [34] Fu, J., Cano, Z.P., Park, M.G., Yu, A., Fowler, M., and Chen, Z. Electrically Rechargeable Zinc-Air Batteries: Progress, Challenges, and Perspectives. Adv Mater 29(7) (2017).
- [35] Farrell, B. Electrochemical cell [Online]. 2003. Available from: [http://edaphos.com/bfarrell/pdf/electrochemistry\\_lecture.pdf](http://edaphos.com/bfarrell/pdf/electrochemistry_lecture.pdf) [October 29, 2016]
- [36] web, A.I.C. The standard hydrogen electrode [Online]. 2012. Available from: [http://alevelchem.com/aqa\\_a\\_level\\_chemistry/unit3.5/s353/02.htm](http://alevelchem.com/aqa_a_level_chemistry/unit3.5/s353/02.htm) [October 29, 2016]
- [37] Services, E.G.T. Fuel cell handbook (7th) [Online]. 2004. Available from: <http://www.brennstoffzellen.rwth-aachen.de/Links/FCHandbook7.pdf> [October 29, 2016]
- [38] Department of physics, U.o.G. Ohm's law [Online]. 1998. Available from: <https://www.physics.uoguelph.ca/tutorials/ohm/Q.ohm.intro.html> [2015, March 30]
- [39] Porter, M.R. Handbook of surfactants, ed. 2. London: Chapman & Hall, 1994.
- [40] Hilder, M., Winther-Jensen, B., and Clark, N.B. The effect of binder and electrolyte on the performance of thin zinc-air battery. Electrochimica Acta 69 (2012): 308-314.
- [41] Daoyong, Y., Fang, H., and Hai, X. Determination of critical concentrations by synchronous fluorescence spectrometry [Online]. 2011. Available from: <http://www.rsc.org/suppdata/ay/c1/c1ay05495c/c1ay05495c.pdf> [May 4]
- [42] Huang, J.-B., Mao, M., and Zhu, B.-Y. The surface physico-chemical properties of surfactants in ethanol-water mixtures. Colloids and surface A: Physicochemical and Engineering Aspects 155 (1999): 339-348.
- [43] Guanghua Li, Ke Zhang, Mohammed Adnan Mezaal, and Rui Zhang, L.L. Effect of electrolyte concentration and depth of discharge for zinc-air fuel cell. International Journal of Electrochemical Science 10 (2015): 6672-6683.
- [44] Ma, H., Wang, B., Fan, Y., and Hong, W. Development and Characterization of an Electrically Rechargeable Zinc-Air Battery Stack. Energies 7(10) (2014): 6549-6557.

**APPENDIX**



จุฬาลงกรณ์มหาวิทยาลัย  
**CHULALONGKORN UNIVERSITY**

## VITA

Miss Jutamart Chotipanich was born in Narathiwat, Thailand on July 7, 1978. She received a B.E. in chemical engineering from Prince of Songkla University in March, 2000, and a M.E. in chemical engineering from Chulalongkorn University in May, 2006. In May 2011 she entered the doctoral program in chemical engineering at Chulalongkorn University.

